FINITE ELEMENT MODELING OF THE ORTHOGONAL METAL CUTTING PROCESS: MODELING THE EFFECTS OF COEFFICIENT OF FRICTION AND TOOL HOLDING STRUCTURE ON CUTTING FORCES AND CHIP THICKNESS.

FINITE ELEMENT MODELING OF THE ORTHOGONAL METAL CUTTING PROCESS: MODELING THE EFFECTS OF COEFFICIENT OF FRICTION AND TOOL HOLDING STRUCTURE ON CUTTING FORCES AND CHIP THICKNESS.

By

SILVIE MARIA TANU HALIM, B. ENG.

A Thesis Submitted

to

the School of Graduate Studies

in Partial Fulfilment of the Requirements for

the Degree Masters of Applied Science

McMaster University

MASTERS OF APPLIED SCIENCE (2008) McMaster University

(Mechanical Engineering) Hamilton Ontario

TITLE: Finite Element Modeling of the Orthogonal Metal Cutting Process: Modeling the Effects of Coefficient of Friction and Tool Holding Structure on Cutting Forces and Chip Thickness.

AUTHOR: Silvie Maria Tanu Halim, B. Eng. (McMaster University)

SUPERVISORS: Dr. Eu-Gene Ng

Dr. M. A. Elbestawi

NUMBER OF PAGES: xv, 128

ABSTRACT

Finite element (FE) method has been used to model the orthogonal cutting process. Currently, FE cutting models appeared to be able to predict cutting force F_c that fits well with experimental results, however, modeled feed force F_t always seems to be under predicted. One of the critical factors to F_t prediction would be to capture the effect of the tool cutting edge radius. Ever since Arbitrary Lagrangian Eulerian (ALE) formulation could be successfully employed into FE cutting models, inclusion of tool cutting edge radius and capturing its effect on machining has become possible. However, even after tool cutting edge included into FE cutting models, approach method made to solve the under predicted F_t did not change. Work done on FE cutting models still focused on capturing the effect of tool cutting edge radius, specifically the ploughing action that caused size effect. The most common solving approach was to identify new friction models or to increase coefficient of friction (COF) along the tool-chip interface. On the other hand, it should be noted that though altering friction models or changing COF value with process parameters could cause predicted F_t closer to the experimental result, predicted F_c, chip thickness t_c and contact length l_c were also affected.

The objective of this research is to develop a methodology to calibrate COF value for FE simulation of orthogonal cutting. The effect of the tool holder geometry on prediction accuracy was also considered. The performance measure used was chip thickness and cutting forces acquired from various experiments. Experimental and predicted results showed that the magnitude of COF should be a function of tool and workpiece material combination, and not a function of process parameters. The results also show that the tool holder geometry has to be included in order to estimate both cutting and feed forces accurately.

ACKNOWLEDGMENTS

I would like to express my heartfelt gratitude to all those who have made it possible for me to complete this thesis. I want to thank the Department of Mechanical Engineering, McMaster University, AUTO21 and Dana Long Manufacturing for financing and sponsoring this research.

I would like to give special thanks to my supervisor, Dr. Eu-Gene Ng, for his guidance, motivation and encouragement in helping me throughout the research and writing of this thesis. His wisdom, insight and professionalism have been of great value to me. The numerous opportunities given by Dr. Eu-Gene Ng in allowing me to be involved in industrial projects and conferences is deeply appreciated. Most importantly, I am deeply grateful for being given the opportunity to be part of this wonderful research.

I would also like to thank my supervisor Dr. M. A. Elbestawi for his financial support throughout this research.

I would like to thank Warren Raynolds for his excellent help and guidance during experimental work throughout my research. Special thanks also to Joe, Jim, Andrew and Ron who were always ready to provide help when needed.

I would like to thank Tan Guang Wang for his friendship and tireless encouragement throughout my research. His understanding is sincerely appreciated. I would also like to thank Aml, Tasneem and Zareena for their friendship.

My father, mother and three sisters, whom I miss so dearly, had also encouraged and supported me throughout my school years. My education would have been impossible without my parents' sacrifice and love. I would like to express my appreciation to Koh Kah Hock, for providing his love, understanding and enduring patience for the past six years. Most importantly, I would like to thank Jesus Christ, my Lord, my Savior, my Teacher and my Friend. Life will be meaningless without His sacrificial love.

TABLE OF CONTENTS

LIST OF FIGURES CAPTIONS

LIST OF TABLE CAPTIONS

NOMENCLATURE AND LIST OF SYMBOLS

v : Cutting speed (m min^{-1})
v_c : Chip velocity (m min^{-1})
f : Feed rate (mm rev^{-1})
t_u : Undeformed chip thickness (mm)
t_c : Chip thickness (mm)
t_{ci} : Initial chip thickness (mm)
w : depth of cut (mm)
R : Resultant force (N)
F_c : Cutting force (N)
F_t : Thrust force (N)
F_z : Axial force (N)
F_s : Shear force (N)
N_s : Normal shear force (N)
F_r : Friction force (N)
N_r : Normal friction force (N)
α : Tool rake angle (deg)
α_e : Tool effective rake angle (deg)
β : Friction angle (deg)
φ : Shear angle (deg)
μ : Coefficient of friction COF (-)
COF : Coefficient of friction (-)
PSZ : Primary shear zone
SDZ : Secondary deformation zone
TDZ : Tertiary deformation zone
BUE : Built-up edge
ρ_e : Tool cutting edge radius (μm)
l_p : Sticking region along the tool-chip interface (mm)
l_c : Contact length along the tool-chip interface (mm)
τ : Shear stress (MPa)
σ : Normal stress (MPa)
τ_{max} : Maximum shear stress (MPa)
A : Apparent area of contact (mm^2)
A_r : Real area of contact (mm^2)
LF : Lagrangian Formulation
ALE : Arbitrary Lagrangian Eulerian
m : (When used in friction models) Shear friction factor (-)
n : (When used in friction models) Constant for variable shear friction model (-)
k : Shear flow stress of workpiece material (MPa)
σ_y : Material yield stress (MPa)
Pb : Lead
AISI : American Iron and Steel Institute

Exp. : Experimental data
WP : Workpiece
A : (When used in J-C equation) Material constant (MPa)
B : (When used in J-C equation) Material constant (MPa)
C : (When used in J-C equation) Strain rate index (-)
ε_{pl} : Plastic strain (-)
$\dot{\varepsilon}_{pl}$: Plastic strain rate (s^{-1})
$\dot{\varepsilon}_0$: (When used in J-C equation) Reference plastic strain rate (s^{-1})
T : Temperature (°C)
T_{ref} : (When used in J-C equation) Reference temperature (°C)
T_{melt} : Workpiece material melting temperature (°C)
m : (When used in J-C equation) Thermal index (-)
n : (When used in J-C equation) Strain hardening index (-)
E : Young's Modulus (GPa)
ρ : Density (kg m^{-3})
α : (When used for material property) Thermal expansion ($°C^{-1}$)
c_p : Specific heat capacity (J kg^{-1} $°C^{-1}$)
k : (When used for material thermal property) Thermal conductivity (W m^{-1} $°C^{-1}$)
CVD : Chemical vapor deposition
CNC : Computer numerical control
δ : Deflection (μm)
δ_x : Deflection in x- direction (μm)
δ_y : Deflection in y-direction (μm)
t_s : Settling time (ms)
ω_n : Natural frequency (Hz)
ξ : Damping ratio (-)
X_s : Steady state value
k : (When used to describe structure dynamic behavior) Stiffness (N mm^{-1})
m : (When used to describe structure dynamic behavior) Mass (kg)

1. INTRODUCTION

1.1 Background

Finite Element (FE) method has been applied to simulate metal cutting. Cutting forces and chip thickness obtained experimentally are commonly used to validate predicted results from the FE cutting models. It has been observed by past researchers [Komvopoulos, 1991, Joyot, 1998] that when tool cutting edge is assumed to be infinitely sharp, the FE cutting models were incapable of thrust force (F_t) prediction. With the improvement of Arbitrary Lagrangian Eulerian (ALE) formulation, tool cutting edge radius into FE cutting models became possible; allowing the possibility of F_t prediction. However, predicted F_t made has always been 30-70% lower than the F_t obtained experimentally [Arrazola, 2008].

A few common approaches to solve the under predicted F_t are: 1) to increase coefficient of friction (COF) value, 2) to change friction models and 3) to calibrate COF with every different cutting condition. Since other researchers are increasingly aware of the problem faced in under predicted F_t, for the past decade, much work has been focused on the critical analysis of friction models and magnitude of COF used in FE cutting models [Filice, 2007, Ozel, 2006, Iqbal, 2007]. The investigation on increasing COF in FE cutting models has concluded that doing so will increase predicted F_t that fits well with experimental results; however, other predicted variables such as cutting force F_c and chip thickness t_c will be over predicted [Ozel, 2006]. Despite of the detailed investigation carried out, there is currently still no conclusion with regards to how to define friction

model or calibrate magnitude of COF to be used in FE cutting models. No conclusion on whether or not COF should be fixed or changed with cutting condition was made. There were fundamental flaws with regards to the definition and usage of COF in FE cutting models:

- At high contact pressure conditions, COF should vary when the combination of tool and workpiece material changes, but not with changes in process parameters [Albrecht, 1960].
- Increasing COF value should not be considered as a solution in solving under predicted F_t. Increased COF produced faulty results in FE cutting models along the tool chip interface, such as stagnated region and chip thickness.

Another important aspect to be addressed is that formation of a stagnated region around the tool cutting edge radius could be captured by FE cutting model using the simple Coulomb friction model. Misconceptions relating to application of high COF on the tool cutting edge radius to capture stagnated region will also be discussed.

The work done for this research is focused on using a new method to solve the under predicted F_t in FE cutting models; not through altering friction models or increasing COF, but through including tool holder geometry in FE cutting models. Misconceptions on friction models and COF will also be thoroughly discussed in this paper. FE cutting models built will be experimentally validated.

1.2 Objectives

The objective of the current project is to solve the current problems faced in force prediction in FE cutting models. Instead of altering friction models, an innovative and groundbreaking approach is used to solve the problem. Basic friction behaviors at the tool chip interface will also be reviewed and discussed. This research work was carried out in three different phases. The three phases are as follows:

- Phase 1: Effect of tool holding structure and workpiece geometry in FE cutting models will be investigated.
- Phase 2: New methodology of calibrating value of COF will be presented.
- Phase 3: Parametric study to test the findings from Phase 1 and Phase 2.

2 LITERATURE REVIEW ON ORTHOGONAL CUTTING

2.1 MECHANICS OF ORTHOGONAL CUTTING

Experimental and analytical reviews in this research will be focused on orthogonal machining. Orthogonal machining, as shown in Figure 2:1, has a tool with a plane cutting face and a cutting edge that is perpendicular to the cutting speed (v) and chip velocity (v_c) vectors. For 2-dimensional (2D) orthogonal machining, the depth of cut (b) has to be at least ten times the feed (f) [Shaw, 2005].

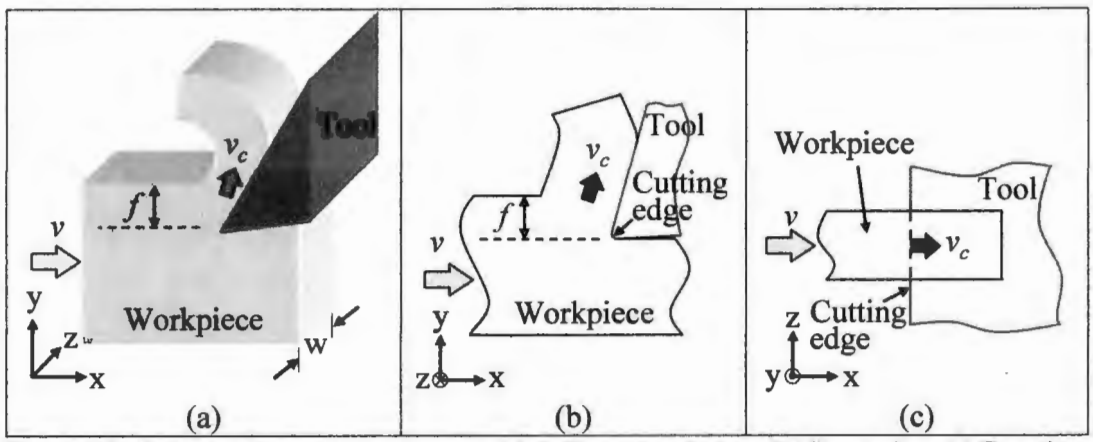

Figure 2.1: Orthogonal machining process. (a) 3-dimensional view. (b) Front view. (c) Top view.

The cutting force circle as shown in Figure 2.2 was suggested by Merchant, thus called Merchant's circle diagram. Merchant's circle diagram is based on the concept of two-dimensional cutting process with homogeneous workpiece material. The model assumed:

- Tool has infinitely sharp cutting edge,
- Plane strain condition,
- Only continuous chip formed with no built-up edge,

In Figure 2.2, the resultant force (R) can be resolved into three components:

1. The cutting force (F_c) and feed force (F_t) in the horizontal and vertical directions respectively.
2. The shear force (F_s) and normal shear force (N_s) along and perpendicular to the shear plane respectively.
3. The friction force (F_r) and normal friction force (N_r) along and perpendicular to the tool rake face respectively.

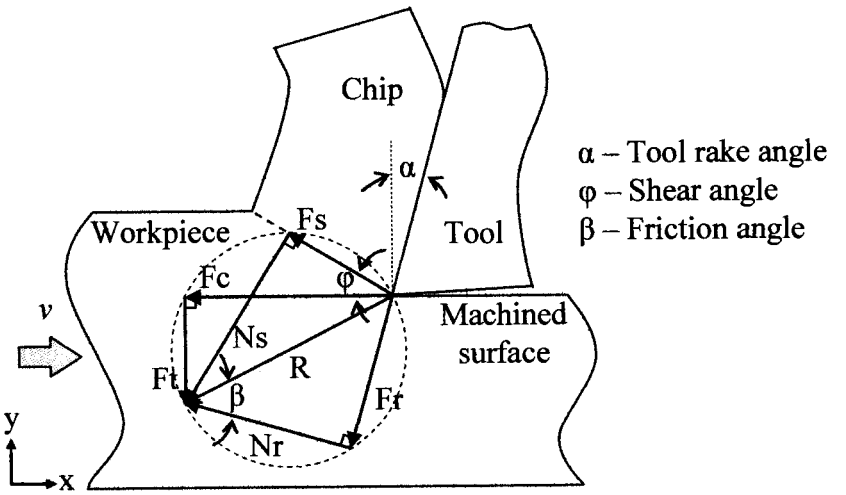

Figure 2.2: Merchant's Circle Diagram

From Merchant's circle, analytical relationships between shear force F_s and friction force F_r in terms of cutting force F_c and feed force F_t could be obtained. Cutting force F_c and feed force F_t could be acquired experimentally by means of a dynamometer. Equation 2.1 and 2.2 shows how friction force F_r and normal friction force N_r are obtained in terms of cutting and thrust force respectively by using Merchant's circle. Equation 2.3 shows how friction angle is obtained from Merchant's circle. However, many had mistakenly determined the average coefficient of friction by using $\mu = \tan\beta = \frac{Fr}{Nr}$. This topic will be further discussed in section 3.2.

$$F_r = F_c \sin\alpha + F_t \cos\alpha \quad \text{----------} \quad (2.1)$$

$$N_r = F_c \cos\alpha - F_t \sin\alpha \quad \text{----------} \quad (2.2)$$

$$\tan\beta = \frac{F_r}{N_r} = \frac{F_c \sin\alpha + F_t \cos\alpha}{F_c \cos\alpha - F_t \sin a} \quad \text{----------} \quad (2.3)$$

During machining, workpiece material will be plastically deformed. Plastic deformation shear zone has three main regions as shown in Figure 2.3: the primary shear zone (PSZ) on the shear plane, secondary deformation zone (SDZ) along the tool rake face, and the tertiary deformation zone (TDZ) on the tool flank face. In machining, no tool has an infinitely sharp cutting edge; the rounded cutting edge radius on the tool will induce plowing. Therefore, the primary shear zone will not be a single plane but a region as illustrated in Figure 2.3. Since the tool is not infinitely sharp, there will be a tertiary deformation zone where there is friction between tool and the newly machined surface.

In finite element (FE) cutting models, inclusion of the cutting edge radius has been a critical factor, especially when much focus was on obtaining thrust force and residual stresses. Modeling friction on the secondary deformation zone along the tool rake face will be the main focus in this research.

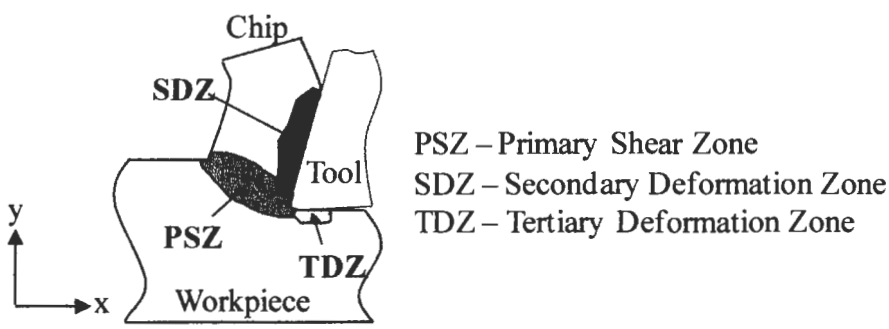

Figure 2.3: Three main plastic deformation zones in workpiece material during machining.

2.2 CHIP FORMATION

There are four basic types of chip formed during metal cutting process; they are 1) continuous chip, 2) continuous chips with built-up edge (BUE), 3) discontinuous and 4) segmental chip. Figure 2.4 (a) shows continuous chip formation. Continuous chips form when shearing occurs at primary shear zone (PSZ). This type of chip is usually obtained when machining ductile materials such as aluminum, mild steel and copper. Machining workpiece with high hardness can also produce continuous chip by using low cutting speed. Cutting conditions that produce continuous chip is regarded as steady state process [Boothroyd, 89]. Formation of continuous chip with BUE is shown on Figure 2.4 (b). Continuous chip with BUE is formed under a high friction condition along the tool-chip interface. The accumulation of welded chip material is referred to as a built-up edge (BUE). BUE will continue to grow and but breaks down when unstable. The broken pieces are carried away by the underside of the chip and the machined surface.

Figure 2.4 (c) shows the formation of discontinuous chip. Discontinuous chip is formed when the workpiece material undergoes severe strain, causing fracture to occur in the primary deformation zone when the chip is only partly formed. This kind of chip is usually formed when machining brittle material or when machining ductile material at very low speeds and very high feed. Discontinuous chip have also been observed when machining ductile material at ultra high cutting speed. Figure 2.4 (d) shows the formation of segmental chip. During machining, segmental chip is basically formed by shear localization due to strain incompatibility of the workpiece microstructure at the shear zone [Shaw, 2005]. The main mechanisms behind segmental chip formation are a) cyclic

crack approach and b) adiabatic shear theory. The mechanism of segmental chip formation varies due to the different physical and thermal properties of the workpiece material and workpiece microstructure [Shaw, 2005].

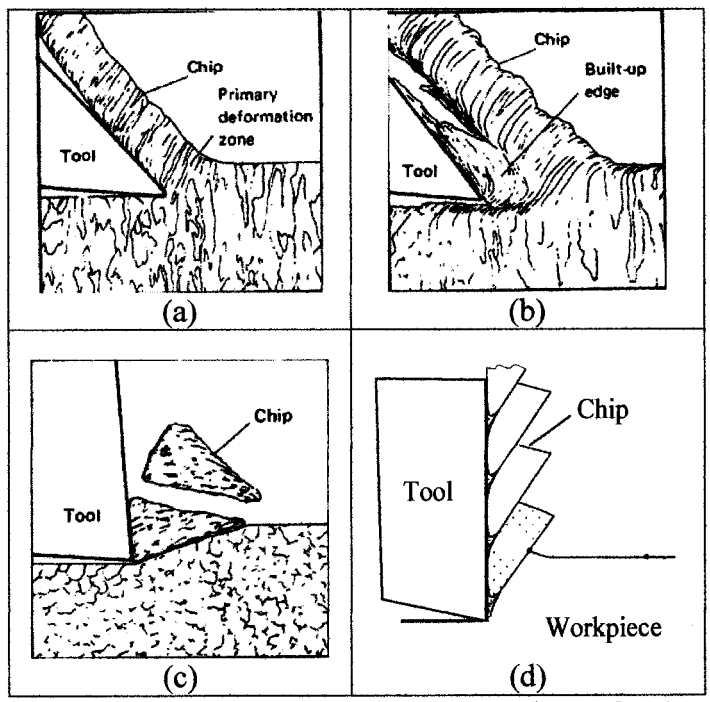

Figure 2.4: Four basic types of chip formation: (a) Continuous chip, (b) Continuous chip with built-up edge (BUE) and (c) Discontinuous chip [Boothroyd, 1989] (d) Segmental chip [Zheng, 1997].

2.3 EFFECT OF TOOL CUTTING EDGE RADIUS

In machining, no matter how sharp a cutting tool is, there will be a finite rounded tool cutting edge radius [Albrecht, 1960] as shown in Figure 2.5. Part of the rounded tool cutting edge will plow through the workpiece material instead of cutting; the plowing action introduces the plowing force component [Boothroyd, 1989]. When feed used is much larger than the tool cutting edge radius, the plowing force forms a small proportion of the resultant force. On the other hand, when the feed value is close or smaller than the tool cutting edge radius, the plowing force forms a large proportion of the resultant force.

The significant effect of cutting edge radius cannot be neglected. The increasing effect of tool cutting edge radius with decreasing feed rate is referred to as 'size-effect' [Boothroyd, 1989].

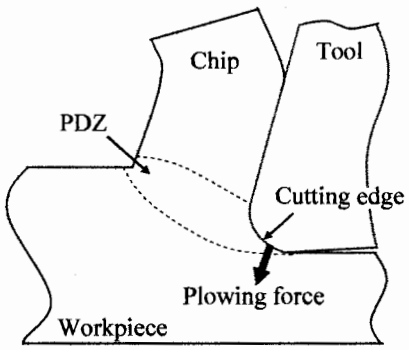

Figure 2.5: Sketch of orthogonal Cutting process with finite tool cutting edge radius.

Previous research has shown that the size effect will also result in a wider primary deformation zone [Liu, 2007]. Depending on the feed rate f range being used, tool cutting edge radius could affect the effective rake angle α_e (actual rake angle). This illustration is shown in Figure 2.6. At a lower feed rate (Figure 2.6 (a)), the effective rake angle α_e would be lower than the tool rake angle α. As feed rate increases (Figure 2.6 (b)), the influence of tool cutting edge on effective rake angle α_e would diminish; the effective rake angle would approach the tool rake angle α [Arsecularatne, 1998]. When the tool cutting edge radius causes the effective rake angle α_e to be more negative than the tool rake angle α in machining, plastic deformation and plowing become the dominant actions rather than cutting [Fang, 2003].

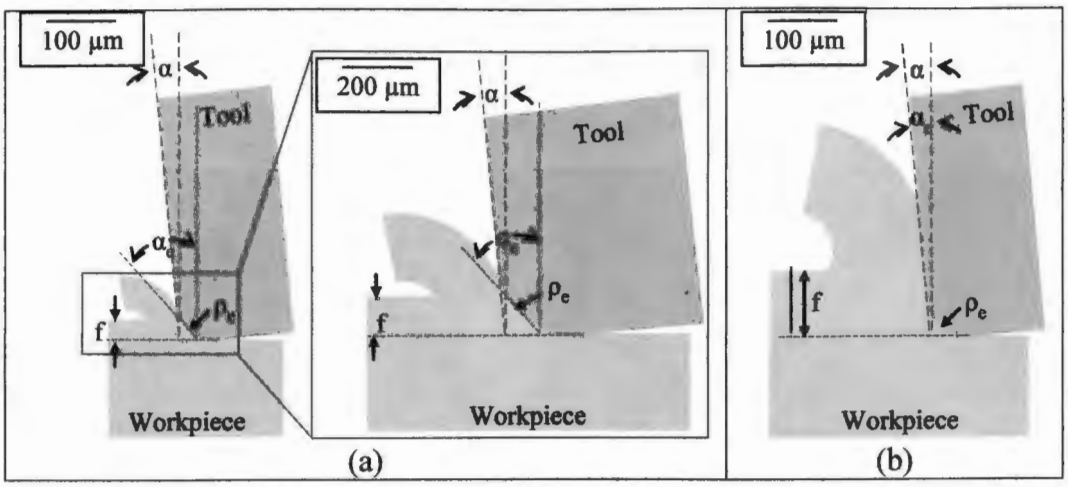

Figure 2.6: Example illustration of cutting edge radius effect. (a) Feed rate *f* near the cutting edge radius ρ_e, effective rake angle α_e lower than tool rake angle α. (b) Feed rate *f* higher than cutting edge radius ρ_e, effective rake angle α_e approaching tool rake angle α.

Figure 2.7 (a) shows the experimental material flow field during machining done by Oxley [Oxley, 1989]. It was observed that stagnation point of the flow exists on the rounded tool cutting edge. Most of the workpiece material will flow above the stagnation point towards the tool rake face to form the chip, but some of the workpiece material is being pushed below the stagnation point into the machined surface. Therefore, stagnation point sometimes is also referred to as separation or neutral point. The stagnation region formed ahead of the tool tip should not be mistaken as BUE. Unlike BUE, stagnation region formed acted as a stable edge, and did not show a cycle of nucleation, growth and dropping out [Ohbuchi, 2003]

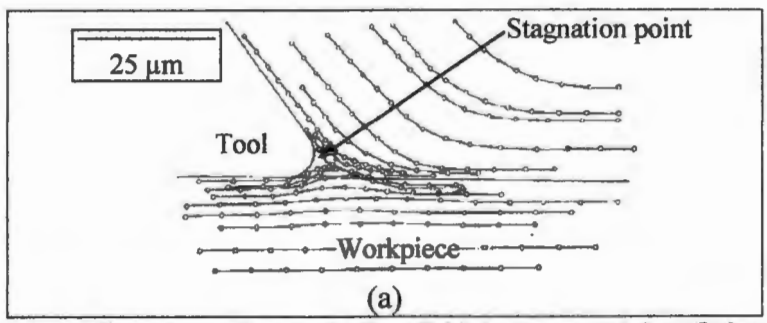

Figure 2.7: (a) Experimental material flow field during machining [Oxley, 1989].

Japer et. al. [Jasper, 2002 b] used a quick stop device to obtain chip root pictures and analyze the effects of tool cutting edge radius on stagnate region. The workpiece used was AISI 1045, and the tool used was uncoated carbide. Figure 2.8 (a) and (b) show chip root pictures when tool cutting edge radius of ρ_e=33 μm and ρ_e=2 μm were used respectively; both radii there approach stagnation point. From the figures obtained, [Jasper, 2002 b] concluded that stagnated point will form no matter how small the tool cutting edge radius.

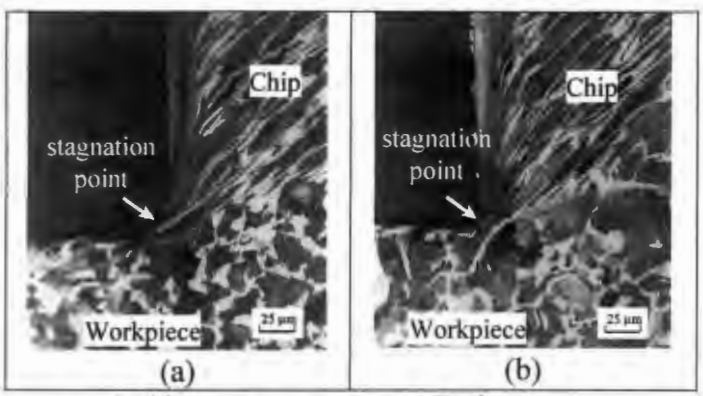

Figure 2.8: Chip root obtained with quick stop device. (a) Tool cutting edge radius ρ_e=33 μm. (b) Tool cutting edge radius ρ_e= 2μm. [Jasper, 2002 b]

As shown, tool cutting edge affects forces, chip formation, temperature on tool-chip interface, machined surface and also tool life [Karpat, 2008]. Therefore, effect of tool cutting edge radius should not be neglected in metal cutting.

2.4 FRICTION IN METAL CUTTING

Friction is the force which causes the motion between two surfaces to be reduced. Coulomb's friction law is the most well known and commonly used theory. Coulomb summarized his results with equation (2.4). Equation (2.4) states that, for surfaces in relative motion, $F=\mu L$, where F is the friction force, L is the normal force and μ is the Coefficient of Friction (COF).

$$F = \mu L \qquad (2.4)$$

Coulomb's friction law states friction coefficient μ is nearly independent not only of L, but also of the sliding velocity v and contact area. As shown in Figure 2.9 (a), all finished surfaces are found to have irregularities, causing the actual area of contact (A_r) to be much smaller that the apparent area of contact (A). Coulomb's friction law was investigated under light load condition, thus the actual contact area of both surfaces is much smaller than the apparent contact area.

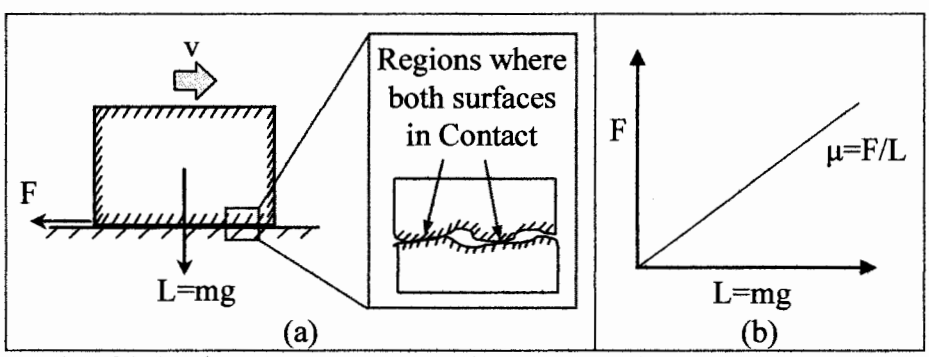

Figure 2.9: (a) The friction force F and the normal force L for sliding contact with velocity v, both surfaces are not 100% in contact. (b) Coulomb's friction law.

In metal cutting, the contact condition between the workpiece and tool undergo extreme conditions: very high sliding velocity, high normal load. Moreover, at the tool-chip interface, the workpiece material undergoes large plastic deformation. When

workpiece material is plastically deformed, the energy being released is mostly transformed into heat. This causes the contact condition along the tool chip interface to go through high temperature, another extreme condition. At the same time, new surfaces were generated at the cutting edge of the tool. Under all these severe contact conditions along the tool-chip interface, Coulomb's friction law no longer holds. Stress distribution along the tool-chip interface proposed by Zorev [1963] shown in Figure 2.10 has been very commonly used as frictional behavior model in orthogonal cutting; where x is the distance from the cutting edge along the tool rake face, σ and τ is the normal and shear stress respectively and l_p and l_c is the sticking region and contact length respectively. Zorev's model assumed continuous chip formation with no built-up edge. The region between sticking region and before the chip moves away from the tool rake face ($l_p < x < l_c$), is termed as sliding region. The normal stress σ is highest at the cutting edge radius, and gradually decreases as the contact length moves away from the cutting edge radius. At sticking region, the shear stress becomes a maximum; at sliding region, the shear stress will be a function of the normal stress. Section 3.2 will detail the discussion of friction models that try to mimic the friction conditions on the tool chip interface.

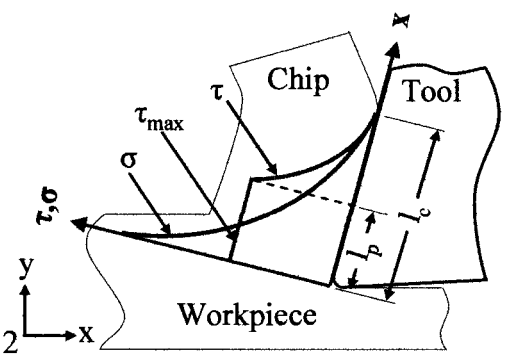

Figure 2.10: Stress distribution along the tool-chip interface proposed by Zorev [1963].

Shaw [2005] suggested that there are three regimes in solid friction as normal stress σ increases. Shaw illustrated the three regimes of solid friction with change in normal stress σ as shown in Figure 2.11 (a-d): Regime I is the classical friction, where normal stress is low (A_r<<A) and Coulomb's friction law holds; Regime III is the deformation friction region, where workpiece shear stress is independent of normal stress, change in load do not change the contact area (A_r=A); Regime II is the transition region between Regimes I and III. As shown in Figure 2.11 (a-d), σ and τ has decreased, and Regime II is the transition regime, located in-between Regime I and III. Shaw commented that the contact stress near the tool cutting edge along the tool-chip interface behave like regime III of the solid friction. Then, the contact stress will eventually behave like regime II and regime I of the solid friction as the chip starts to curl away from the tool rake face.

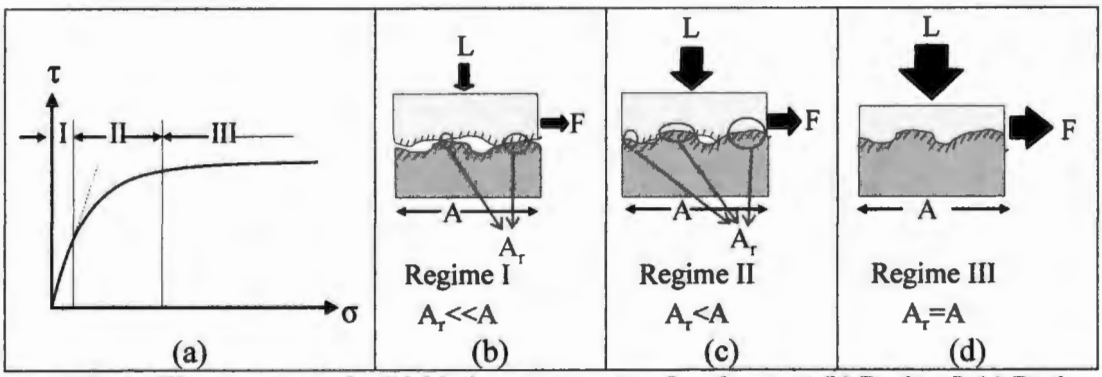

Figure 2.11: (a) Three regimes of solid friction. Apparent and real area at (b) Regime I, (c) Regime II and(d) Regime III [Shaw, 2005].

3. LITERATURE REVIEW ON FE MODELING IN METAL CUTTING

3.1 FINITE ELEMENT FORMULATIONS

There are three different types of finite element formulations that are commonly used in FE cutting models. These are: Lagrangian, Eulerian and Arbitary-Lagrangian Eulerian (ALE) formulations. Each individual formulation has its unique advantages and disadvantages. Choosing the type of formulation to be used in FE cutting model will depend on the limitations of individual formulation techniques.

3.1.1 Lagrangian Formulation

Lagrangian approach is for solid-mechanics analysis, where the FE mesh grids are attached completely to the material. Figure 3.1 shows the simple illustration of the element mesh grids and material deformation when Lagrangian formulation is used. Figure 3.1 (a) shows the initial position of the element mesh grid and material. Figure 3.1 (b) shows the final deformed material; the element mesh grids are still attached to the material and are deformed with the deformation of the material.

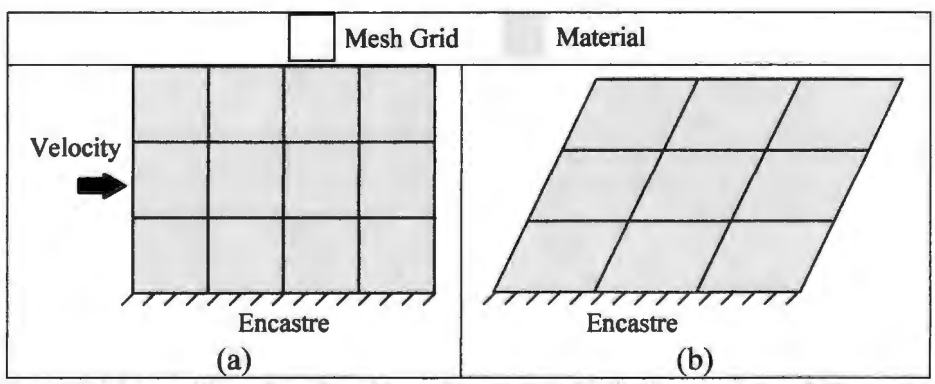

Figure 3.1: (a) Initial position of mesh grids and material. (b) Both material and element mesh grid deformation after the velocity is applied.

Lagrangian formulation (LF) has been commonly used for simulating cutting process. Figure 3.2 (a) shows a typical example of the initial mesh and boundary condition used in Lagrangian approach; there is a predefined parting line on the workpiece geometry positioned right below the feed rate, *f*. The thin predefined parting line will be deleted as the tool cut through the workpiece to form the chip. Figure 3.2 (b) shows an example of continuous chip formation with Lagrangian formulation. When using Lagrangian approach, the chip and contact length is formed through natural deformation as the tool cut through the workpiece, thus no initial assumption of chip geometry is required. However, large mesh distortion is inherent for this approach. When the mesh distortion gets severe, the elements turn inside out, forcing the model to terminate. The requirement of having a predefined parting line is one of the major drawbacks when using Lagrangian formulation. This is because the damage criterion applied on the parting line lacks generality.

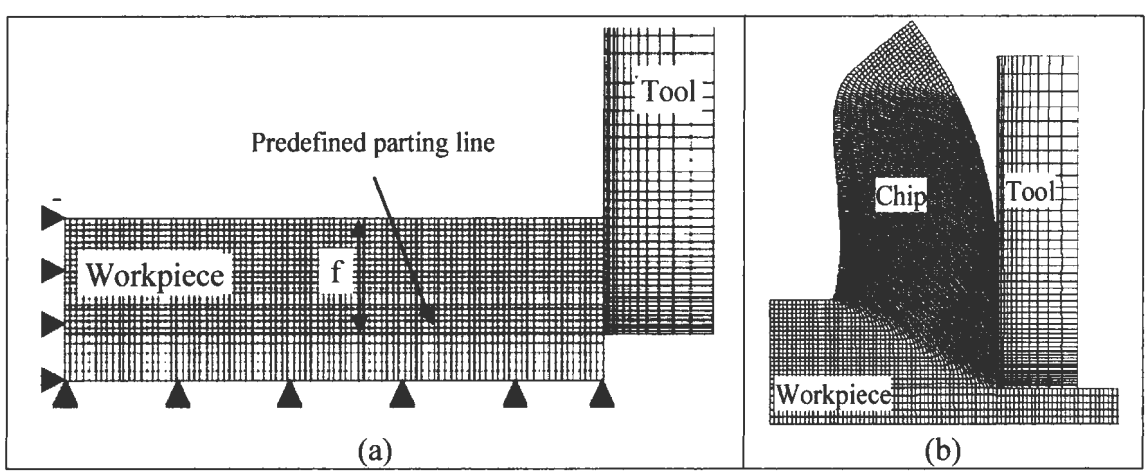

Figure 3.2: Initial boundary condition and geometry when using Lagrangian formulation in FE cutting models. (b) Continuous chip formation using Lagrangian formulation [Ng, 2002 a].

The damage criterions used in Lagrangian are detailed in Table 3.1. Even after the type of criterion had been chosen properly, there is no physical indication as to what

criterion value should be adopted. Moreover, choosing the type and value of damage criterion has great influence on the results obtained from the FE model. Huang and Black [1996] did a detailed analysis of material separation criteria or criterion in orthogonal machining, which included an evaluation of separation criteria based on nodal distance, equivalent plastic strain, energy density and stresses. Huang and Black [1996] concluded that neither geometrical nor physical criterion could simulate incipient cutting correctly. Another limitation of using Lagrangian formulation is that the modeled tool has to be assumed as perfectly sharp. This is because thin partition line for damage criterion is not possible with the presence of tool cutting edge. Tool cutting edge radius will also induce large deformation and severe mesh element distortion on the workpiece material around the tool cutting edge. The severe mesh distortion will most probably cause the simulation to be terminated. When the tool cutting edge is modeled as perfectly sharp, valuable information such as plowing, size effect and stagnation zone at the tool cutting edge will not be captured by the model. Meanwhile, it should also be noted that when FE cutting model requires damage criterion or/and assumed perfectly sharp tool, the model is incapable of predicting feed force F_t. Research done on FE cutting models that had employed Lagrangian formulations either did not present feed force F_t results, or predicted feed force F_t that were very low when compared to experimental results. For example, refer to authors shown in Table 3.1. FE cutting models that employed Lagrangian formulation with adaptive mesh option were also incapable of predicting feed force F_t accurately [Fang, 2004].

Damage Criterion	Authors
Nodal distance	• [Shih, 1995] • [Komvopoulos, 1991] • [Mamalis, 2002]
Effective plastic strain	• [Ng, 2002 a] • [Yang, 2002] • [Guo, 2002 a and b]
Stress-based damage criterion	• [Shi, 2002] • [McClain, 2002] • [Shet, 2000]
Energy density	• [Lin, 1992]

Table 3.1: Damage criterion on the predefined parting line.

Despite of these limitations mentioned above, Lagrangian approach is still commonly used for FE cutting models. This is because FE cutting models that used Lagrangian formulation have successfully modeled chip formations that includes workpiece microstructure [Simoneau, 2006], segmental chip formation [Ng, 2002 a], [Baker, 2003] and 3-dimensional cutting models [Ng, 2002 b]. The advantages of using Lagrangian formulations are shown in Figure 3.3 (a-c).

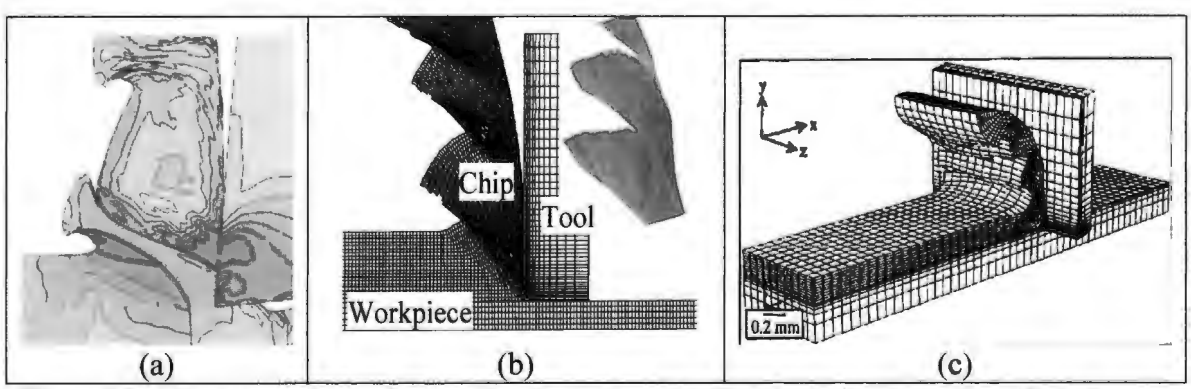

Figure 3.3: Advantages of using Lagrangian formations: (a) Chip formation including effect of workpiece microstructure [Simoneau, 2006]. (b) Segmental chip formation [Ng, 2002 a]. (c) 3-dimensional FE cutting model [Ng, 2002 b].

3.1.2 Eulerian Formulation

In Eulerian formulation, material will flow through the mesh which is fixed spatially. Figure 3.4 shows simple illustrations of the mesh grids and material flow when

the Eulerian approach is employed. Figure 3.4 (a) shows the initial mesh grid and position of the material; Figure 3.4 (b) shows the final position of the mesh grid and the material flow when velocity is being applied. The material will flow through the mesh grids whose positions have been fixed, thus causing no mesh distortion.

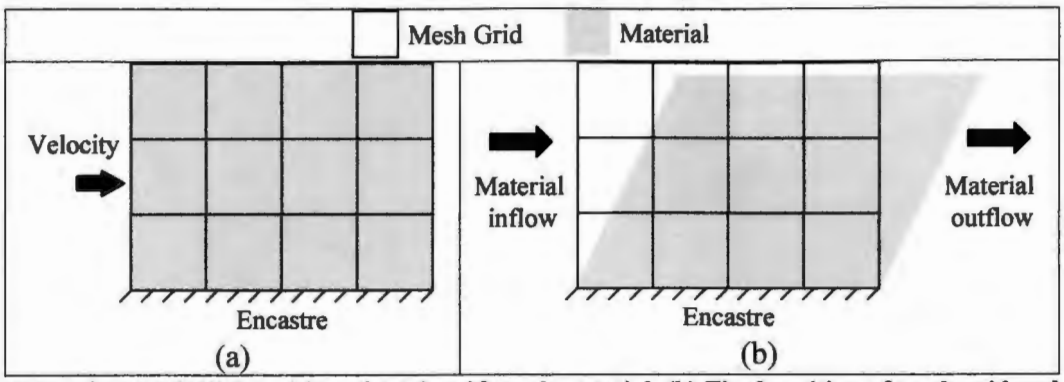

Figure 3.4: (a) Initial position of mesh grids and material. (b) Final position of mesh grid and material flow when using Eulerian formulation.

When Eulerian formulation is employed in FE cutting models, the workpiece material will nicely flow through the mesh grids that have been designed, causing no element separation or chip breakage. Since there is no longer mesh distortion nor chip separation criterion, including the tool cutting edge radius became possible. Raczy [2004] used Eulerian formulation to build a FE cutting model that included the tool cutting edge geometry; prediction of stress and strain distributions in the material ahead of the tool tip was successfully carried out. However, prior knowledge of the chip geometry and chip-tool contact length is required. An example of the FE mesh geometry design that used Eulerian formulation is shown in Figure 3.5 (a). To overcome the shortcomings of initial assumptions, iterative procedures are required [Childs, 1990], [Kim, 1999]. Examples of such iterative procedures are shown in Figure 3.5 (b) used by Kim [1999]. The iterative procedure involved changing the boundary, adjustment of the mesh until convergence

was achieved. Another limitation of using Eulerian approach is that the workpiece material is being modeled as viscoplastic, thus ignoring the elastic property of the workpiece. Therefore residual stress (R. S.) prediction on the machined surface is not possible [Movahhedy, 2002].

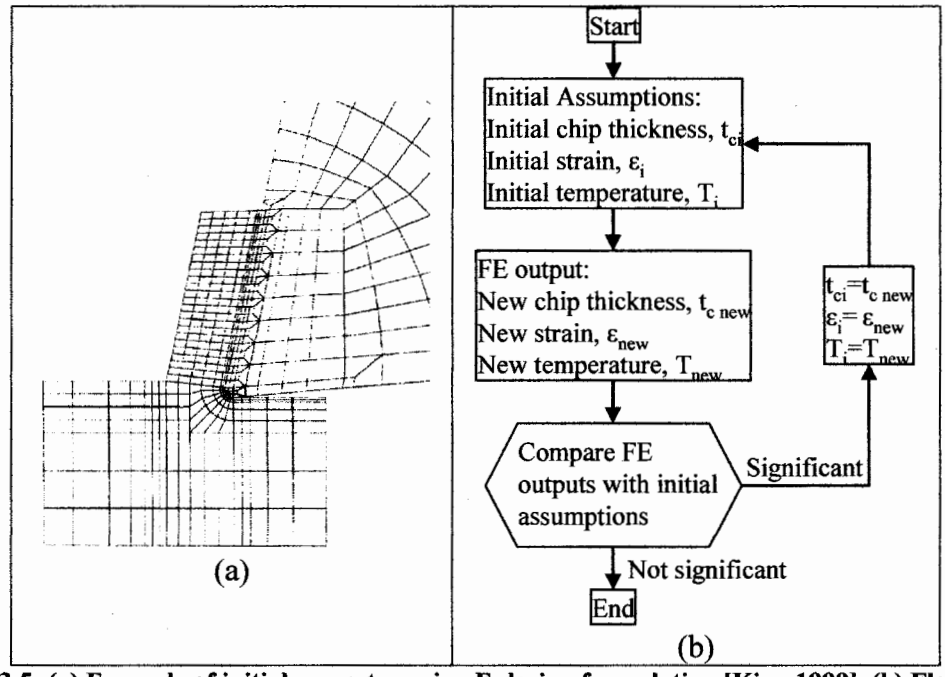

Figure 3.5: (a) Example of initial geometry using Eulerian formulation [Kim, 1999]. (b) Flow chart showing the iteration process when employing Eulerian formulation [Kim, 1999].

3.1.3 Arbitrary Lagrangian Eulerian Formulation

ALE formulations combined both Lagrangian and Eulerian techniques, obtaining their advantages while minimizing the limitations. To this day, research done on applying ALE formulation in FE cutting models have been carried out simply by using adaptive mesh option on the workpiece elements, thus allowing the workpiece to remesh during deformation [Miguelez, 2006, Arrazola, 2008, Ozel, 2007]. Figure 3.6 shows the results of applying ALE formulation only by using adaptive mesh option. However, as shown in Figure 3.6 (a), using adaptive mesh option on the workpiece elements could not fully

solve the sever deformation problem near the tool cutting edge. Avoiding numerical problems was achieved by using only small tool cutting edge radius in FE cutting models [Miquelez, 2006]. Ozel and Erol [2007] solved the severe mesh distortion problem around the tool cutting edge radius by using very fine mesh around the tool cutting edge radius region as shown in Figure 3.6 (b)- a computationally expensive procedure.

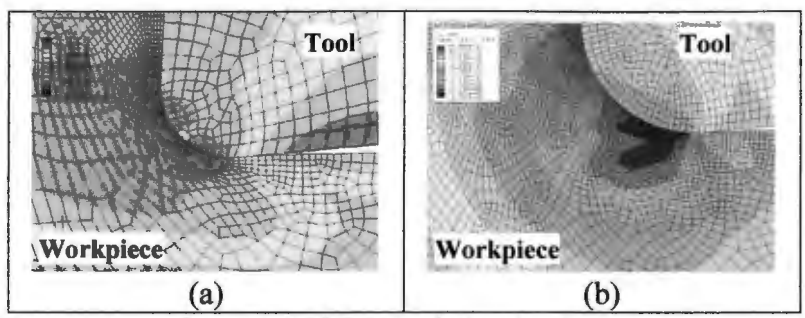

Figure 3.6: Consequences of applying ALE formulation simply by using adaptive mesh option, without assigning specific Eulerian region around the tool cutting edge. (a) Large mesh distortion around tool cutting edge. (b) Very fine mesh size around the tool cutting edge region. [Ozel, 2007]

The proper ALE method applied in FE cutting models was explained in detail by [Movahhedy, 2000 b]; the solution to avoiding severe element distortion was to assign Eulerian mesh on the workpiece region near the tool cutting edge while Lagrangian mesh on the other regions. Figure 3.7 (a) and (b) shows the initial and final geometry mesh of the FE simulation respectively. The chip is already formed at initial condition; however, the final chip formed will not be affected by the initial chip geometry [Movahhedy, 2000, Nasr, 2007].

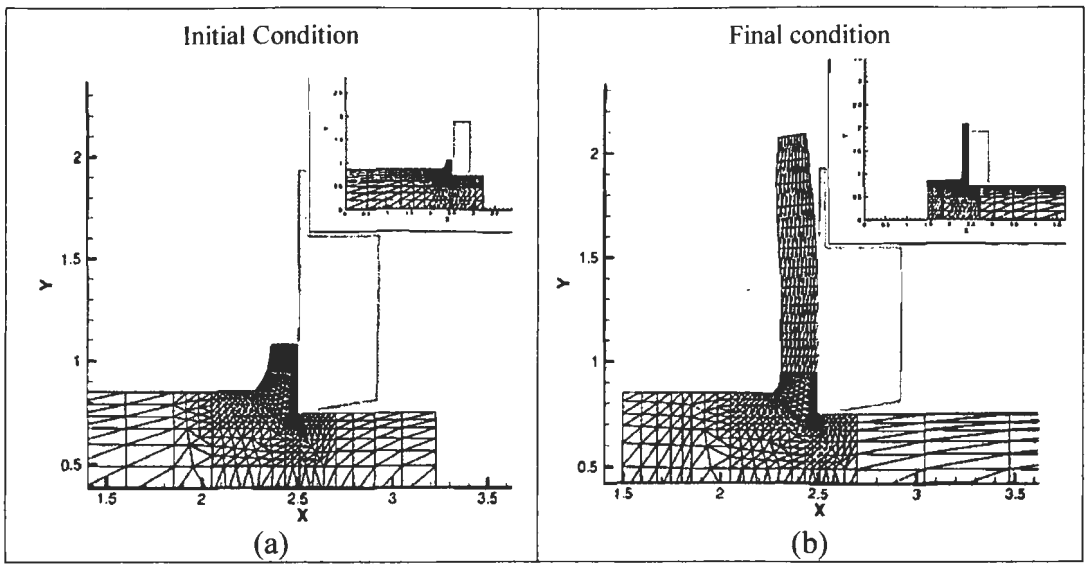

Figure 3.7: (a) Initial geometry, (b) final geometry when ALE formulation is used in FE cutting models [Movahhedy, 2002 a].

Figure 3.8 shows the partitioning scheme employed by Movahhedy et. al. [2002 a]. The shaded area around the tool cutting edge is modeled as Eulerian, which means material will flow through the element mesh without any mesh deformation. Part of the initial chip shape and feed rate were also assigned as Eulerian region. The unshaded part of the workpiece was modeled as Lagrangian, where the element mesh will follow the material deformation. The region where Eulerian mesh is assigned made it possible for FE cutting model to include the tool cutting edge radius into consideration, preventing severe element distortion and eliminating the need for chip separation criteria.

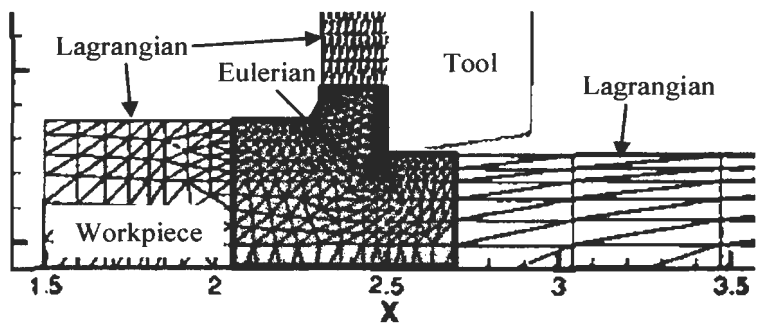

Figure 3.8: ALE partitioning scheme showing the Eulerian and Lagrangian region designed by [Movahhedy, 2000 a].

ALE technique in FE cutting model has been further improved by Nasr et. al. [2007]. An example of a similar, but better portioning scheme, is shown in Figure 3.9. The Eulerian region is located around the same area (region B in Figure 3.9); however initial chip shape and the feed rate were assigned as Lagrangian region. The main purpose of the Eulerian region assigned is for the workpiece material to flow towards the chip and the machined surface, preventing excess element distortion and eliminating chip separation criterion.

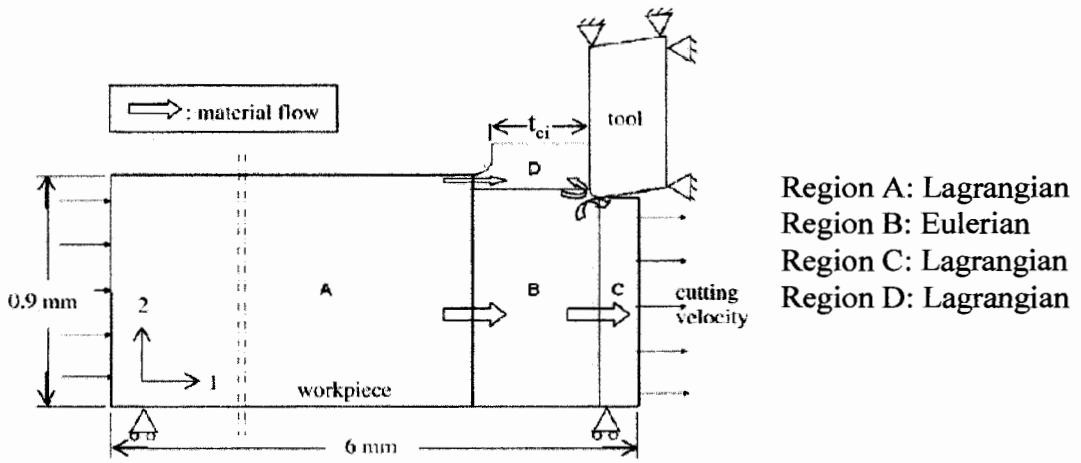

Figure 3.9: Boundary conditions, partitioning scheme and material flow when employing ALE formulation in FE cutting models [Nasr, 2007].

By assigning the initial chip shape area as Lagrangian region, the final shape of the chip will be absolutely formed based on the material deformation (as shown in Figure 3.10). For decades, research on the prediction of R.S., effect of different sizes of tool cutting edge radius [Nasr, 2007] and temperature prediction [Coelho, 2007] have been successfully done using ALE technique. Although the effectiveness of utilizing ALE technique is tested and proven, there are still limitations to overcome. For example, modeling the effect of heterogeneous workpiece material using ALE technique is still not

achievable. This was due to the designed remeshing scheme adapted in ALE formulation. Moreover, ALE technique is still limited to model orthogonal cut with continuous chip formation.

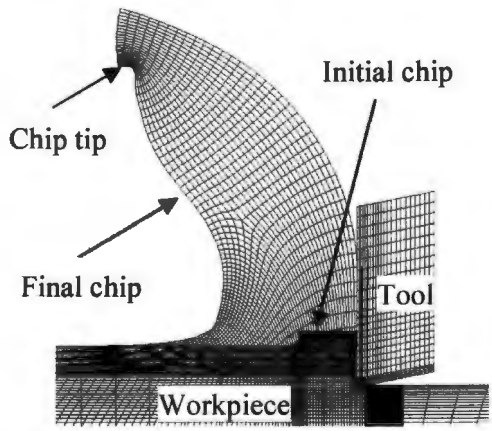

Figure 3.10: Final deformation geometry superimposed with initial geometry [Nasr, 2007].

Choosing the type of formulations to be used in FE cutting models will strongly depend on the area of research interest. Table 3.2 summarizes the advantages and limitations of each individual formulation.

Formulation	Advantages	Limitations
Lagrangian	• Chip formation and contact length form as a nature of workpiece deformation • Able to include workpiece microstructure • Able to build 3-dimensional model • Able to model segmental chip formation	• Large Mesh distortion • Perfectly sharp tool • Chip separation criterions • Incapable of F_t prediction
Eulerian	• Include tool cutting edge radius • No mesh distortion • No chip separation criterion required	• Initial chip geometry assumptions • Iteration process required • Viscoplastic material used • Homogeneous workpiece only
Arbitrary Lagrangian Eulerian (ALE)	• Chip formation and contact length form as a nature of workpiece deformation • Include tool cutting edge radius • No chip separation criterion required • No mesh distortion around the tool cutting edge • Able to predict residual stress	• Homogeneous workpiece only • Continuous chip formation only • Orthogonal cut only

Table 3.2: Advantages and limitations of the three different finite element formulations.

3.2 FRICTION MODELS

Accuracy of predicted results in FE cutting models is highly dependent on the friction condition along the tool-chip interface. Using different friction models and different μ (COF) in FE cutting models will produce different results in contact length, chip thickness, tool rake temperature and cutting forces. The following are some of the most commonly used friction models in FE cutting simulation.

Model I: Coulomb's Friction Law

Based on Coulomb's Friction law shown in equation (3.1), the frictional stress τ along the tool rake face is proportional to the normal stress σ on the tool rake face, and μ is the constant COF.

$$\tau = \mu\sigma \quad \text{----------} \quad 3.1$$

In FE cutting models, to employ Coulomb's Friction law, COF must be estimated as an input. Bil et. al. [2004] had described Coulomb's Friction Law as over simplified and unable to capture sticking and slipping region, and its inability to show the true stress distribution along the tool-chip interface. The most common method used to estimate the value of COF needed in equation 3.1 was by using Merchant's circle (equation (3.2)) [Ozel, 2006]. With this equation, COF will be a function of the magnitude of cutting force F_c and feed force F_t, which is a function of process parameter. Section 3.4 will further discuss the effect of magnitudes of COF used in FE cutting models on cutting forces and chip thickness.

$$\mu = \frac{F_c \sin\alpha + F_t \cos\alpha}{F_c \cos\alpha - F_t \sin a} \quad \text{----------} \quad 3.2$$

Model II: Constant Shear friction model

Constant shear friction model assumed a constant frictional stress τ on the rake face, which is equal to a constant shear friction factor m multiply by the shear flow stress of the workpiece material k (equation (3.3)).

$$\tau = mk \quad \text{----------} \quad 3.3$$

In FE cutting models, the shear friction factor m and material shear flow stress k must be estimated as an input. The average shear flow stress for the work material k and the shear angle ϕ can be estimated using equation 3.4 (a) and 3.4 (b) respectively, where t_u is the undeformed chip thickness, t_c is the chip thickness and w is the depth of cut [Childs, 2006]. Cutting force F_c, feed force F_t and chip thickness t_c have to be experimentally measured.

$$k = \frac{F_c \cos\phi - F_t \sin^2\phi}{t_u w} \quad \text{----------} \quad 3.4\ (a)$$

$$\phi = \tan^{-1}\frac{(t_u / t_c)\cos\alpha}{1-(t_u / t_c)\sin\alpha} \quad \text{----------} \quad 3.4\ (b)$$

Model III: Constant Shear Model in sticking and Coulomb friction in sliding.

A common approach used to model two distinct regions (sticking and sliding) is to use constant shear friction in sticking region (equation 3.5 (a)), and use Coulomb friction in sliding region (Equation 3.5 (b)).

$$\tau = mk \text{ when } 0 < x < l_p \quad \text{----------} \quad 3.5\ (a)$$

$$\tau = \mu\sigma \text{ when } l_p < x < l_c \quad \text{----------} \quad 3.5\ (b)$$

In order to employ this friction model into FE cutting models, shear friction factor m, material shear flow stress k and COF have to be estimated as inputs. The parameter l_p and l_c have to be determined and estimated experimentally. There are many different ways to

observe the markings on the tool rake face caused by machining; however there is no definite way to measure l_p and l_c. Moreover, l_p and l_c will vary all the time while cutting, cause further difficulty in defining the value of l_p and l_c as inputs in FE cutting models.

Model IV: Zorev's Sticking-Sliding Friction Model

According to Zorev's model (Figure 3.11), there are two distinct friction regions on the tool-chip interface- sticking and sliding region. At sticking region ($0 < x < l_p$), the contact friction stress τ cannot be larger than the workpiece shear stress limit τ_{max}; at sliding region ($l_p < x < l_c$), frictional stress was assumed to be dependent on the normal stress σ. Zorev's model is also known as the maximum shear stress limit friction model.

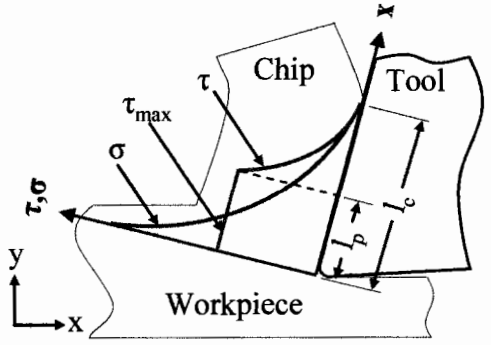

Figure 3.11: Curves representing normal and frictional stress distributions on the tool rake face according to Zorev.

To apply Zorev's friction model in FE cutting models, equations 3.6 (a) and 3.6 (b) were used, where μ is the COF and τ_{max} were assumed to be the workpiece maximum shear stress. The difference between model IV and model III is that in model IV, the distances of sticking region l_p and contact length l_c do not need to be experimentally measured and estimated as an input in the FE cutting model.

$\tau(x) = \tau_{\max}$ when $\mu\sigma(x) \geq \tau_{\max}$ ---------- 3.6 (a)

$\tau(x) = \mu\sigma(x)$ when $\mu\sigma(x) < \tau_{\max}$ ---------- 3.6 (b)

In FE cutting models, τ_{max} and μ have to be estimated as input. Researchers have estimated that the limiting shear stress τ_{max} as $\sigma_y/\sqrt{3}$ where σ_y is the yield stress of the workpiece material adjacent to the surface [Li, 2002, Kishawy, 2006]. Filice et. al. [2007] used the shear flow stress of the workpiece material k as the value of limiting stress τ_{max}.

Model V: Variable shear friction at the entire tool-chip interface

The stress distribution on the tool rake face had been obtained mainly by three methods: 1) Photoelastic method, 2) split tool method and 3) composite tools [Lee, 1994]. The advantages and limitations of each individual method have been described in detail by [Buryta, 1994]. The stress distribution information obtained from split tool test were used to create friction models. Two variable shear friction models will be discussed here: variable shear friction model [Dirikolu, 2001] and stress-based polynomial variable shear friction model [Yang, 2002].

Usui and Shirikashi [1982] proposed a variable shear friction model that relates frictional stress τ and normal stress σ on the tool chip interface as shown in equation 3.7 (a), where k is the material shear flow stress, and μ is the COF. At low normal stress σ, equation 3.7 (a) reduces to equation 3.1; at high normal stress σ, equation 3.7 (a) saturated to the value of material shear flow stress k. Equation 3.7 (a) was modified to equation 3.7 (b) by adding a shear friction factor m. The purpose of adding shear friction factor m was mainly to consider the effect of solid lubricant produced at the tool-chip interface while cutting. At high normal stress, the solid lubricant might reduce the saturation value mk, where $0 < m < 1$. Equation 3.7 (c) is the further refinement to equation 3.7 (b), with a constant n added into the equation to add the effect of transition of τ between $\tau = \mu\sigma$ to

$\tau = mk$ [Dirikolu, 2001]. To apply the friction model shown in equation 3.7 (c) into FE cutting models, COF μ, shear friction factor m, constant n, and material flow stress k have to be estimated as inputs. Material flow stress k can be estimated with equation 3.4 a, whereas COF μ, shear friction factor m, constant n have to be experimentally determined.

$$\tau = k\left[1 - e^{-(\mu\sigma/k)}\right] \quad \text{---------- 3.7 (a)}$$

$$\tau = mk\left[1 - e^{-(\mu\sigma/mk)}\right] \quad \text{---------- 3.7 (b)}$$

$$\tau = mk\left[1 - e^{-(\mu\sigma/mk)^n}\right]^{1/n} \quad \text{---------- 3.7 (c)}$$

Dirikolu et. al. [2001] investigated the friction behavior on the rake face by using the split-tool test. The workpiece materials tested were leaded low carbon free cutting steel (PbLCFCS), plain low carbon free cutting steel (LCFCS) and medium low carbon free cutting steel (MCFCS). The tool used was uncoated cemented carbide with 0° rake angle. The feed rate and dept of cut were 0.1 mm/rev and 2.5 mm respectively and the cutting tests were neither done with lubrication nor cooling. The measured shear stress and normal stress was fitted to the form of equation 3.8, which is shown in Table 3.3. The detailed explanations on the significant effect of the constant (μ, m, n) on frictional stress could be looked up on [Dirikolu, 2001].

Cutting speed (m/min)	PbLCFCS			LCFCS			MCFCS		
	μ	m	n	μ	m	n	μ	m	n
50	0.75	0.05	1.3	0.8	0.75	2.2	1.5	0.70	1.0
100	0.77	0.52	1.3	0.9	0.78	2.2	1.6	0.68	1.0
150	0.80	0.54	2.2	1.0	0.80	1.7	1.7	0.66	1.0
200	1.05	0.64	1.8	1.3	0.80	1.7	1.6	0.67	1.0
250	1.30	0.74	1.8	1.6	0.80	1.7	1.5	0.66	1.0

Table 3.3: Friction constants for equation 3.8 from split tool tests. [Dirikolu, 2001]

From the results shown in Table 3.3, different workpiece material having different process parameter will have different value μ, m and n for equation 3.7 (c). Thus a disadvantage of using equation 3.7 (c) as the friction model in FE is that extensive experimental tests have to be done to obtain the required constants. Moreover, Buryta et. al. [1994] commented that the stress distributions obtained along the tool chip interface were highly dependent on how the measure force data were smoothed or fitted, and the stress distribution was highly sensitive to the curve fitting method. Furthermore, the normal stress is high on the tool rake face, especially near the tool cutting edge. However, normal stress cannot always increase to levels that exceed the strength of the tool material or else tool breakage would always occur.

The second variable shear friction model is proposed by Yang and Liu [2002]. The tool and workpiece investigated were uncoated carbide and 304 stainless steel respectively. The tool and workpiece material were chosen from the availability of stress distribution from literature done by Barrow et al [1982]. The technique used by Barrow [1982] was the split tool test. The shear stress τ and normal stress σ distribution obtained is shown in Figure 3.12. Yang and Liu [2002] then created a friction model to fit the σ-τ curve, as shown in Figure 3.12.

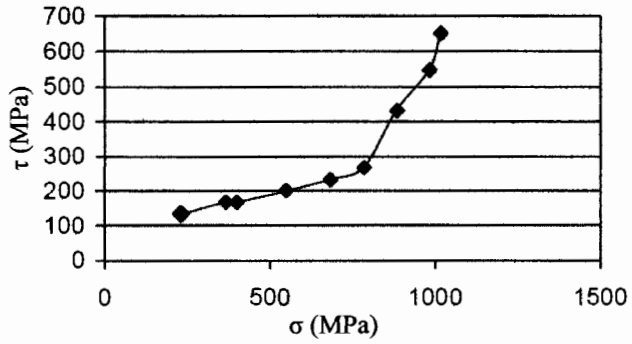

Workpiece: 304 stainless steel
Tool: Uncoated carbide
Method: Split tool
Feed rate, f : 0.356 mm/rev
Cutting speed, v : 120 m/min
Rake angle, α: 30°

Figure 3.12: σ-τ relationship on the tool rake face in metal cutting obtained using split-tool test [Barrow, 1982].

Yang and Liu [2002] proposed a general relationship between normal stress and shear stress as shown in equation 3.8 (a) - shear stress as a function of normal stress. Furthermore Yang and Liu made use of the versatility of polynomials and proposed equation 3.8 (b) that represented the relationship between shear stress and normal stress. Equation 3.8 (c) shows the final equation that was proposed by Yang to represent the curve shown in Figure 3.12. From equation 3.8 (c), the constants at higher order of normal stress are low and therefore could be ignored. Therefore, using high order of polynomial function to represent the curve might not be necessary. To apply friction model shown in equation 3.8 (c), stress distributions from the split tool test has to be carried out. The constants will also change with cutting conditions.

$$\tau = f(\sigma) \quad \text{----------} \quad 3.8\text{ (a)}$$

$$\tau = \sum_{n=0}^{n-4} a_n \sigma^n \quad \text{----------} \quad 3.8\text{ (b)}$$

$$\tau = \begin{cases} 655 & \text{If } \sigma \geq 1016 \text{ MPa} \\ 9.5E-10\sigma^4 + 6.2E-7\sigma^3 - 2.5E-3\sigma^2 + 17.2\sigma - 175 & \text{If } 262 \text{ MPa} < \sigma \leq 1016 \text{ MPa} \\ 0.45\sigma & \text{If } \sigma < 262 \text{ MPa} \end{cases} \quad 3.8\text{ (c)}$$

Model VI: Variable COF at the entire tool chip interface

Few authors have come out with methods on how to use Coulomb friction law with variable COF at the entire tool chip interface. The work done by [Ozel, 2006], [Arrazolla, 2008], and [Haglund, 2008] will be discussed here.

Ozel [2006] used variable COF along the tool rake face by considering COF as a function of normal stress along the entire tool-chip interface. The stresses on the tool rake face have to be obtained experimentally and the variable COF is shown in equation 3.9.

$$\mu = \frac{\tau(x)}{\sigma(x)} \quad \text{----------} \quad 3.9$$

The workpiece and tool material Ozel [2006] used was LCFCS and uncoated carbide respectively. The experimentally measured stresses on the tool rake face were used to calculate the variable COF. The experimentally measured stresses and calculated variable COF are shown in Figure 3.13 (a) and Figure 3.13 (b) respectively; the calculated COF will serve as input in the FE cutting models when machining LCFCS with uncoated carbide tool. However, it is worth observing the calculated COF shown in Figure 3.13 (b). COF is high when normal stress σ is low and COF decreases as normal stress σ increases. The result shown contradicts with the concept of sticking and sliding region on the tool rake face. Extra caution has to be taken when utilizing the variable COF shown in Figure 3.13 (b) on FE cutting models because when a high μ value is applied at the sliding region (low normal stress region), the workpiece will stick on the tool.

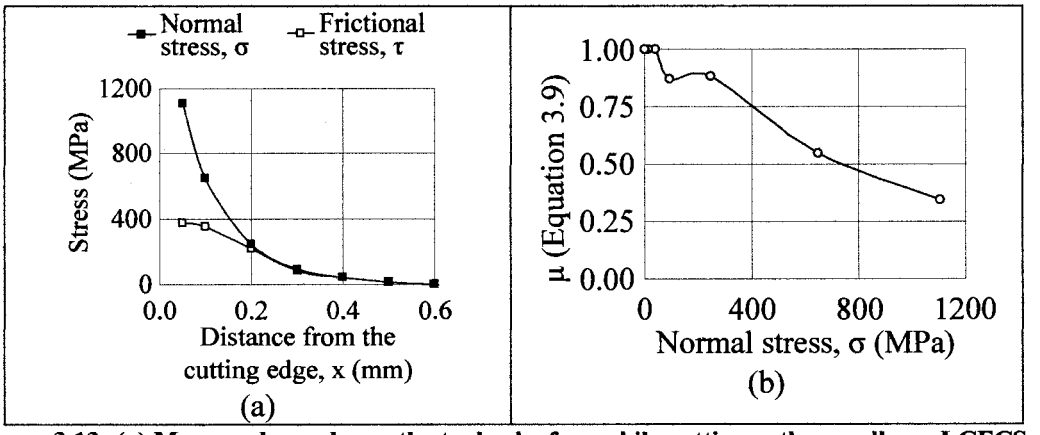

Figure 3.13: (a) Measured σ and τ on the tool rake face while cutting orthogonally on LCFCS at v=150 m/min and f=0.1 mm/rev. [Kato, 1972] (b) Measured variable COF as function of normal stress along the tool rake face, based on (a). [Ozel, 2006]

Arrazola et. al. [2008] also came out with a method to calculate the variable COF along the tool chip interface to be used in FE cutting models. Arrazola's main objective in developing the new variable friction model along the tool chip interface was to capture the ploughing effect on the tool cutting edge. Arrazola et. al. [2008] suggested that the missing ploughing effect was the main problem that caused the problem of under predicting feed force F_t in FE cutting models. The tool and workpiece material investigated were uncoated carbide and AISI 4140 respectively. The cutting speed was fixed at 300 m/min with a rake angle of 6°. Their method of calculating the variable COF along the tool-chip interface can be summarized into four steps:

1. Experimental tests on orthogonal cutting for feed rates ranging from 0.05 mm/rev to 0.35 mm/rev, and obtain cutting force F_c, feed force F_t, and contact length l_c.
2. Plot the cutting forces with different feed rates as shown in Figure 3.14 (a)
3. Find the function of feed force F_t in terms of cutting force F_c, and find the function of cutting force F_c in terms of contact length, l_c.

4. When the two equations in step 3 are ready, the variable friction coefficient will be presented as shown in equation 3.10, where α is the tool rake angle. Since in step 3, cutting force F_c is being written as a function of contact length l_c, the variable μ will be in terms of contact length l_c on the tool rake face. Figure 3.14 (b) shows the calculated variable μ along the contact length on the tool rake face done by [Arrazola, 2008].

$$\mu = \tan\left(\tan^{-1}\left(\frac{dF_t}{dF_c}\right) + \alpha\right) \quad \text{----------} \quad 3.10$$

From Figure 3.14 (b), COF is high when the contact length is near the cutting edge radius, and COF decreases as contact length further away from the cutting edge radius. It shows that Arrazola et. al. [2008] tried to capture the ploughing effect on the tool cutting edge radius by implementing high friction. Take note that this model can only be applied to one combination of workpiece material and tool. The major disadvantage to this friction model is that intense experimental work has to be done prior to obtaining the friction model.

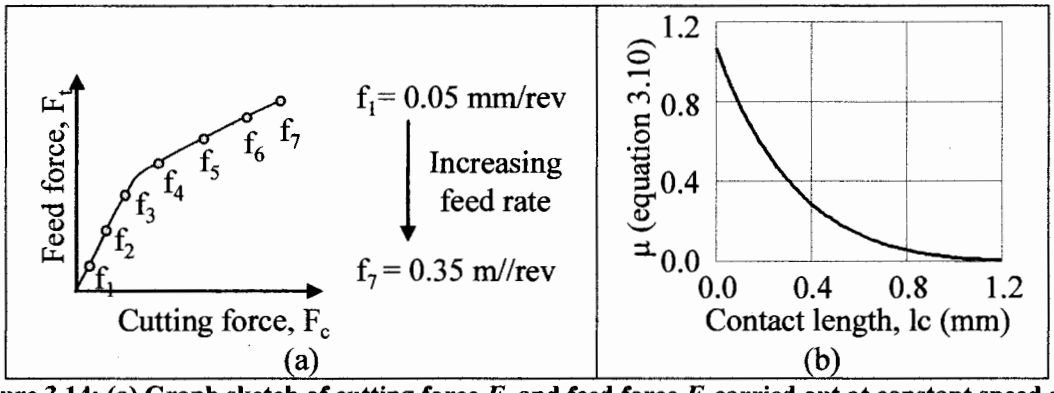

Figure 3.14: (a) Graph sketch of cutting force F_c and feed force F_t carried out at constant speed and with different feed rates, f. (b) Calculated variable COF as a function of contact length, l_c. [Arrazola, 2008]

Haglund et. al. [2008] continued to further expand the work done by Arrazola et. al.[2008]. Haglund's FE cutting models used experimental work carried out by Arrazola et. al. [2008] to validate. Tool and workpiece material investigated by Haglund was the same as Arrazola's. Take note that Arrazola et. al. [2008] carried out experimental work at v=300 m/min, while FE models simulated by Haglund et. al [2008] were carried out at v=200 m/min. Two methods to apply variable COF were used by Haglund et. al. [2008].

In the first method, Haglund et. al. [2008] simply divided the tool rake face into two regions, and defined two different COF in each individual region. The setback of this method was that there was no fixed method to define the regions, and there was no fixed explanation or method to assign the value of COF in each region. In the second method, Haglund et. al. [2008] created a temperature-dependent COF. A constant of μ=1.0 was assumed to temperatures up to 625 °C, but COF decreased linearly to zero as temperature increased to the workpiece melting temperature (1520°C). Once again, having no explanation or fixed method to assign the value of COF on the temperature specified is a major drawback.

For the simplicity of reading the results, friction models will be labeled as below:

Model I: Coulomb's friction

Model II: Constant shear friction

Model III: Shear Friction on sticking region and Coulomb's friction on sliding region

Model IV: Sticking-sliding friction [Maximum shear stress friction model]

Model V: Variable shear friction at tool-chip interface

Model VI: Variable COF at tool-chip interface

3.3 CONTACT ALGORITHM IN ABAQUS

Understanding the contact algorithm used in ABAQUS is very important. Figure 3.15 shows the concept of different friction models that relate the maximum allowable friction stress τ across the interface to the normal contact pressure σ between the two contacting bodies before sliding could occur [ABAQUS, 2003]. In Figure 3.15, the shaded region is the sticking region and the un-shaded region is the sliding region. In Figure 3.15 (a), it shows that when the contact friction stress between two bodies is lower than the normal stress multiplied by a constant COF ($\tau < \mu\sigma$), the two bodies will stick; sliding of the surface will only occur when $\tau \geq \mu\sigma$. Figure 3.15 (b) shows the condition when a maximum shear stress limit option is included. At low normal contact stress σ, the contact condition between two bodies follows the coulomb friction model; at high normal contact stress σ, the maximum allowable contact shear stress τ_{max} becomes independent of the normal contact stress. Meanwhile, regardless of the magnitude of the normal contact stress, sliding will occur if the shear stress reaches the value of τ_{max} [ABAQUS, 2003].

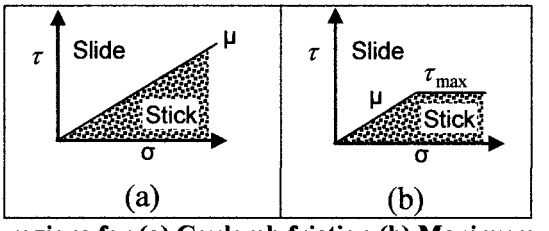

Figure 3.15: Slip and stick regions for (a) Coulomb friction (b) Maximum shear stress limit friction model [ABAQUS, 2003].

When maximum shear friction model (Model IV) is being used in FE cutting models, the purpose of including the option of τ_{max} value is to capture the sticking region on the tool cutting edge. However, this contradicts with the contact algorithm in commercially available finite element software; including τ_{max} value option in FE model

is to capture the sliding instead of sticking. The majority of the authors who utilized Model IV in FE cutting models had the same misconception, except [Woon, 2008]. Therefore, extra precaution has to be taken when utilizing Model IV; sliding might occur at the tool cutting edge radius region where normal contact stress is high.

3.4 PREDICTED FORCES IN FE CUTTING MODELS

Different friction models that are currently being used commonly by many authors have already been discussed in section 3.2. Section 3.4 of this research is dedicated to review the accuracy of predicted cutting force F_c, feed force F_t with different friction conditions when modeling the orthogonal cutting process. Currently, FE cutting models appear to be able to estimate cutting force F_c that fits well with experimental results; however, modeled feed force F_t always seems to be underestimated by 10%-50%. The predicted feed force F_t produced by FE cutting models depends heavily on the FE formulation being used. It is only when adopting FE formulation where chip separation criterion is not required that a smaller range of difference of predicted feed force F_t from experimental results can be produced. This effect could be observed by comparing results shown in [Kompovopoulos, 1991] who used Lagrangian formulation and results shown in [Joyot, 1998] who used ALE formulation. Another important factor to improve the predicted feed force F_t is to include tool cutting edge radius into FE cutting models. When tool cutting edge radius is included, the model could capture the ploughing effect. Ploughing effect plays an important role in feed force component, especially when cutting with small feed rates due to its size effect. FE cutting models that include tool cutting edge radius have already been successfully built by Movahhedy et. al. [2000 a]. However,

the problem of under predicted F_t still exists. Attempts were made by several authors to solve the problem in the underestimated modeled feed force F_t. Currently, the most common solving approach is to develop new friction models along the tool-chip interface or to alter the value of COF with process parameters. Typically, authors would increase magnitude of COF to fit the predicted feed force F_t, but at the expense of overpredicting cutting force F_c and chip thickness t [Haglund, 2008, Arrazola, 2008].

3.4.1 Effect of Using Different Friction Models

Yang and Liu [2002] built FE cutting models that use Lagrangian formulation to compare two different friction models; Model IV and Model V. The tool and workpiece material used were uncoated carbide and stainless steel 304 respectively. The detailed information regarding obtaining the polynomial equation for model V proposed by Yang [2002] is shown in Section 3.2. The predicted cutting force F_c obtained by Yang is shown in Figure 3.16. Recall from Section 3.2 that FE cutting models that utilize Lagrangian formulation is incapable of feed force F_t prediction due to perfectly sharp tool assumption. Therefore, FE cutting models built by Yang [2002] could only predict cutting force F_c. The results obtained by Yang [2002] were not experimentally validated but it could still give valuable information regarding the effect of different friction models on the predicted forces. Figure 3.16 shows that the results obtained by friction model IV and friction model V are similar. This is clear evidence that the extra step taken to obtain the complicated polynomial equation was unnecessary.

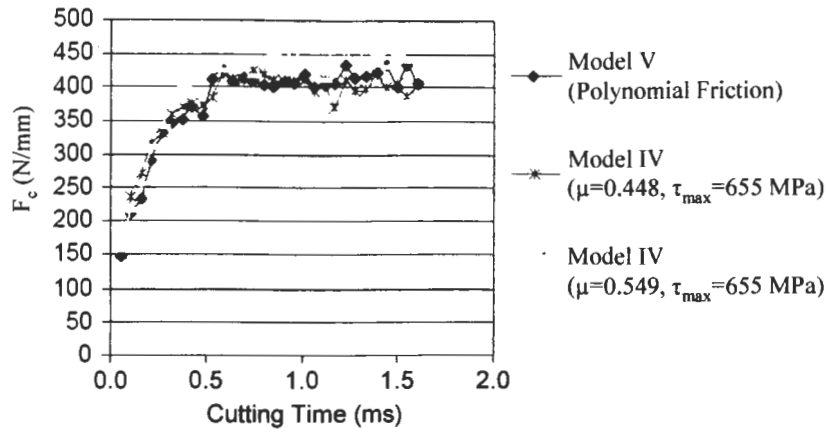

Figure 3.16: Comparison of predicted cutting force (F_c) with different friction models. FE models were done at v=120m/min, f=0.356 mm/rev, α=30°. [Yang, 2002]

Sartkulvanich et al. [2005] developed FE cutting models to compare two different friction models: model I and model II. The workpiece and tool material used were AISI 1045 and uncoated tungsten carbide respectively. The FE formulation and software employed was LF with adaptive mesh option and Deform-2D respectively. For comparison purposes, μ=0.27 for model I was used, and m=0.3 for model II was used. Figure 3.17 compares the predicted forces with experimental results. Cutting force F_c from both models were over predicted and feed force F_t from both model were under predicted.

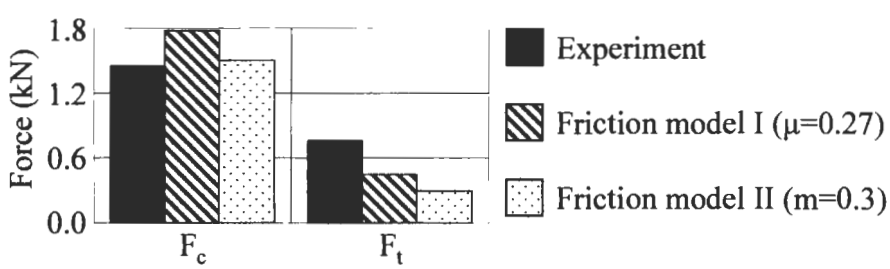

Figure 3.17: Comparison of forces using two different friction models with experimental results. FE models and experiment were done at v=198 m/min , f=0.25 mm/rev , α=6 °. [Sartkulvanic, 2005]

Ozel [2006] did a more thorough investigation on the influence of friction models on FE cutting simulations. Tool and workpiece material investigated were uncoated

cemented carbide and LCFCS respectively. Ozel [2006] employed Merchant's circle (equation 2.3) to estimate the COF; friction model with variable COF along the tool-chip interface (model VI) was also developed. Figure 3.18 summarized the predicted results from the FE models using various friction models compared with experimental results. Overall, cutting force F_c from all the models were significantly being over predicted, feed force F_t values were also over predicted even though they were closer to experimental result. This showed that the value of COF used (which uses merchant circle) were too high, thus the magnitude of COF calculated using Merchant's circle could not be used in FE cutting models. The results also showed that the various friction models investigated here produced similar predicted results, and none of them produced both cutting force F_c and feed force F_t that agree well with experimental results.

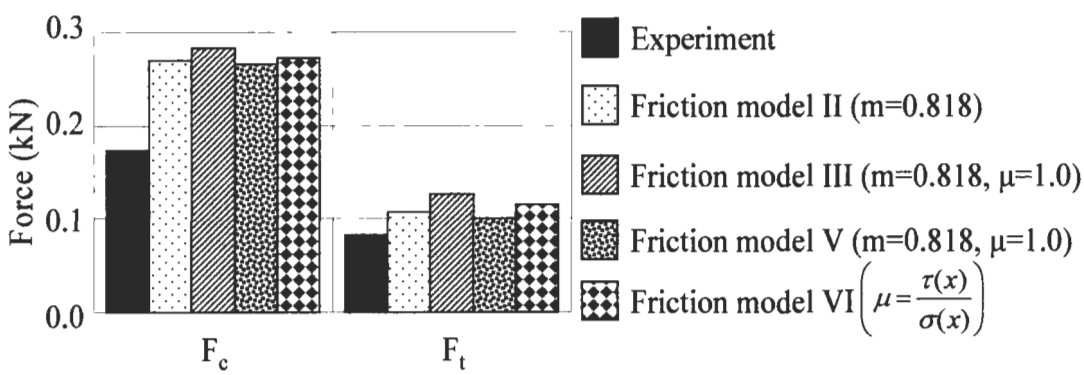

Figure 3.18 Comparison of Forces using four different friction models with experimental results. FE models and experimental were done at v=150 m/min , f=0.1 mm/rev , α=0 °. [Ozel, 2006]

Filice L. et al. [2007] then investigated thoroughly on the effect of using five different friction models on forces. The tool and workpiece material investigated were uncoated carbide and AISI 1045 respectively. The FE formulation and software used were Lagrangian formulation with adaptive mesh option and Deform-2D respectively. Figure 3.19 shows the best results from each friction model. All the predicted cutting

force F_c were close to experimental results but feed force F_t were under predicted. These results concluded that the different friction models did not provide significant differences on the predicted forces. From the results found by Filice et. al. [2007], it was concluded that different friction models could be applied and produce similar results as long as the value of friction coefficients were being altered.

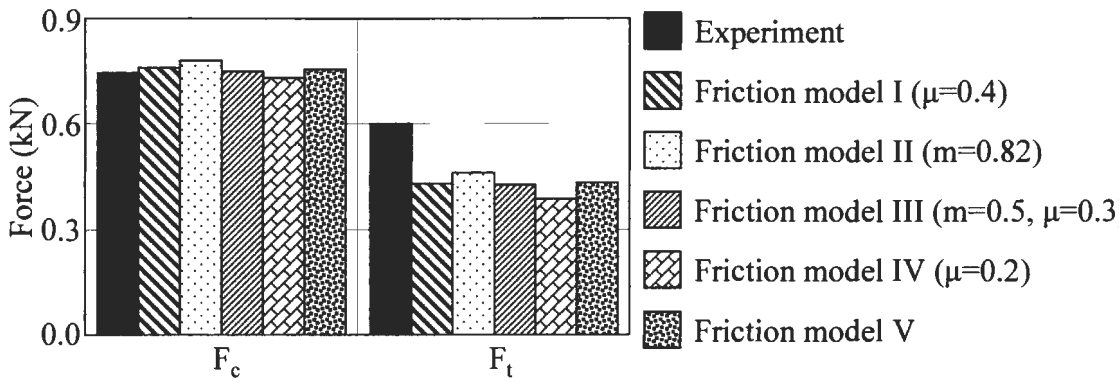

Figure 3.19: Comparison of best predicted forces for each friction model with experimental results. FE models and experiment were done at v=100 m/min, f=0.1 mm/rev, α=0 °. [Filice, 2007]

Iqbal et. al. [2007] also did an evaluation of the effect of friction and flow stress models on FE cutting forces with the same workpiece material (AISI 1045 with uncoated tool) as what Filice et. al.[2007] used. Iqbal et. al. [2007] did experimental work and FE cutting models on a wide range of cutting speeds (198 m/min – 879 m/min), investigating the friction models I, model II, model III, model V and model VI. With the five different friction models, two different flow stress models (Johnson-Cook and Oxley flow stress models) and four different cutting speeds being tested, all of his results agreed with the results found by Filice et. al. [2007]- that feed force F_t was being under predicted between 7% - 71%.

As mentioned in Section 3.2, Arrazola et. al. [2008] suggested that the under predicted feed force F_t was caused by the limitation of friction models, which were

unable to capture the ploughing effect of tool cutting edge radius. The workpiece and tool material used were AISI 4140 and uncoated carbide respectively. The FE formulation and software used were Lagrangian formulation and ABAQUS respectively. Arrazola et. al. [2008] proposed a new friction model that used variable COF along the tool rake face. Comparison of cutting force F_c and feed force F_t with different friction models and experimental results is shown in Figure 3.20. Feed rates investigated varied from 0.05 mm/rev to 0.35 mm/rev. From Figure 3.20, the following observations were made:

1. When using Coulomb friction (Model I), at all feed rate, predicted cutting force F_c were within 10% difference with experimental data. However, feed force F_t were always under predicted up to 67% difference from experimental data.
2. With variable COF along the tool rake face (Model VI), from f=0.1 mm/rev to f=0.35 mm/rev, predicted cutting force F_c were within 10% difference from experimental data. However, at low feed rate of 0.05 mm/rev, cutting force F_c was over predicted by 40%.
3. When employing Variable COF along the tool rake face (Model VI), predicted feed force F_t was within 10% difference from experimental data.

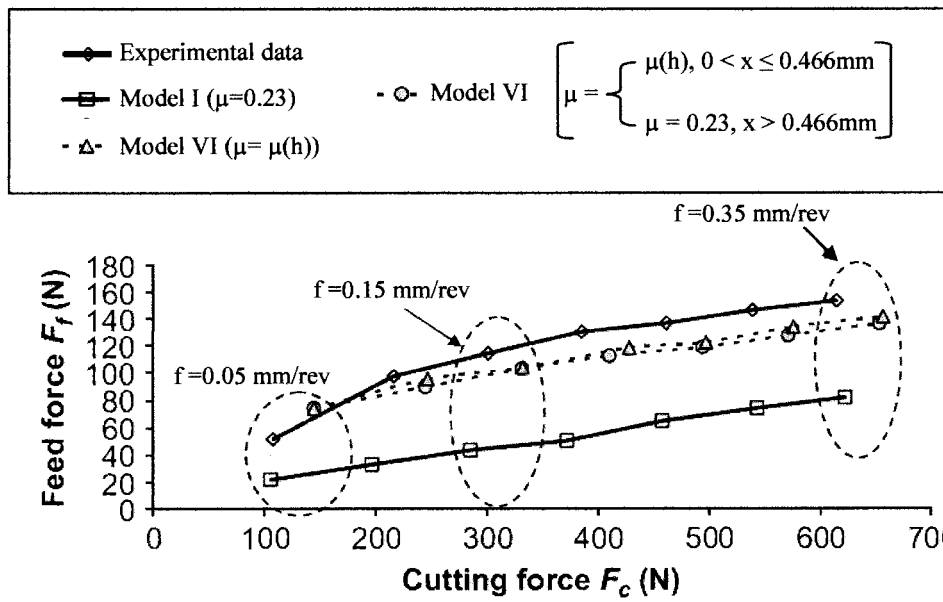

Figure 3.20: Comparison of different friction models with experimental results at varying feed rate. FE models and experiment were done at v=300m/min, α=6°. [Arrazola, 2008]

Haglund et al. [2008] continued the work done by Arrazola et. al. [2008] by developing new variable COF models. The tool and material investigated were uncoated carbide and AISI 4140. The FE formulation and software used were Lagrangian formulation and ABAQUS respectively. Haglund et. al. [2008] used experimental work carried out by Arrazola et. al. [2008] to validate their models. FE cutting models built by Haglund et. al. [2008] were all simulated at a cutting speed of v=300 m/min while Arrazola et. al. [2008] had carried out all their experimental work at a cutting speed of v=200 m/min. Figure 3.21 shows the result obtained by different friction models compared with experimental results. Haglund et. al. [2008]'s best FE cutting model was able to produce predicted feed force F_t that was being underestimated by only 1.3%. However, cutting force F_c would be 11.5% over predicted. Since the predicted results

were being compared with experimental result that was done at different cutting speeds, one should be wary when making conclusions based on the results obtained.

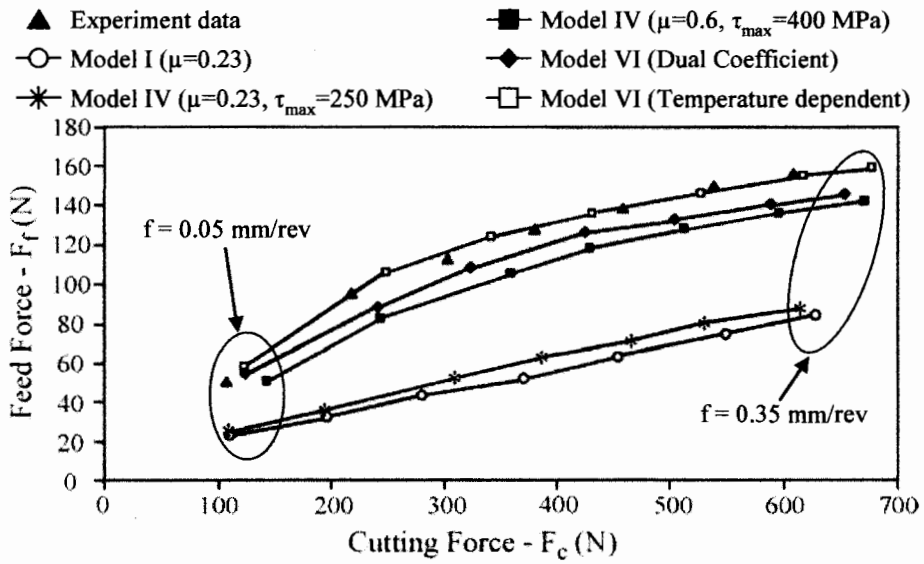

Figure 3.21: Comparison of predicted forces for different friction models with experimental results. FE models were done at v=200m/min, f=0.1 mm/rev, α=6 ° [Haglund, 2008]. Experimental work were done at v=300 m/min, f=0.1 mm/rev, α=6 °. [Arrazola, 2008]

From the results obtained by past authors [Filice, 2007, Arrazola, 2008, Haglund, 2008], it showed that to date, none of these friction models could predict cutting force F_c, feed force F_t and chip thickness t_c altogether.

3.4.2 Effect of Using Different Commercial FE Codes

Bil et. al. [2004] investigated the results of predicted cutting force F_c, feed force F_t and chip thickness t_c by using three different commercial software that were used for plane strain orthogonal metal cutting operations. The commercial software tested was MSC.Marc, Deform2D and Thirdwave AdvantEdge. FE cutting models were built to investigate the effect of different feed rates and rake angles. The tool and workpiece material used were high speed steel and C15 steel respectively. Figure 3.22 shows the

comparison between predicted cutting and feed force using three different commercial FE cutting software with experimental result. All three commercial software MSC.Marc, Deform2D and Thirdwave AdvantEdge under predicted feed force F_t, and over predicted cutting force F_c. Thirdwave AdvantEdge produced a predicted F_t value that was closest to experimental work, however, the cutting force F_c value was the most over predicted among the other commercial software. Deform2D could predict cutting force F_c that was close to experimental result but it was incapable of predicting feed force F_t. The results obtained thus further highlighted the problem of under predicted feed force F_t even when using commercial FE codes that were widely used by the manufacturing industry. Bil et. al. [2004] concluded that all the commercial FE codes being tested failed to achieve a satisfactory correlation with both measured predicted cutting force F_c, feed force F_t.

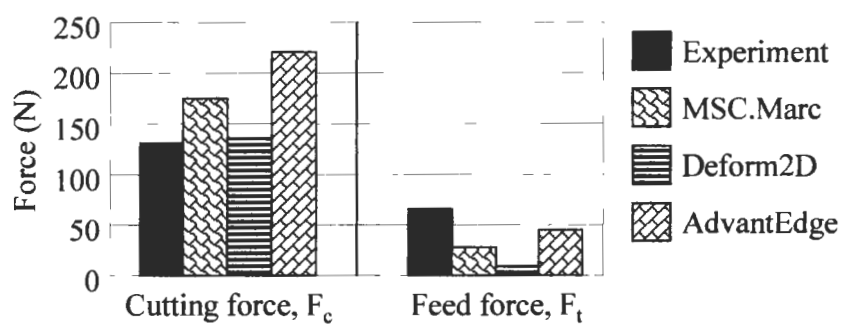

Figure 3.22: Comparison on predicted cutting force F_c and Feed force F_t using different commercial software with experimental result. FE models and experiment was done at v=22 m/min, f=0.1 mm/rev and α=20° [Bil, 2004].

3.4.3 Effect of Using Different Values of COF

Bil et. al. [2004] investigated the effect of value of COF used in the commercial FE codes. Figure 3.23 shows the effect of different COF used on both cutting force F_c and feed force F_t obtained by Thirdwave AdvantEdge; Thirdwave AdvantEdge employs coulomb friction law (model I) along the tool chip interface. Both cutting force F_c and

feed force F_t increased with magnitude of COF. Predicted cutting force F_c were closer to experimental result when lower COF was being used; however feed force F_t will be under predicted. The effect of COF value was also tested on two other commercial FE codes, MSC.Marc and Deform2D; both FE codes produced similar trends as the ones obtained by Thirdwave AdvantEdge.

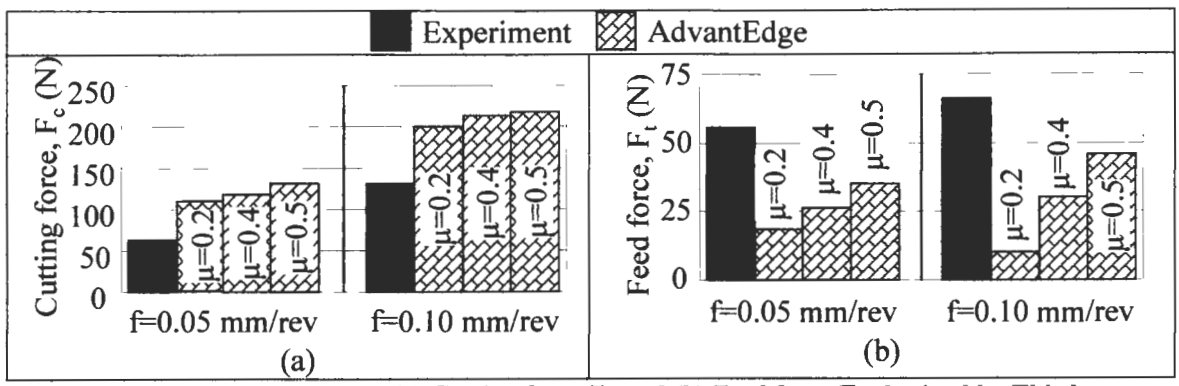

Figure 3.23: Effect of COF on (a) Cutting force Fc and (b) Feed force Ft obtained by Thirdwave AdvantEdge. FE models and experiment was done at v=22 m/min and α=20°. [Bil, 2004]

Yen et. al. [2004] investigated using constant shear friction model (Model II) with varying shear friction factor *m*. The tool and workpiece material used were uncoated carbide and AISI 1020 respectively. The FE formulation and software used were Lagrangian formulation and Deform-2D respectively. Figure 3.24 summarized the force comparison between the experiment and simulation with different shear friction factor *m*. Both predicted cutting force F_c and feed force F_t increased with shear friction factor *m*; however the predicted feed force F_t was significantly lower than the experimental results. Yen et. al. [2004] suggested that the reasons for under predicted feed force F_t are as follows:

1. The extrapolation errors of the material flow stress data at high strain rates and temperatures.

2. The simplified friction model used for the tool-chip interface.

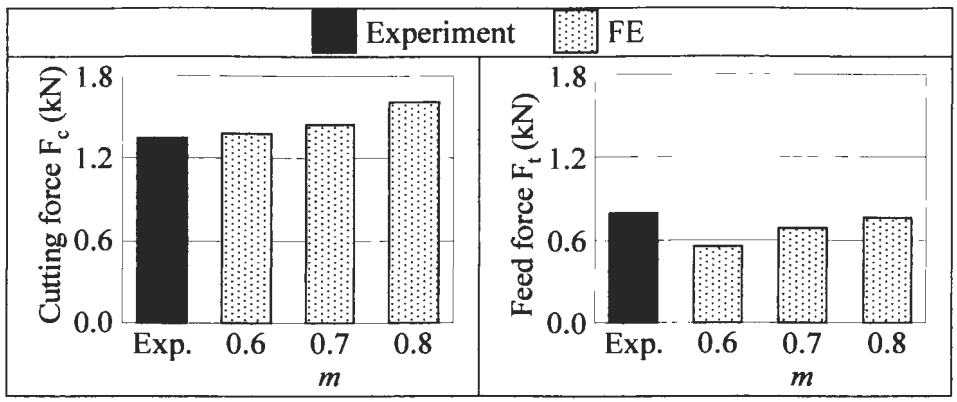

Figure 3.24: Effect of shear friction factor m on (a) Cutting force F_c and (b) Feed force F_t. FE models and experiment was done at v=130 m/min, f=0.2 mm/rev and α=12°. [Yen, 2002]

Sartkulvanich et. al. [2005] built FE cutting models to test the effect of using different values of COF and m used in friction model I and model II respectively. The tool and workpiece material investigated were uncoated tungsten carbide and AISI 1045 respectively. The FE formulation and software used were Lagrangian formulation and DEFORM-2D respectively. The values of m varied were between 0.3 to 0.9, and the values of COF varied were between 0.1 to 0.5. The analysis showed that cutting force F_c results were over predicted by 3% - 42% while feed force F_t were under predicted by 8% - 62% when compared to experimental data.

Filice et. al. [2007] did an excellent investigation of the effect of both friction models and friction constant value on forces. Figure 3.25 showed the effect of increasing COF when Coulomb friction law was applied. The trend on the effect of COF on predicted forces obtained by Filice et. al. [2007] concurred with the trend obtained by Bil et. al. [2004], Yen et. al. [2004] and Sartukulvanich et. al. [2005]; increasing COF caused both cutting force F_c and feed force F_t to increase. The predicted feed force F_t obtained by Filice et. al. [2007] also could not match with experimental results, even at high value

of COF. Similar tests like the one shown in Figure 3.25 were also done using other friction models (model II, model III and model IV). All the friction models tested showed similar trends; increasing constant COF or m caused both cutting force F_c and feed force F_t to increase, but feed force F_t was always under predicted.

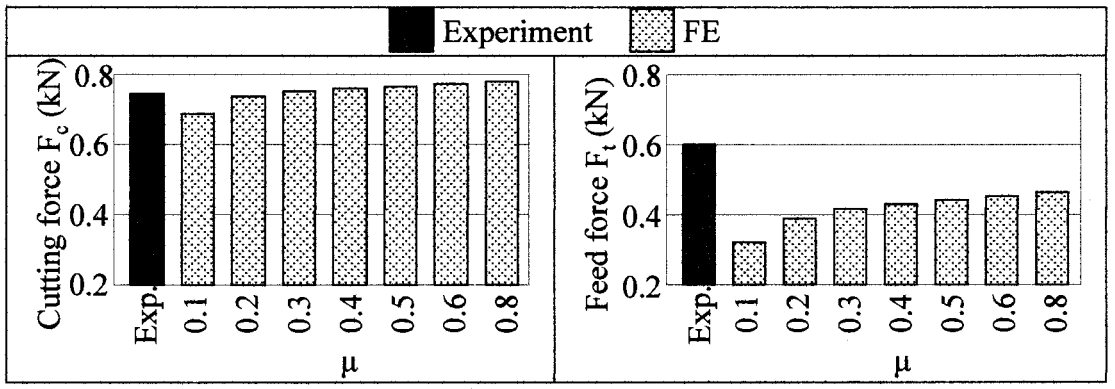

Figure 3.25: Effect of COF on (a) Cutting Force F_c and (b) Feed force F_t. FE models and experiment was done at v=100 m/min, f=0.1 mm/rev and α=0°. Coulomb friction model was used. [Filice, 2007]

Despite the tremendous effort put into investigating predicted cutting force F_c and feed force F_t by using different friction models, different commercial FE codes, and different magnitudes of COF, different workpiece materials, and different cutting process parameters, none of the FE models were able to predict both cutting force F_c and feed force F_t that fit well with experimental results. When predicted cutting force F_c agreed well with experimental results, feed force F_t was under predicted; on the other hand,when predicted feed force F_t agreed well with experimental result, cutting force F_c was over predicted.

The main objective of this research was focused on the problem of under predicted feed force F_t, however, by using a new approach. Instead of focusing friction behavior on the tool-chip interface, new FE cutting models were built having tool and workpiece geometry that followed closely with that of the experimental set up. Effects of

adding tool holder geometry and using the actual dept of workpiece geometry into the FE cutting model were investigated. A new combined experimental/computational approach to calibrate COF for a combination of tool and workpiece material was also presented. Correlation of predicted FE results with experimental work is a critical criterion.

Author	WP/ Tool Material	FE formulation/ Software	Friction Models						| μ |	| m |	τ_{max} (MPa)	| μ |/| m | changes/fix with process parameter	Tool Holder	% Difference $e(\%) = \frac{FE - Exp.}{Exp.} \times 100\%$				Remarks:
			I	II	III	IV	V	VI						e_{Fc}	e_{Ft}	e_{tc}	e_{tc}	
[Haglund, 2008]	AISI 4140/ Uncoated WC	LF with adaptive mesh/ ABAQUS	√						0.23	-	-	Fix	No	-9.3 to 7.3	-62.4 to -45.0	-3 to 7	-63 to -45	- Vary feed rates - Temperature dependent COF. - FE models simulated at 200 m/min, experimental results carried out at 300 m/min
						√			0.23	-	250			-2.5 to 11.8	-68.4 to -51.5	-13 to 3.4	-55 to -42	
						√			0.6	-	400			6.2 To 25.5	-17.9 To 4.0	-10 To 8.1	-55 to -42	
								√	0 to 1.0	-	-			11.0 to 15.1	3.3 to 15.8	2 to 12	-29 to -26	
[Arrazola, 2008]	AISI 4140/ Uncoated WC	LF with adaptive mesh/ ABAQUS	√						0.23	-	-	Not Commented	No	~0	-70.0 to -47.6	~0	-	- vary feed rates - Experimental cutting force ratio up to F_c/F_t=7.
								√	0 to 1.2	-	-			7.4 to 16.6	-6.7 to 10.5	2 to 12	-	
[Iqbal, 2007 b]	AISI 1045/ Uncoated WC	LF with adaptive mesh/ Deform-2D	√						-	-	-	Not commented	No	17 to 26	-62 to -31	-	-	- Tested on many different cutting speeds - Friction models tested unable predict both F_c and F_t together
				√					-	-	-			15 to 49	-71 to -48	-	-	
					√				-	-	-			23 to 28	-25 to 2	-	-	
							√		-	-	-			6 to 27	-53 to -25	-	-	
								√	-	-	-			14 to 29	-42 to -26	-	-	

Table 3.4: Compilation of orthogonal FE cutting models part A. LF: Lagrangian Formulation

Author	WP/ Tool Material	FE formulation/ Software	Friction Models						|μ|	|m|	τ_{max} (MPa)	|μ|/|m| changes/fix with process parameter	Tool Holder	% Difference $e(\%) = \frac{FE - Exp.}{Exp.} \times 100\%$				Remarks:
			I	II	III	IV	V	VI						e_{Fc}	e_{Ft}	e_{fc}	e_{lc}	
[Filice, 2007]	AISI 1045/ Uncoated WC	LF with adaptive mesh/ Deform-2D	√						0.1 to 0.8	-	-	Not commented	No	- 7.7 to 4.6	-46.3 to -22.3	-44 to -31	-58 to -46	- Different friction models could predict forces as long as value of constants are calibrated - Unable to predict both F_c and F_t together
				√					-	0.30 to 0.90	-			-3.2 to 8.7	-45.3 to -15.5	-45 to -28	-66 to -44	
					√				0.1 to 0.3	0.40 to 0.82	-			-1.1 to 1.3	-36.7 to -28.7	-34 to -31	-62 to -32	
						√			0.2 to 0.4	-				-1.9 to 2.8	-35.5 to -28.0	-34 to -31	-56 to -48	
							√		1.6	0.68	-			1.3	-28.0	-31	-56	
[Ozel, 2006]	LCFCS/ Uncoated WC	LF with adaptive mesh/ Deform-2D		√					-	0.818	-	Not commented	No	55	30	-	-37	
					√				1.0	0.818	-			63	52	-	-37	
							√		-	1.0	-			52	27	-	-43	
								√	-	-	-			56	39	-	-22	
[Sartkulvanich, 2005]	AISI 1045/ Uncoated WC	LF with adaptive mesh/ Deform 2D	√						0.1	-	-	Not Commented	No	7.8	-61.1	2.0	-32.8	
			√						0.5	-	-			26.4	-36.8	12	-20.7	
				√					-	0.3	-			3.9	-61.5	-4.0	-34.5	
				√					-	0.9	-			42.3	-7.8	28.0	3.4	
[Bil, 2004]	C15/ Rigid tool	LF/ MSC.Marc		√					-	0.2 to 0.7	-	Not commented	No	-4.0 to 31.3	-	-40.7 to -18.5	-	- unable to use single value of friction parameter to predict both F_c and F_t - Low friction parameter suits to predict F_c - High friction parameter suits to predict F_t
		LF with adaptive mesh/ Deform-2D		√					-	0.1 to 0.7	-			-16.7 to 4.2	-83.3 to -33.3	-55.6 to -48.1	-	
		LF with adaptive mesh/ AdvantEdge	√						0.2 to 0.5	-	-			50.0 to 66.7	-85.2 to -31.5	-33.3 to -14.8	-	
[Shi, 2004]	HY-100/ Uncoated WC	LF/ ABAQUS				√			1.6	-	-	Not commented	No	-3.3	-8.8	-5.6	-	- Assumed infinitely sharp tool - used chip separation criterion

Table 3.5: Compilation of orthogonal FE cutting models Part B. LF: Lagrangian Formulation

Author	WP/ Tool Material	FE formulation/ Software	Friction Models						|μ|	|m|	τ_{max} (MPa)	|μ|/|m| changes/fix with process parameter	Tool Holder	% Difference $e(\%) = \frac{FE - Exp.}{Exp.} \times 100\%$				Remarks:
			I	II	III	IV	V	VI						e_{Fc}	e_{Ft}	e_{tc}	e_{lc}	
[Yen, 2004]	AISI 1020/ Uncoated cemented carbide	LF with adaptive mesh/ Deforem-2D		√					-	0.6 to 0.7	-	Not Commented	No	2.2 to 19.3	-31.3 to -5.0	-	-	
[Yen, 2004 b]	AISI 1045/ CVD coated WC	LF with adaptive mesh/ Deforem-2D		√					-	0.5	-	Not commented	No	11.1	-29.7	8.7	-	- Overpredict F_c and under predict F_t.
[Yang, 2002]	304 Stainless steel/ Rigid tool	LF/ ABAQUS				√			0.549	-	655	Yes	No	-	-	-	-	- No experimental validation - Did not present predicted F_t
								√	0.45	-	655			-	-	-	-	
[Shi, 2002]	AISI 4340/ Rigid tool	LF/ ABAQUS				√			0.3	-	549	Not commented	No	-15 to -7.4	-	-	-	- Did not present predicted Ft - Possibility to calibrate COF
[Mamalis, 2001]	AISI 1018/ Tunsten Carbide	LF/ MARC	√						0.4	-	-	Not commented	No	-12.5	-	-	-	- Lagrangian formulation incapable of F_t prediction - incapable of high temperature prediction on tool cutting edge
[Klocke, 2001]	AISI 1045/ Uncoated carbide	LF with adaptive mesh/ Deform 2D	√						0.2	-	-	Not commented	No	~10.0	-	12.0	-	- Tested at a very high speed of 3000 m/min

Table 3.6: Compilation of orthogonal FE cutting models Part C. LF: Lagrangian Formulation

Author	WP/ Tool Material	FE formulation/ Software	Friction Models						|μ|	|m|	τ_{max} (MPa)	|μ|/|m| changes/fix with process parameter	Tool Holder	% Difference $e(\%) = \frac{FE - Exp.}{Exp.} \times 100\%$				Remarks:
			I	II	III	IV	V	VI						e_{Fc}	e_{Ft}	e_{tc}	e_{lc}	
[Marusich, 2001]	AISI 4130/ Chip breaker UM Grade 4025	LF with adaptive mesh/ AdvantEdge	√						0.5	-	-	Not commented	No	0 to 8.0	-45.5 to -37.5	16.0 To 25.0	-	- Published by AdvantEdge thirdwave system - Tested on different cutting conditions - Under predict F_t, over predict t_c
[Dirikolu, 2001]	PbLCFCS/ Uncoated WC	LF/ -					√		1.3	0.74	-	Yes	No	~0	20.0	-	-	- Uses Iterative Convergence Method (ICF) - Uses split-tool technique to measure constants
	LCFCS/ Uncoated WC						√		1.6	0.80	-			-4.7	7.1	-	-	
	MCFCS/ Uncoated WC						√		1.5	0.66	-			~0	~0	-	-	
[Movahhedy, 2000 b]	LCFCS/ Uncoated carbide	ALE/ ABAQUS					√		1.0	-	-	Not commented	No	19.0	15.7	-	-8	
[Ozel, 2000]	P20 mold steel/ uncoated WC	LF with adaptive mesh/ Deform 2-D				√			0.5 to 0.7	-	907 to 954	Yes	No	<10	<10	-	-	- Use Merchant's circle to obtain COF - Experimentally Calibrate COF - Contradicts with the findings made by [Bil, 2004] -Contradict with [Ozel, 2006]

Table 3.7: Compilation of orthogonal FE cutting models Part D. LF: Lagrangian Formulation

Author	WP/ Tool Material	FE formulation/ Software	Friction Models						| μ |	| m|	τ_{max} (MPa)	| μ |/| m| changes/fix with process parameter	Tool Holder	% Difference $e(\%) = \frac{FE - Exp.}{Exp.} \times 100\%$				Remarks:
			I	II	III	IV	V	VI						e_{Fc}	e_{Ft}	e_{tc}	e_{tc}	
[Kalhori, 2000]	AISI 1045/ Uncoated Carbide	LF/ ABAQUS	√						0.3	-	-	Not Commented	No	-27.6	-73.5	1.0	3.4	- Lagrangian Formulation incapable of F_t prediction
		LF/ SiMPle	√						0.3	-	-			-41.3	-73.5	1.0	1.7	
		LF/ AdvantEdge	√						1.0	-	-			-15.9	-37.1	-5.6	-10.3	
[Shet, 2000]	AISI 4340/	LF/ ABAQUS				√			0.0 to 0.6	-	549	Not Commented	No	-	-	-	-	- Investigated on the effect of varying COF - Presented results on F_c but not F_t
[Behrens,1999]	C15 steel/ Rigid tool	LF/ ABAQUS		√					-	0.4	-	Not Commented	No	-36.0	-	-	-	
[Joyot, 1998]	42CD4/ Carbide	ALE/ -	√						0.32	-	-	Not commented	No	3.6	-34	42.9	-	- Under predict F_t, over predict t_c
[Komvopoulos, 1991]	AISI 4340/ Rigid tool	LF/ ABAQUS	√						0.0	-	-	Not Commented	No	-38	~-100	11.4	-	- Tested the effect of varying COF - Assumed infinitely sharp tool
			√						0.15					-22.7	-87.9	13.6	-	
			√						0.5					4.0	-6.2	16.1	-	

Table 3.8: Compilation of orthogonal FE cutting models Part E. LF: Lagrangian Formulation

4. MODELING OF ORTHOGONAL METAL CUTTING

4.1. Finite Element Simulations

All the FE cutting models in this research will be simulated using general FE code ABAQUS/Explicit version 6.4-1, unless specified otherwise. In order to include the tool cutting edge geometry and to eliminate the use of chip separation criteria in the FE cutting model, ALE formulation will be used. The initial assumed chip shape does not affect the final chip shape or the mechanics of cutting [Movahhedy, 2000, Nasr, 2007]. Plane strain, quadrilateral, linearly interpolated, and thermally coupled element type was used. Coupled temperature-displacement analysis is used to allow for temperature-dependent properties and heat transfer. Plane strain condition with continuous chip formation was assumed in FE cutting models. The effect of workpiece microstructure will not be taken into consider. In all the FE cutting models built, heat loss through convection or radiation was neglected. FE cutting models built will assume no tool wear. A major portion of the FE simulations will be focused on the effect of adding tool holder geometry on the predicted results.

4.2. *Material Properties*

The workpiece material being investigated here is AISI 1045 with hardness of 200 – 220 BHN, and the cutting tool used is Sandvik Coromant TNMG 432 grade GC 4225 (CVD coated carbide with TiN+Al_2O_3+TiCN). Coated tool was used instead of uncoated (Sandvik uncoated carbide grade H13A) because crater wear was observed when cutting with uncoated tools. The customized tool holder is made from AISI 4140. The mechanical and physical properties of workpiece material, tool and tool holder is given in Table 4.1. The Johnson-Cook (J-C) plasticity model (equation 4.1) is used to model the plastic behavior of the workpiece material. J-C constitutive equation is a function of plastic strain ε_{pl}, strain-hardening index n, stain rate index C, plastic strain rate $\dot{\varepsilon}_{pl}$, workpiece material melting temperature T_m, temperature T, and thermal index m. The reference temperature used is T_{ref} = 25 °C. J-C plastic model is suitable for modeling cases with high strain, strain rate, strain hardening, and non-linear material properties. The J-C material constant for workpiece material AISI 1045 is shown in Table 4.1 and was obtained by using split Hopkinson pressure bar (SHPB) [Jasper, 2002 a].

$$\sigma = \left(A + B{\varepsilon_{pl}}^{n}\right)\left(1 + C\ln\left(\frac{\dot{\varepsilon}_{pl}}{\dot{\varepsilon}_0}\right)\right)\left(1 - \left(\frac{T - T_{ref}}{T_{melt} - T_{ref}}\right)^{m}\right) \qquad (4.1)$$

		Workpiece [Kalhori, 2000] and [Jasper, 2002 a]	Carbide tool [Kalohori, 2000]	Holder [Ng, 2002 a]
Young's Modulus, E (GPa)		205	560	210
Poisson's ratio, ν		0.3	0.22	0.3
Density, ρ (kg/m^3)		7850	14500	7800
Thermal expansion, α ($^\circ C^{-1}x10^6$)		10.1 (20 °C) 12.0 (200 °C) 13.0 (400 °C) 15.3 (600 °C)	5.4 (20 °C) 5.3 (200 °C) 5.4 (400 °C) 5.6 (600 °C)	13.7
Specific heat capacity, c_p (J/kg °C)		220	220	475
Plasticity Johnson-Cook Material Constant	**A (MPa)**	553.1	-	-
	B (MPa)	600.8	-	-
	n	0.234	-	-
	C	0.0134	-	-
	m	1.0	-	-
	$\dot{\varepsilon}_0$ (s^{-1})	1.0	-	-

Table 4.1: Mechanical and physical properties of workpiece, tool and holder.

The temperature dependent thermal conductivity of workpiece material AISI 1045 is shown in Figure 4.1. The cutting tool used in experimental work is CVD coated ($TiN+Al_2O_3+TiC$). Initial trial using uncoated carbide showed crater wear after <10 seconds of cutting. Since FE cutting models assumed no tool wear, therefore in this research, CVD coated carbide was used. The main function of TiN coating is to act as a diffusion barrier and act as hard lubricant thus reducing friction on the tool-chip interface [Grzesik, 1999]. Since friction behavior is the major component for TiN coating, it is assumed that its mechanical and thermal properties can be neglected in FE cutting model. The important property of Al_2O_3 is its low thermal conductivity at high temperature. Since the experimental work done was at relatively high speed with high temperature

generated along the tool chip interface, it is important to incorporate thermal conductivity of Al_2O_3 into FE cutting models. Moreover, the thermal conductivity of the cutting tool will affect contact length and also influenced the chip thickness formation [Balaji, 1999]. The thermal conductivity of Al_2O_3 as a function of temperature, as shown on Figure 4.1, will be used as an input on the tool's thermal conductivity property on FE cutting models.

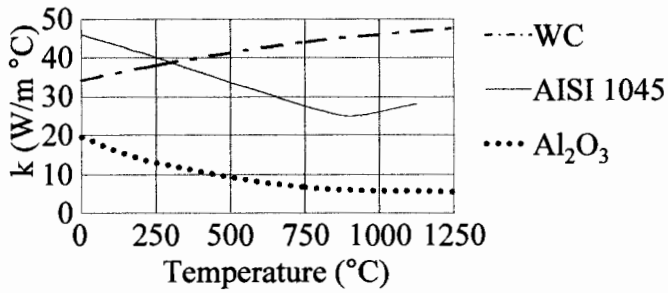

Figure 4.1: Thermal conductivity of tool and workpiece material as a function of temperature [Jawahir, 1993].

Two initial FE cutting models were built to simulate the effect of including both thermal and mechanical properties of Al_2O_3 (labeled as FE simulation B), and when only the thermal conductivity property of Al_2O_3 was used (labeled as FE simulation A).

FE Simulation A: The whole tool has the mechanical and physical properties of carbide, however, with thermal conductivity k of Al_2O_3.

FE Simulation B: The tool has mechanical and physical properties of carbide. CVD coating layer of (surrounding the tool) has the mechanical, physical and thermal conductivity properties of Al_2O_3.

Figure 4.2 compares the final geometry of the tool cutting edge for the two different simulations. The workpiece material used was AISI 1045, with cutting condition of f=0.1 mm/rev and v=250 m/min. When mechanical and physical properties of Al_2O_3 were used, the elements mesh on the tool cutting edge geometry expererienced 'hourglass' effect, as

shown on Figure 4.2 (b). Hourglassing occurred because the mechanical and physical properties on the layer of CVD coating could not withstand the high contact load [ABAQUS, 2003]; density of Al_2O_3 is much lower than density carbide. The effect of 'hourglassing' on predicted FE results was not investigated, thus preferred to be avoided if possible.

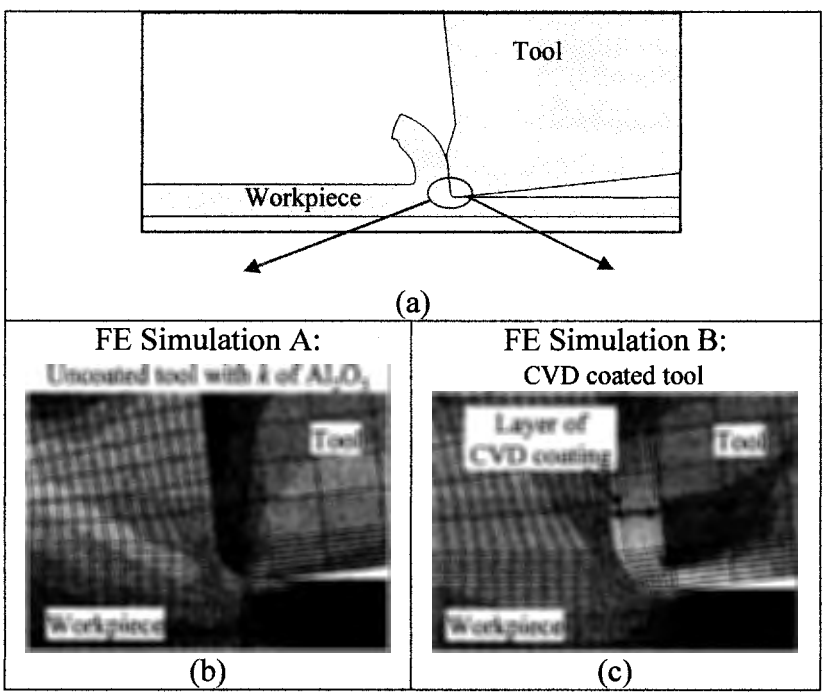

Figure 4.2: (a) Final condition of chip formation. (b) Final tool cutting edge geometry of FE simulation A. (c) Final tool cutting edge geometry of FE simulation B.

Figure 4.3 compares the predicted forces obtained from FE simulation A and FE simulation B. The obtained results showed that including the mechanical and physical properties of layer of CVD coating has no significant effect on the predicted forces. Since predicted forces in FE cutting models are the main concern in this current work, all the tools in the FE cutting models built would have mechanical and physical properties of carbides, however with thermal conductivity of Al_2O_3. This was done to prevent hourglassing effect.

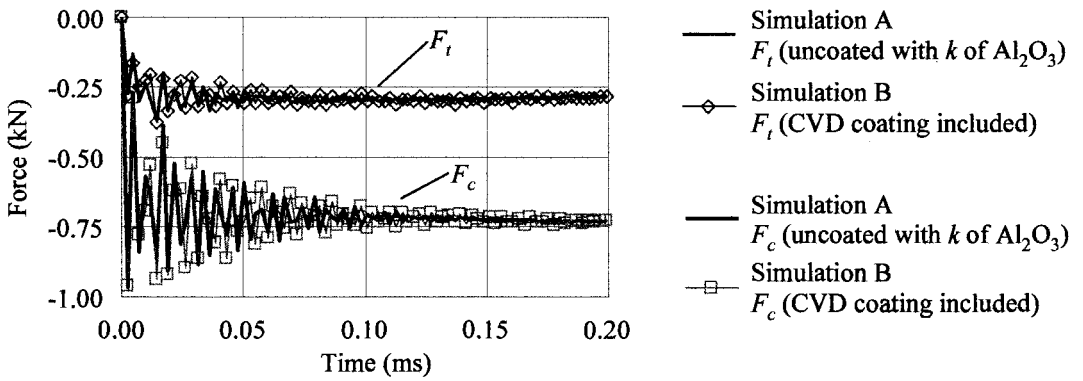

Figure 4.3: Comparison of predicted forces when physical and mechanical properties of CVD coating was not used (Simulation A) and used (Simulation B).

4.3. GEOMETRY AND BOUNDARY CONDITIONS

The cutting tool used in the experimental work has chip breaker profile as shown on Figure 4.4 (a). Since the FE cutting models built are two-dimensional (2-D), the chip breaker profile has to be assumed as shown on Figure 4.4 (b). Figure 4.4 (c) shows the geometry of cross section area of AA' of Figure 4.4 (b) which will be used as the geometry dimension of the tool in FE cutting model. Detail explanation on chip breaker dimension measurement will be discussed in section 5.4. Past research on FE cutting models that include the effect of tool cutting edge radius did not mention on how the tool cutting edge radius dimensions were obtained, arbitrary number might be used [Grzesik, 2005, Yen, 2004 b]. The measured tool cutting edge radius of the insert used in experimental and FE cutting model is ρ_e=35 μm.

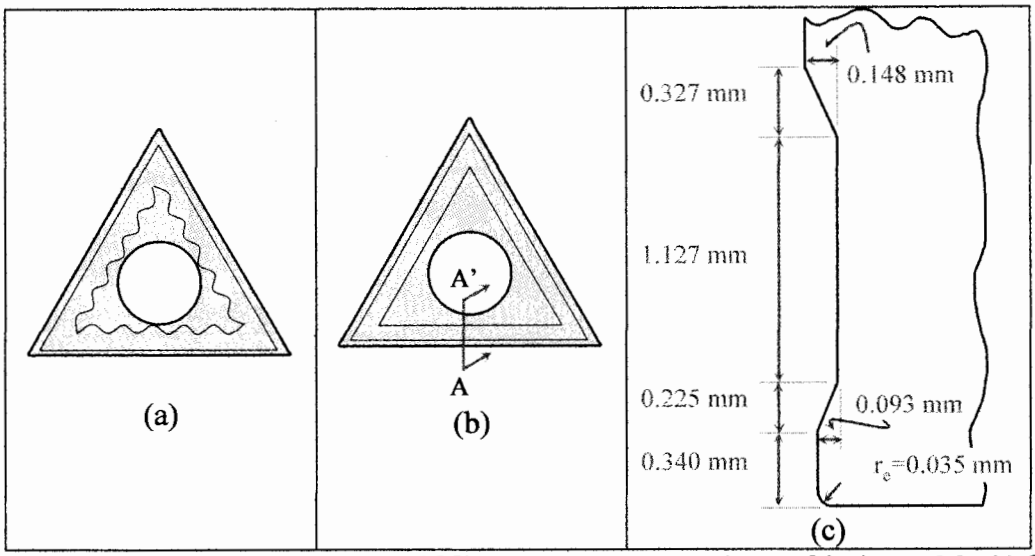

Figure 4.4: (a) Sketch of insert TNMG 432 MR. (b) Assumed dimension used in FE models. (c) Cross section dimension of AA' from sketch (b).

Different geometry configurations of FE cutting models were built. Conventional and newly designed geometry used in FE cutting models will be shown and discussed. Figure 4.5 (a) and (b) shows the experiment set up for plunging process on the front view and side view respectively. Orthogonal cutting was carried out in the experiment. In Figure 4.5, the tool holder has an overhang of 25 mm away from the dynamometer which measures the forces while cutting. For all cutting processes, the width of cut was fixed at 3 mm, and rake angle of α=-6° was used. The workpiece plunging depth will be kept constant at 10 mm.

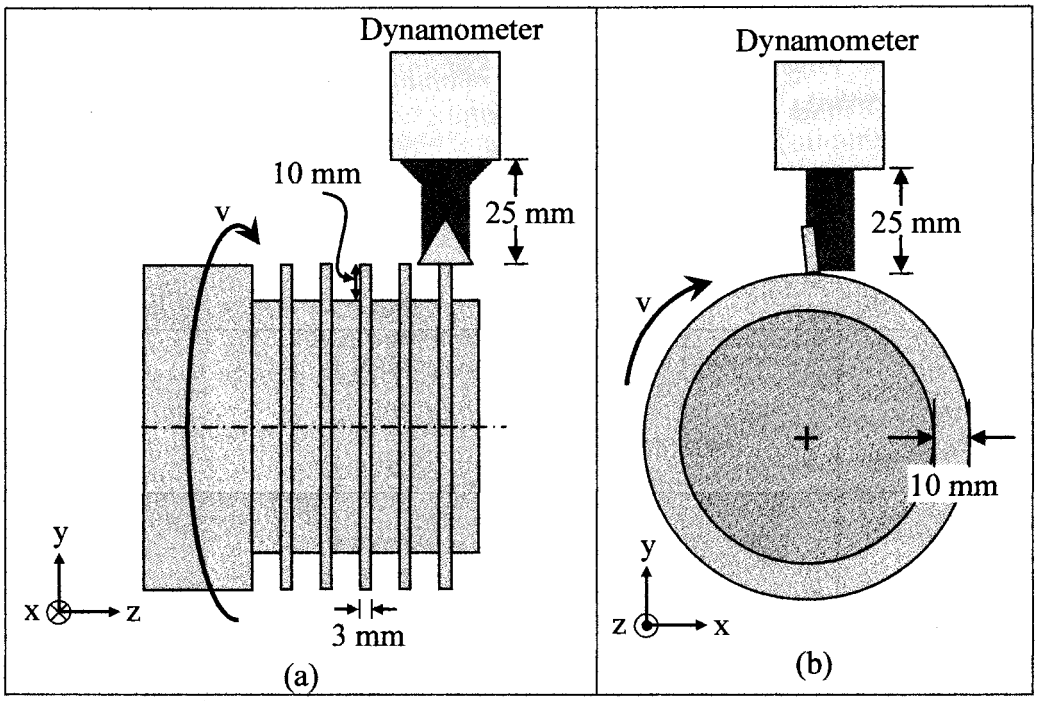

Figure 4.5: Experiment set up for plunging process. (a) Front view. (b) Side view.

Figure 4.6 (b) shows the geometry used by conventional FE cutting model. For the ease of reading, it will be labeled as FE (Tool). The circle drawn on Figure 4.6 (a) shows the portion of the experiment set up being taken into consider on the model FE (Tool); only a small portion of the insert and the workpiece is being taken into consider, and the tool holder is not included into the model. With ALE formulation, the moving object will be the workpiece material, and the tool will be fixed. For orthogonal plunging process, only the region on the top of the tool has to be defined as encastre. The bottom of the workpiece will be constrained in the y-direction; however, it is free to move in the x-direction.

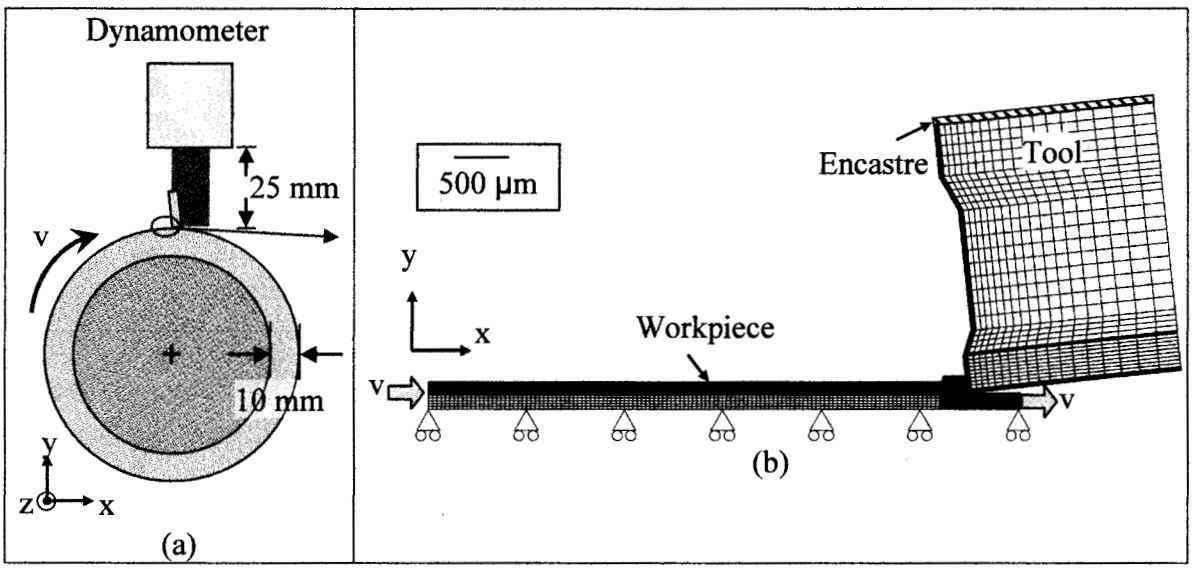

Figure 4.6: (a) Portion of experiment set up being modeled. (b) B.C. for FE cutting model that only include tool, labeled as FE (Tool).

The newly designed geometry for FE cutting model is shown on Figure 4.7 (b), where the tool holder is included. For the ease for reading, it will be labeled as FE (Tool + Holder). Figure 4.7 (a) shows the portion of the experiment set up being taken into consider on the model FE (Tool + Holder), the whole insert and tool holder overhang are included in the model. In FE (Tool + Holder) model, the forces are being extracted from the encastre region on top of the tool holder. The length of the tool holder geometry away from the encastre region was 25 mm. During actual cutting, the tool holder has an overhang of 25 mm away from the dynamometer. The boundary conditions on the workpiece material are the same as the one shown on Figure 4.6 (b). As it can be seen, the newly designed FE (Tool + Holder) model was built to follow closely to the experimental set up configuration.

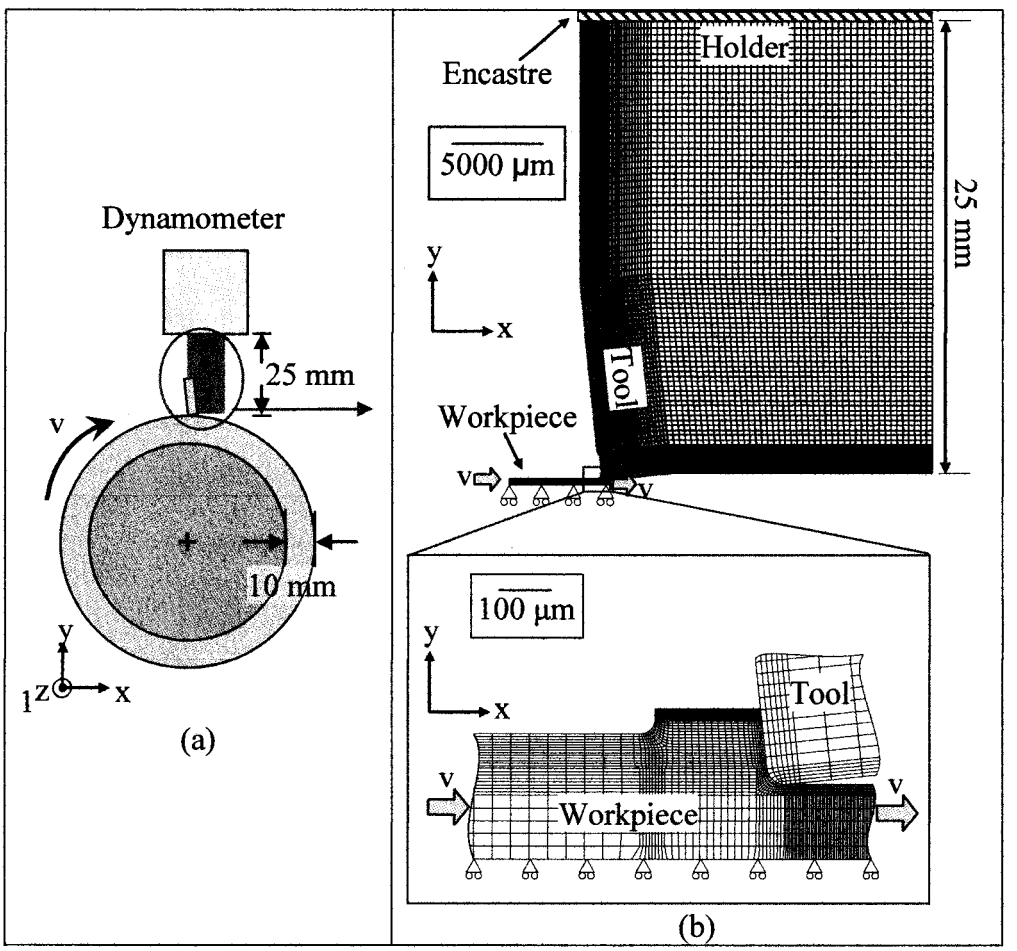

Figure 4.7: (a) Portion of experiment set up being modeled. (b) B.C. for FE cutting model that include tool and holder, labeled as FE (Tool + Holder).

Figure 4.8 (b) shows another newly designed FE cutting model where not only the tool holder was taken into consideration, but also the geometry of the full cutting depth of the workpiece material. Also, for the ease of reading, the model will be labeled as FE (Tool + Holder + WP). The region being circled in red on Figure 4.8 (a) shows portion of experimental set up being taken into consider on FE (Tool + Holder + WP); the whole insert, tool holder overhang, and the full cutting depth of the workpiece material. The boundary conditions on FE (Tool + Holder + WP) are the same as on FE (tool + holder).

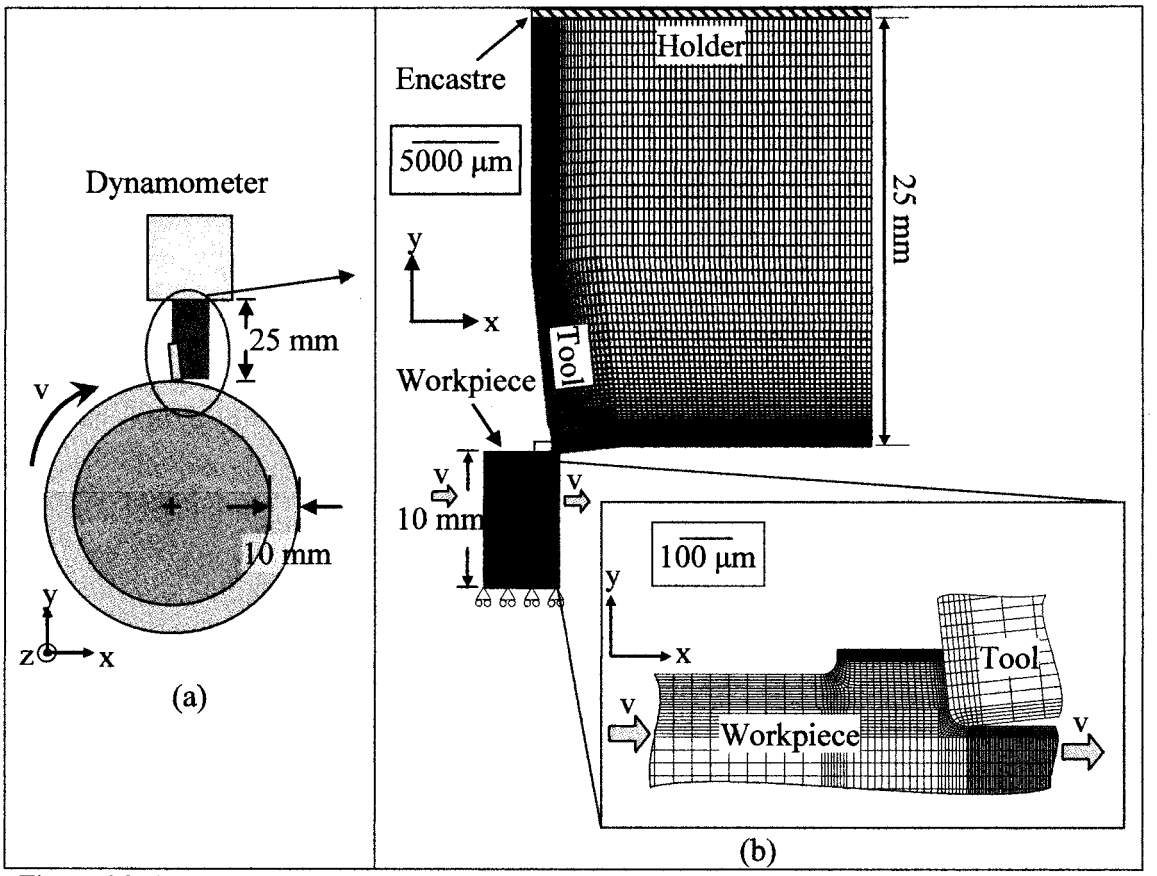

Figure 4.8: (a) Portion of experiment set up being modeled. (b) B.C. for FE cutting model that include tool, holder and workpiece cutting depth, labeled as FE (Tool + Holder + WP).

The portions of eulerian and lagrangian regions are shown in Figure 4.9. The shaded region employ Eulerian formulation and the rest employ updated Langrangian formulation with adaptive remeshing. As it can be seen from Figure 4.9, the workpiece geometry on FE cutting model includes initial chip thickness (t_{ci}) geometry and initial corner radius (r_i). Previous works that employed ALE formulation commented that the geometry dimensions of t_{ci} and r_i does not affect the final chip shape or the mechanics of cutting. This is because the steady state chip thickness (t_c) has the ability to reshape itself and grow automatically, and it is determined solely by the deformation process. Even

though when the initial designed shape of t_{ci} and r_i are far away smaller than the final chip shape, The chip still has the ability to reshape itself to reach steady state chip thickness.

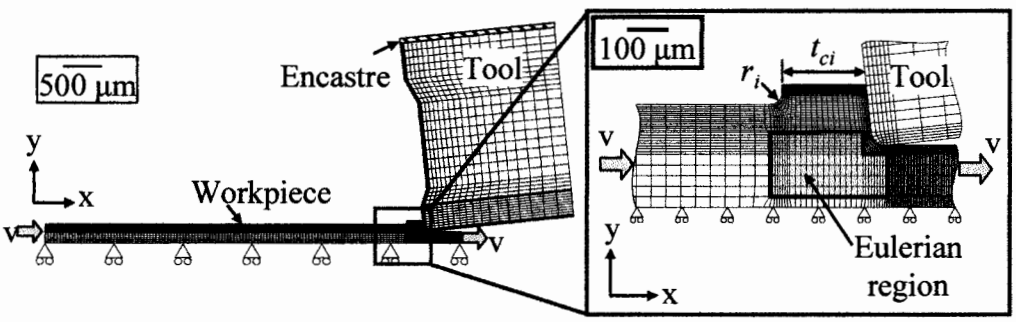

Figure 4.9: Boundary conditions (B.C.) of FE cutting models using ALE formulation.

Figure 4.10 shows the effect of different size of initial chip thickness on the final chip thickness. Both models shown on Figure 4.10 were built very similar, except the size of initial chip thickness t_{ci}; Figure 4.10 (b) has t_{ci} bigger than Figure 4.10 (a) by almost 51%. The final chip thickness t_c produced by both models were different by only about 2.5%. The results found agreed well with the findings by Movaheddy et. al. [2002] and Nasr et. al. [2007], therefore, by using ALE formulation, it is not necessary to do trial and error design for t_{ci}.

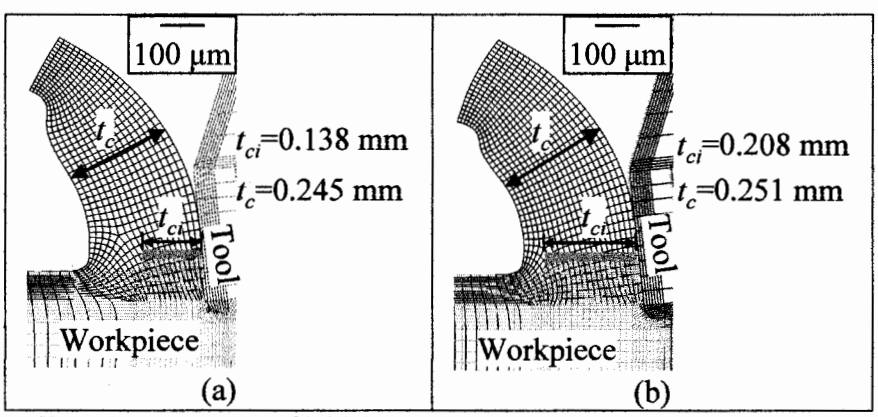

Figure 4.10: Effect of different size of initial chip thickness (t_{ci}) on final chip thickness (t_c). FE model (a) has smaller t_{ci} compared to (b). FE models carried out at v=250 m/min, f=0.1 mm/rev and μ=0.1.

4.4. *Contact behavior on Tool-Chip Interface*

In metal cutting, main sources of heat are generated by material plastic deformation and friction between two contact surfaces. The model assumed that 90% of plastic deformation was converted into heat energy. Along the tool-chip interface, the fraction of dissipated energy converted into heat during frictional slip was 100%. The fraction of heat due to sliding friction channeled into the chip β, was calculated using Equation (4.2) and (4.3), where k, ρ and c_p is the thermal conductivity, density and heat capacity of the material respectively. The letter c as a subscript on E, k, ρ and c_p refers to the chip (workpiece) and the letter t as a subscript refers to the tool. The average value of β calculated and employed was 70%. The gap conductance between two contact surfaces was assumed to be 500 kW m^{-2} $°C^{-1}$.

$$E_{c,t} = \sqrt{k_{c,t} \times \rho_{c,t} \times c_{p_{c,t}}} \qquad (4.2)$$

$$\beta = \frac{E_c}{E_c + E_t} \qquad (4.3)$$

The friction behavior along the tool chip interface will employ model I: Coulomb friction law. Previous works had commented that Coulomb friction law is a simplified friction model and could not be employed for FE cutting models [Haglund, 2008 and Arrazola, 2008]. However, as shown on section 3.3, tremendous works had done on different friction models, and all still facing the same problems of under predicted F_t. Therefore, this current research will not focus on employing friction models that require immense detail along the tool chip interface. Nevertheless, a new method of calibrating of COF to

be used on Coulomb friction law will be discussed on section 6.2. The work on section 6.2 will also emphasize on COF is a function of workpiece and tool material combination, and not a function of process parameter.

4.5. Modeling Test Matrix

The FE cutting models built were divided into three phases as follows:

Phase 1:

Three different FE models were investigated in this phase. These were FE (Tool), FE (Tool + Holder) and FE (Tool + Holder + WP). For these three models, process parameter was all held constant.

Phase 2:

Phase 2 of the research will focus on the new method of calibrating COF to be used for tool and workpiece material combination for coated tungsten carbide and AISI 1045 respectively. All the models were built with the same process parameter and cutting conditions, except using different values of COF.

Phase 3:

Main objective of phase 3 is to carry out parametric study to examine the findings from phase 1 and 2.

The FE cutting models built will be experimentally validated. Figure 4.11 shows the flow chart for the FE cutting models and experimental work validation methodology.

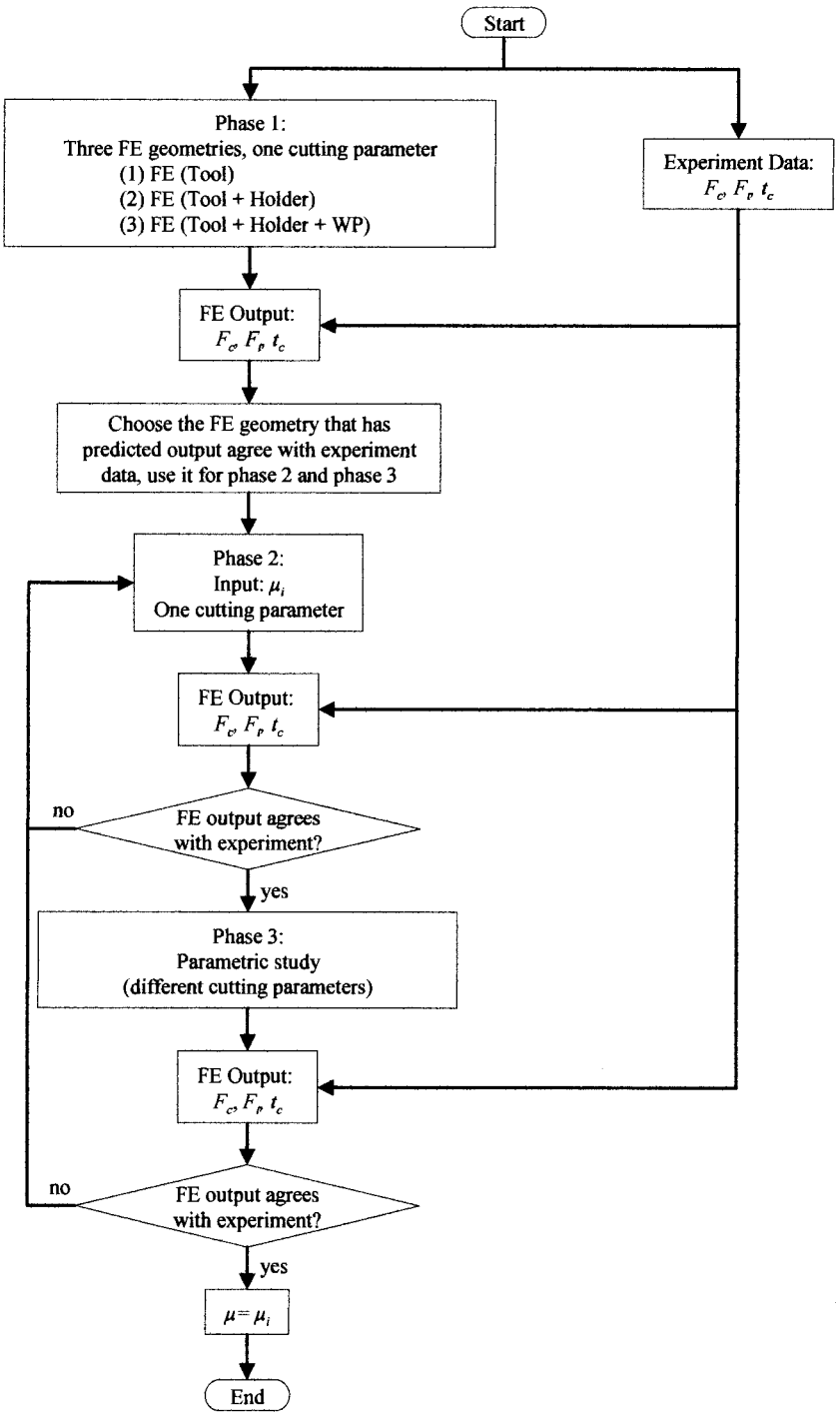

Figure 4.11: Chart flow for the FE cutting models and experimental work methodology.

Table 4.2 summaries the modeling test matrix for Phase 1 to Phase 3. All cutting models have the same α=-6°, width of cut of 3 mm, same tool and workpiece material of coated

WC and AISI 1045 respectively. The results from the FE cutting models will be experimentally validated.

	v (m/min)	250				150			200			250		
	f (mm/rev)	0.10				0.05	0.10	0.20	0.05	0.10	0.20	0.05	0.10	0.20
	COF, μ	0.10	0.15	0.20	0.50	0.10								
Phase 1	FE (tool)	√												
	FE (tool + holder)	√												
	FE (tool + holder + wp)	√												
Phase 2	FE (tool)	√	√	√	√									
	FE (tool + holder)	√	√	√	√									
Phase 3	FE (tool)					√	√	√	√	√	√	√	√	√
	FE (tool + holder)					√	√	√	√	√	√	√	√	√

Table 4.2: Modeling test matrix.

5. EXPERIMENTAL WORK

5.1. EXPERIMENTAL SET UP FOR ORTHOGONAL CUTTING

Experimental work was carried out to validate the FE cutting models built for Phase 1 to Phase 3. All the cutting tests were carried out orthogonally and in a dry environment. Table 5.1 shows the experimental test matrix carried out.

Speed, v (m/min)	150			200			250		
Feed, f (mm/rev)	0.05	0.10	0.20	0.05	0.10	0.20	0.05	0.10	0.20
Phase 1								√	
Phase 2							√	√	√
Phase 3	√	√	√	√	√	√	√	√	√

Table 5.1: Experimental test matrix.

Orthogonal cutting tests were carried out on a Nakamura Tome SC-450 (CNC) lathe. The experimental set up is shown on Figure 5.1 (a) and (b).

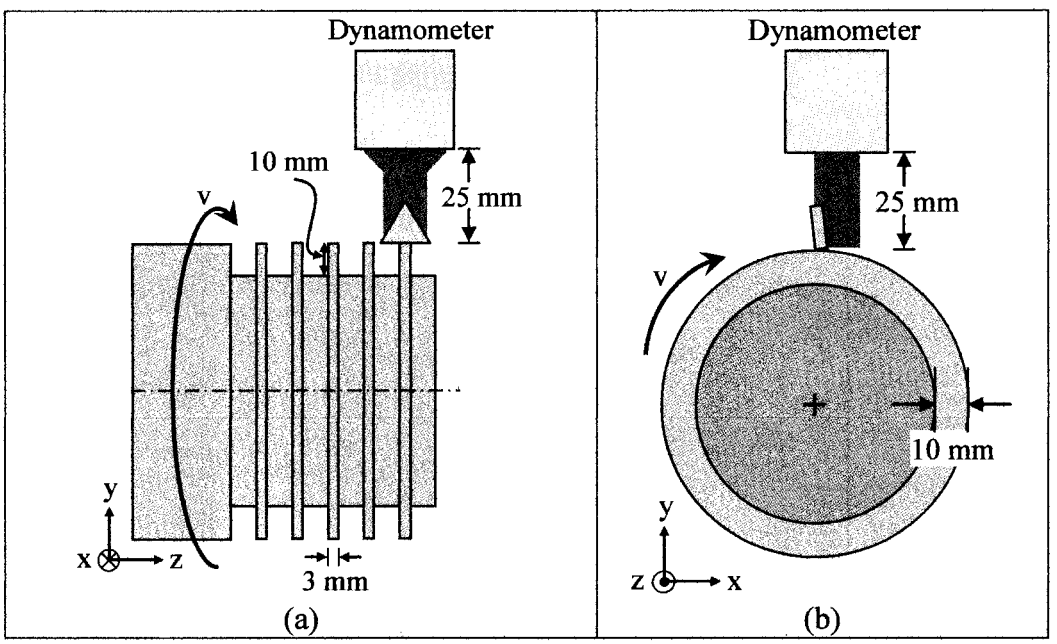

Figure 5.1: Experimental set up for orthogonal cutting. (a) Front view. (b) Side View.

A three axis Kistler type tool-post piezoelectric dynamometer was used to measure the cutting force F_c, thrust force F_t and axial force F_z. Sampling rate was fixed at 2 kHz. The rake and clearance angles employed were -6 deg and 6 deg respectively. Orthogonal cutting tests were carried out with a 3 mm width of cut. Figure 5.2 shows an example of forces obtained experimentally (taken from one of the cutting condition from Table 5.1); obtained F_z was approximately 0 N, thus plane strain assumption is acceptable for modeling.

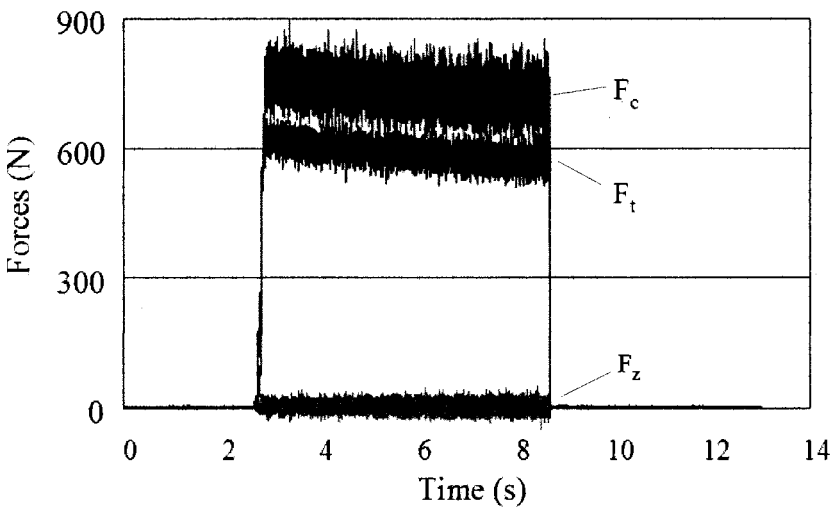

Figure 5.2: Example of obtained forces experimentally. F_z obtained ~0 N. Cutting condition at f=0.1 mm/rev, v=250 m/min.

5.2. TOOL HOLDER DESIGN

The tool holder used for experimental work was custom designed and made. Figure 5.3 (a) to (e) shows the tool holder design specification. The tool holder was designed for orthogonal plunging process, and has an overhang of exactly 25 mm from the dynamometer.

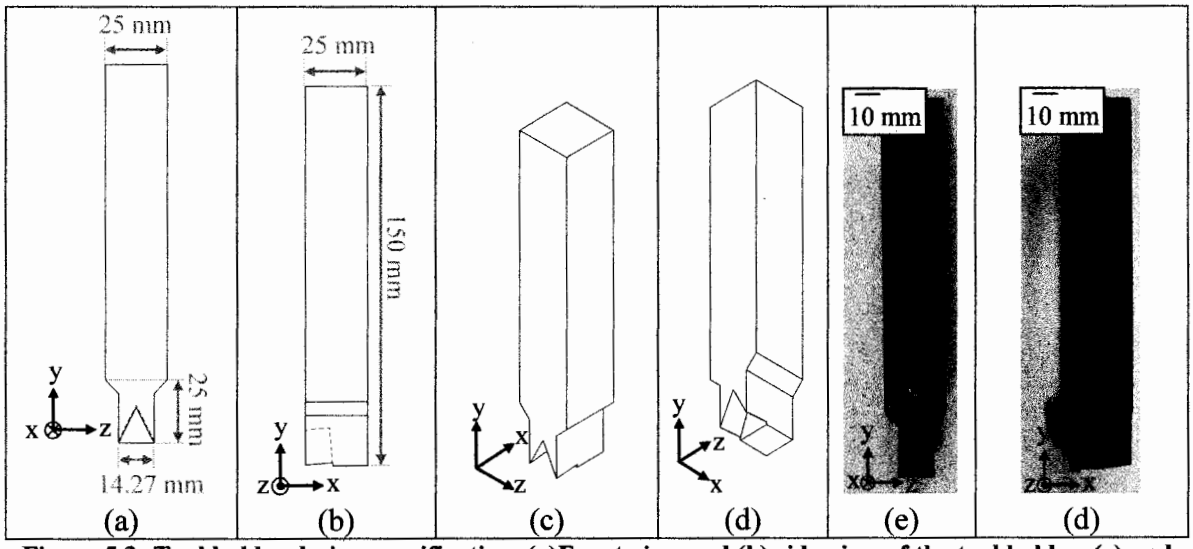

Figure 5.3: Tool holder design specification. (a)Front view and (b) side view of the tool holder. (c) and (d) are the 3D views of tool holder. (e) and (f) are the pictures of the tool holder.

5.3. CUTTING WORKPIECE AND TOOL MATERIAL

The workpiece material investigated was AISI 1045 with a bulk hardness of 200-220 BHN. Figure 5.4 shows the microstructure of the workpiece material AISI 1045 used for experimental work. The darker region of the microstructure shows the harder pearlite grains while the white region is the softer ferrite grains [Simoneau, 2007].

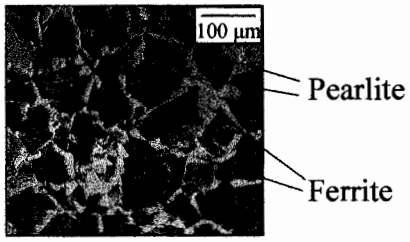

Figure 5.4: Picture of the microstructure of the workpiece AISI 1045 steel. Darker region showing the harder pearlite grains, while the white region showing the softer ferrite grains.

The cutting tool used was commercially available Sandvik Coromant TNMG 432 MR, with CVD coating GC 4225 (coating of $TiN+Al_2O_3+TiCN$).

5.4. TOOL CUTTING EDGE RADIUS MEASUREMENT

The dimension information of the tool cutting edge radius was not readily available; therefore the tool dimensions had to be captured manually. The equipment used to capture images of the insert profile was the microscope Nikon AZ100 Multizoom. The digital camera was used to capture many layers 2-dimensionals (2D) pictures of the insert profile; distance between each layer 5 μm. The software Nikon's NIS-Elements took multiple shots of the 2D pictures and combined to form 3D picture based on the distance between each layer. Figure 5.5 shows an example of the 3D picture of insert profile obtained by compiling 35 layers of 2D pictures. The obtained 3D picture could be rotated and measured.

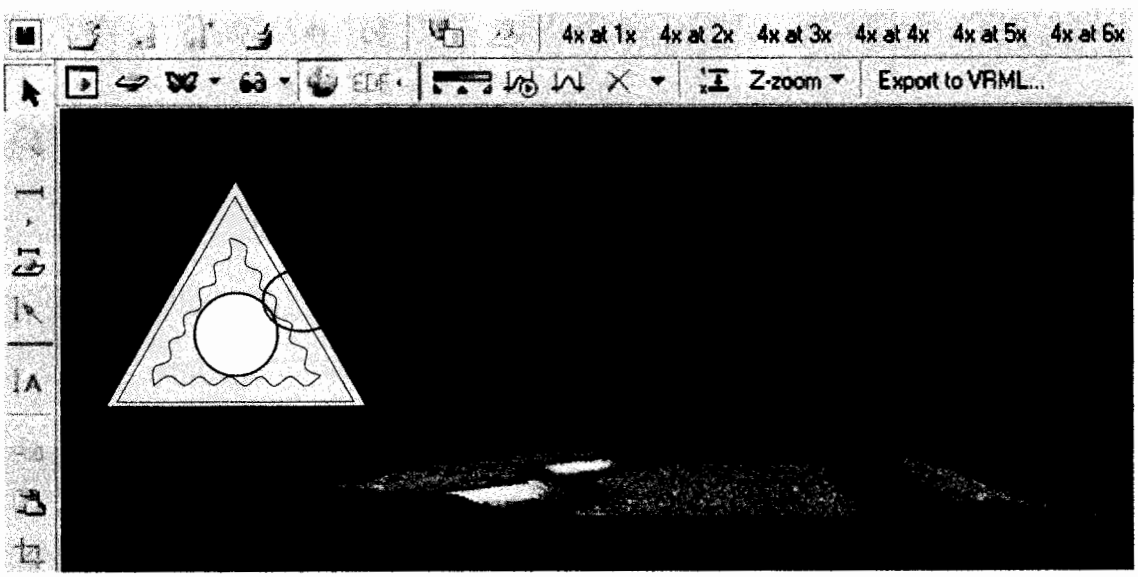

Figure 5.5: Example of 3D view of the insert profile of TNMG 432 MR.

Figure 5.6 shows an example of how the insert profile dimension was being captured. The measurement was taken at least five times; the average value was calculated and used. The picture shown in Figure 5.6 was taken at high magnification; however the picture still

showed clearly the full depth of view. This is because the picture in Figure 5.6 was a compilation of 35 layers of 2D pictures. Since distance between each layer of 2D picture is 5 μm, the compiled 3D picture was able to show a clear picture with a full depth of view of 175 μm.

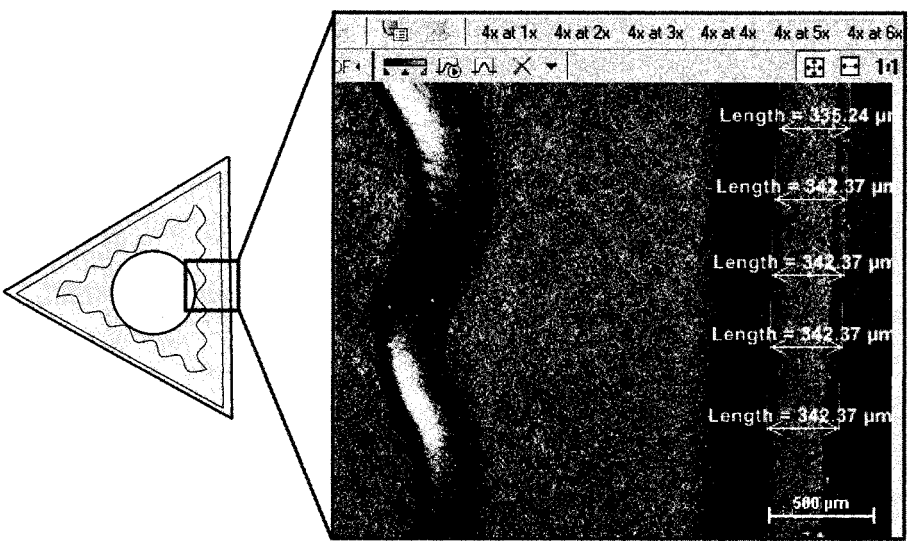

Figure 5.6: An example of measuring dimension of the insert profile.

Figure 5.7 shows the method on how the tool cutting edge radius was measured. The insert was tilted in a way that the tool cutting edge was pointing directly towards the lens of the digital camera. 15 layers of 2D pictures of the tool cutting edge were taken from the top of the tool tip till a distance of 75 μm below the tool cutting edge. The layers of 2D pictures were then compiled to form the 3D image as shown in Figure 5.7 (a). It is assumed that the shiny part of the insert is the curvature of the tool cutting edge radius. Figure 5.7 illustrates how the tool cutting edge radius was measured and calculated. The measurements were made at least 5 times and the average value was calculated and used.

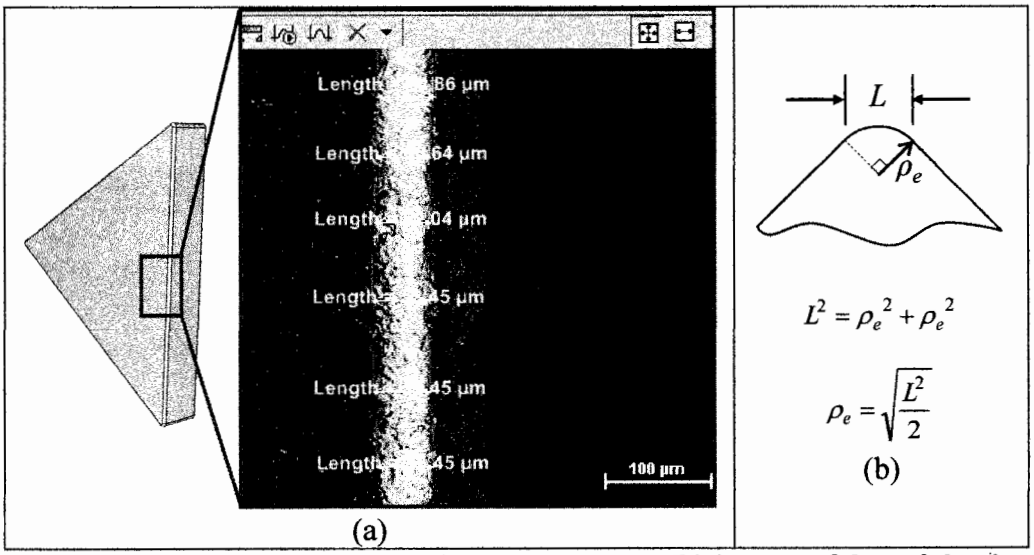

Figure 5.7: Method of measuring tool cutting edge radius. (a) Shining part of the tool showing the curvature of the tool cutting edge radius. (b) Method of calculating the tool cutting edge radius.

Figure 5.8 (a) shows the sketch of the insert used for experimental work. Since the FE cutting models built were 2D, an assumed dimension of Figure 5.8 (b) was used in FE models. The final dimension of the insert measured is shown on Figure 5.8 (c). The obtained measured tool cutting edge radius is 35 µm.

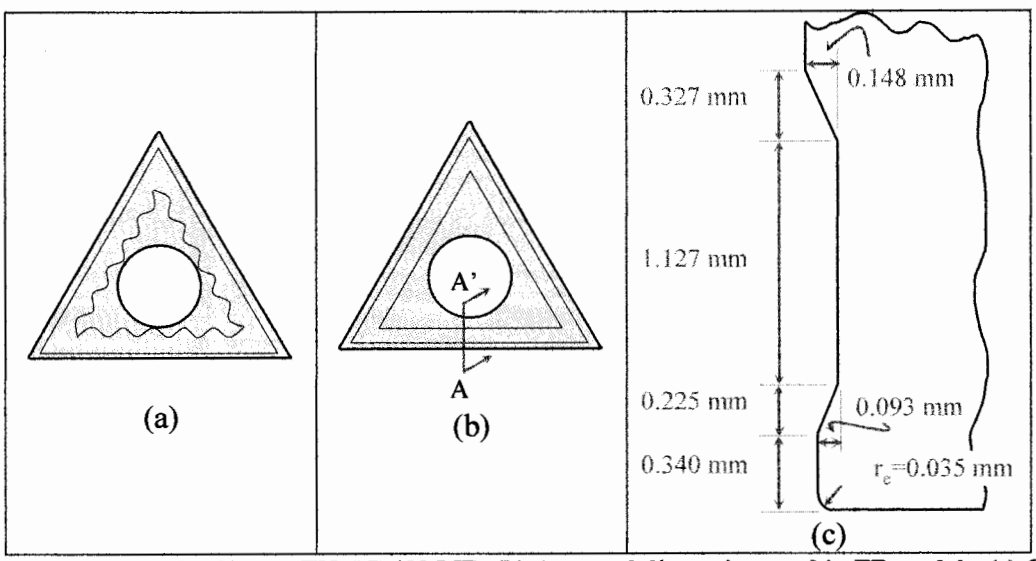

Figure 5.8: (a) Sketch of insert TNMG 432 MR. (b) Assumed dimension used in FE models. (c) Cross section dimension of AA' from sketch (b).

6 RESULTS AND DISCUSSIONS

6.1 PHASE 1: GEOMETRICAL CONSIDERATION IN FEM

The main objective of Phase 1 was to investigate the effect of workpiece geometries when FE modeling the cutting process. Figure 6.1 shows the flow chart for Phase 1 methodology. Three different FE cutting models were built based on one cutting conditions, however, geometry designs were varied. The predicted output made by each model was compared with experimental results. The geometry of FE cutting model that could predict results which agreed closely to experimental data was used in Phase 2 and Phase 3 works.

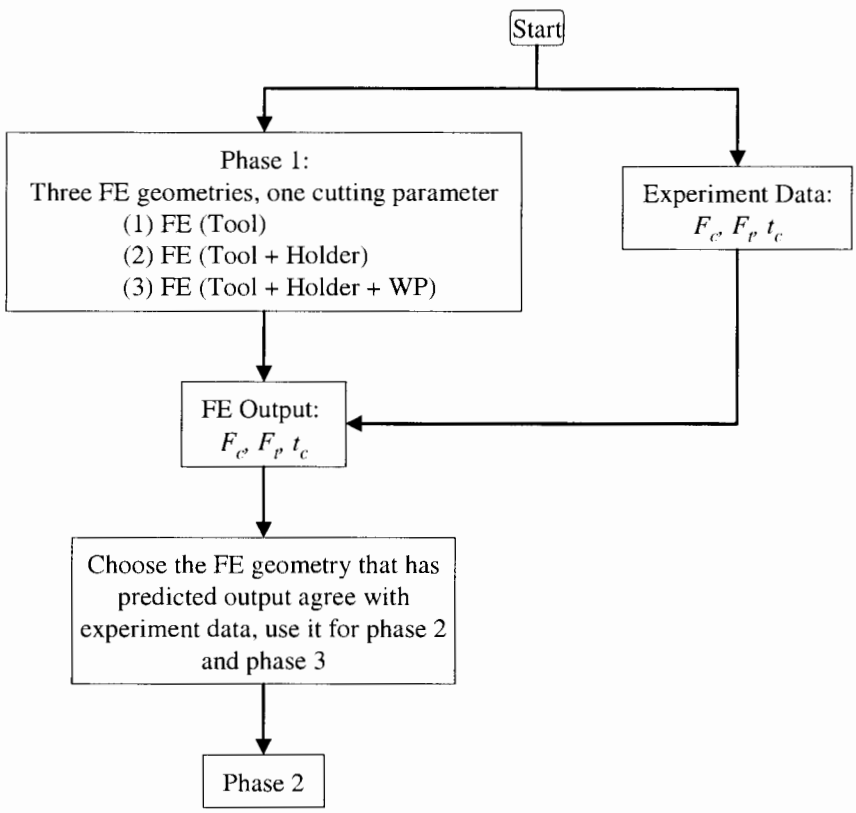

Figure 6.1: Flow chart for Phase 1 methodology

6.1.1 Effect of Tool Holder and Workpiece Consideration in FE Cutting Models

Three different FE cutting models were built; FE (Tool), FE (Tool + Holder) and FE (Tool + Holder + WP). To normalize the effect of other variables, the three FE cutting models and experiment were carried out using the same tool rake angle of -6°, speed of 250 m/min and feed of 0.1 mm/rev. The value of COF employed by the three FE cutting models in Phase 1 was kept constant at 0.1. Table 6.1 summarizes the test matrix for Phase 1.

	FEM	Experiment
Speed (m/min)	250	
Feed (mm/rev)	0.1	
COF, μ	0.10	
FE (Tool)	√	
FE (Tool + Holder)	√	
FE (Tool + Holder + WP)	√	
Experiment		√

Table 6.1: Phase 1 test matrix.

Figure 6.2 compared the predicted cutting force F_c, feed force F_t and chip thickness t_c from the FE cutting models built with experimental results. The three FE cutting models produced similar values of F_c and t_c, but different values of F_t. The predicted F_c and t_c from all three models agreed well within 4% and 13% difference with experimental data respectively. However, only FE (Tool + Holder) and FE (Tool + Holder + WP) predicted feed force F_t that has 6% and 13% difference with experimental data respectively. FE (Tool) predicted F_t that has 52% difference with experimental results. This large difference value of predicted F_t from experimental result was also being obtained by Iqbal et. al. [2007 b] and Ozel [2006]. Both predicted F_t and F_c from

FE (Tool + Holder) and FE (Tool + Holder + WP) agreed well with experimental results. Previous works on FE orthogonal modeling could not accurately predict both F_c and F_t that agreed with experimental results (refer to compilations on table 3.4 to table 3.8). The drastic increase with F_t in FE (Tool + Holder) and FE (Tool + Holder + WP) compared to FE (Tool) could be explained by comparing the forces (F) and tool deflection (δ) signatures.

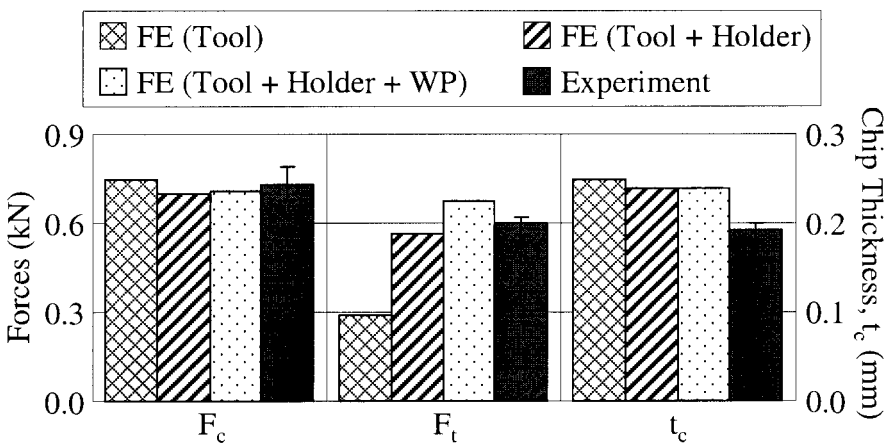

Figure 6.2: Comparison of predicted F_c, F_t and t_c taken from different FE models with different geometry with experimental data.

For all FE cutting models in this research, the tool deflection measurement was taken from the same point, near the cutting edge as shown in Figure 6.3. Deflection measurement was taken near the cutting edge because at this point, maximum magnitude for tool deflection was observed in the FE models.

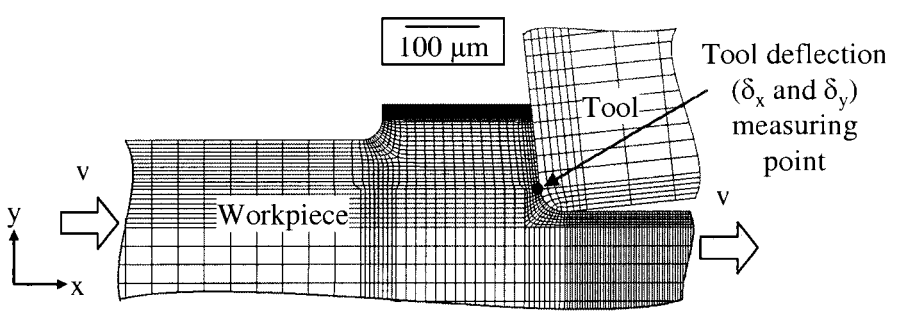

Figure 6.3: All FE cutting model will take the same point to measure tool deflection.

Figure 6.4 (a), (b) and (c) shows the forces (F) and deflection (δ) signatures taken from FE (Tool), FE (Tool + Holder) and FE (Tool + Holder + WP) respectively. In FE cutting models, the tool deflection in x-direction (δ_x) influenced the value of F_c, and tool deflection in y-direction (δ_y) influenced the value of F_t. As shown on Figure 6.4, the δ_x and δ_y magnitudes obtained by FE (Tool) were substantially smaller when compared to FE (Tool + Holder) and FE (Tool + Holder + WP). This was because the distance between the tool cutting edge and encastre region of the tool for FE (Tool) was only 2.5 mm, whereas those for both FE (Tool + Holder) and FE (Tool + Holder + WP) were set at 25.0 mm. During the actual cutting test, the distance between the cutting edge and dynamometer was 25.0 mm. Therefore, the distance between the cutting edge and dynamometer had to be considered in FE cutting model for realistic simulation. The forces and tool deflection signatures in Figure 6.4 show the dynamic behavior in the FE cutting models. The dynamic characteristics were time dependent and affected by the part geometry and material properties. The addition of tool holder overhang not only changed the geometry of the overall tool, but also changed the material properties; Young's modulus of AISI 4140 is smaller than carbide, thus causing the overall structure in FE (Tool + Holder) to be less rigid than FE (Tool). When the overall structure became less rigid, higher deflection occurred when force was being applied. When tool holder was included, the deflection of the tool was up to 2.8 μm. With FE (Tool) the maximum deflection was only 0.6 μm.

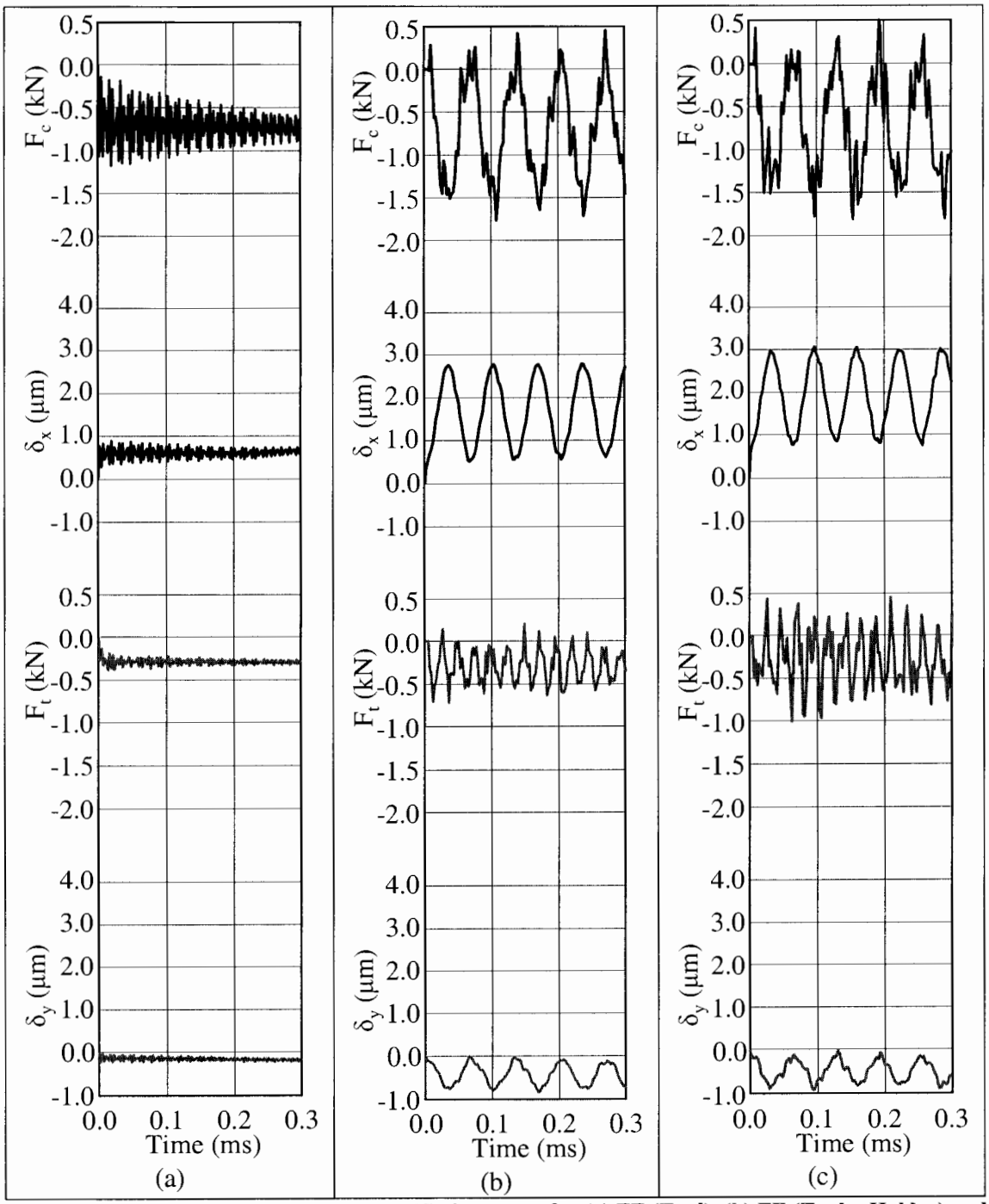

Figure 6.4: Forces (F) and tool deflection (δ) signatures for (a) FE (Tool), (b) FE (Tool + Holder) and (c) FE (Tool + Holder + WP).

For illustration purposes, a good example to explain the different magnitude of tool deflection obtained by FE (Tool) and FE (Tool + Holder) was to compare two beams

with the same square cross sectional area as shown in Figure 6.5 (a) and (b). Beam A was made of carbide material and had a short length of 0.04 m. Beam B was made of AISI 4140 steel and had a length ten times longer than beam A. Both beams had each end being fixed onto a wall. 10 kN force was applied to the other end of both beams. The results from both FE models built showed that beam A had a maximum of $\delta_x = -3.0\times10^{-7}$ m and $\delta_y = -8.0\times10^{-7}$ m, and beam B had a maximum of $\delta_x = -5.1\times10^{-5}$ m and $\delta_x = -1.4\times10^{-3}$ m. A larger deflection was observed with Beam B because of lower structural stiffness when compared to Beam A. The deflection on the cutting edge on FE (Tool + Holder) was larger than on FE (Tool) also because of the same reason; FE (Tool + Holder) had overall lower structured stiffness when compared to FE (Tool).

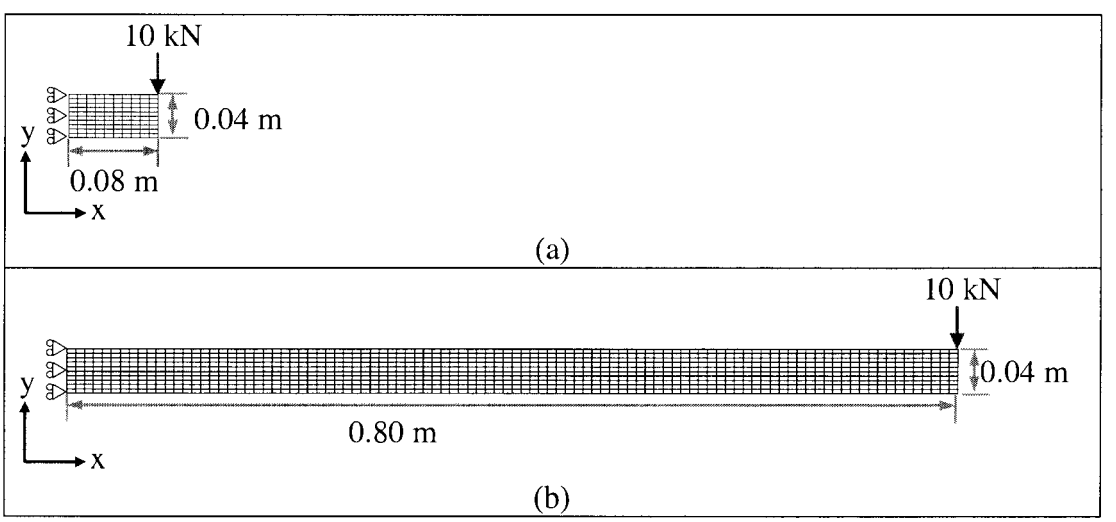

Figure 6.5: (a)Example Beam A. (b) Example Beam B.

6.1.2 Obtaining Predicted Forces from Force signatures

The method to obtain F_c and F_t from the forces signature from the model FE (Tool), FE (Tool + Holder) and FE (Tool + Holder + WP) was explained in this section.

6.1.2.1 Obtaining Predicted F_c and F_t from forces signature on FE (Tool)

F_c and δ_x signature obtained from FE (Tool) is shown in Figure 6.6 (a). During the transition region, both F_c and δ_x signatures initially oscillated at a higher magnitude. The oscillation magnitude range decreased with time and finally died down to a near steady state value. Oscillation magnitude of both F_c and δ_x signature finally settled between the maximum and minimum value. Thus the average value from the F_c force signature was taken as the predicted F_c from FE (Tool).

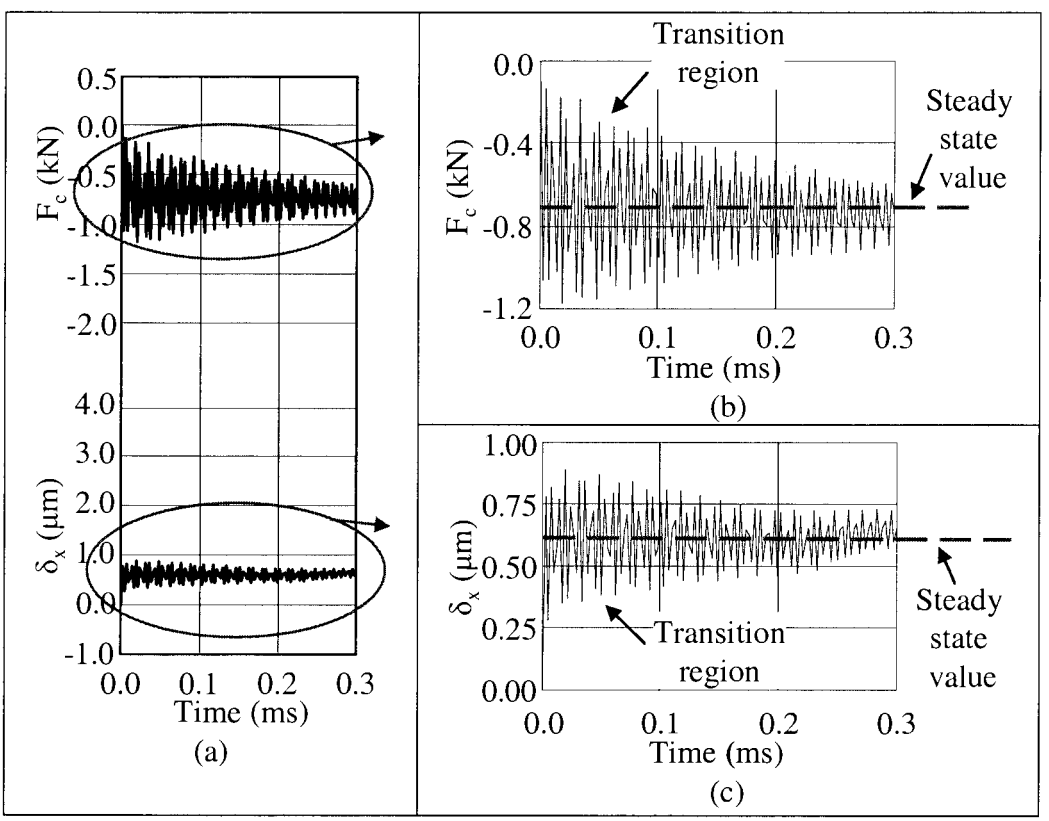

Figure 6.6: (a) F_c and δ_x signature taken from FE (Tool). (b) Blown up graph of F_c signature from (a). (c) Blown up graph of δ_x signature from (a).

Figure 6.7 shows F_t and δ_y signature obtained from FE (Tool). Similar to the F_c and δ_x signature obtained from FE (Tool), F_t and δ_y signature also had its transition region. The oscillation magnitude range also decreased with time and finally died down to a near

steady state value. However, the difference was that the oscillation magnitude of both F_t and δ_y signature finally settled near its maximum value. Thus, the average value of the peaks valley from F_t force signature was taken as the predicted F_t from FE (Tool).

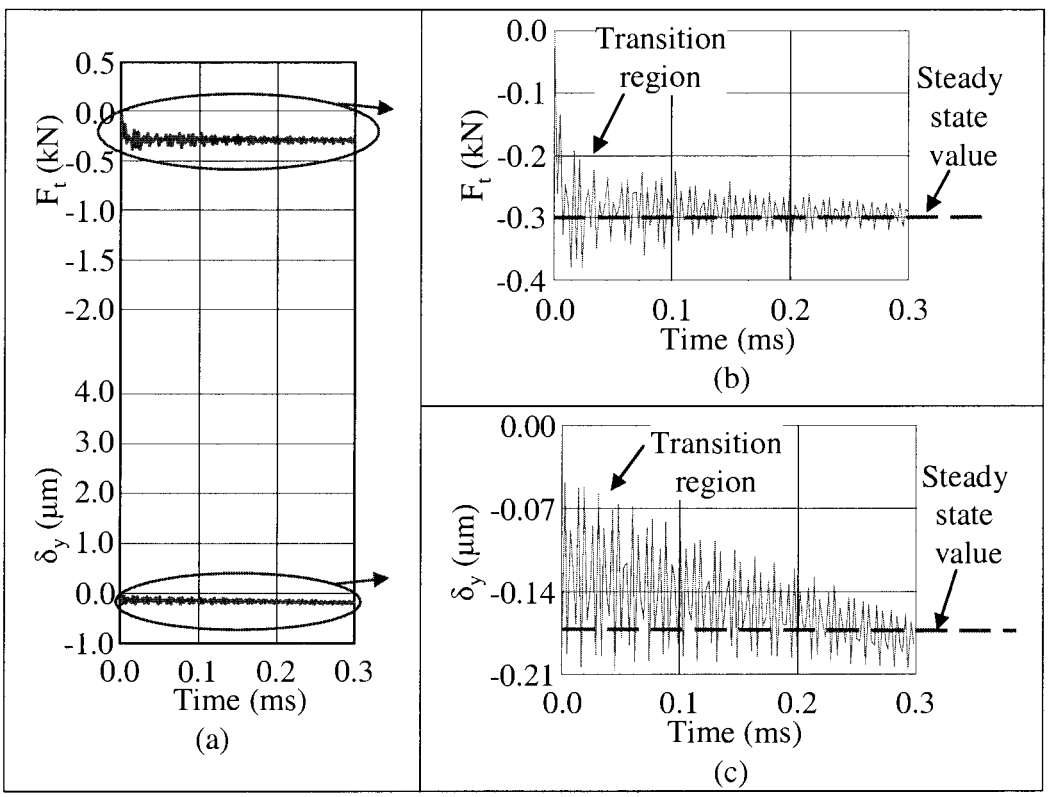

Figure 6.7: (a) F_t and δ_y signature taken from FE (Tool). (b) Blown up graph of F_t signature from (a). (c) Blown up δ_y signature from (a).

Three key observations were observed with FE (tool) model. They were:

- Both F_c and F_t signatures initially went through transition region and later reached a steady state value.
- Oscillation of F_c signature settled between its maximum and minimum value; therefore value of predicted F_c was obtained by taking the average value from the F_c signature.

- Oscillation of F_t signature settled at its maximum value; therefore value of predicted F_t was obtained by taking the average of the peak values from the F_t signature.

6.1.2.2 Obtaining Predicted F_c and F_t from forces signature on FE (Tool + Holder)

F_c and F_t signatures obtained from FE (Tool + Holder) are shown in Figure 6.8 (a) and (b) respectively. Both F_c and F_t signatures were still going through the transition region. Since the model was not built long enough to reach steady state, the same method as from FE (Tool) was used to obtain predicted F_c and F_t. Predicted F_c from FE (Tool + Holder) was obtained by taking the average value from the F_c signature while predicted F_t was obtained by taking the average of the maximum peak values from the F_t signature. See detail in Appendix A

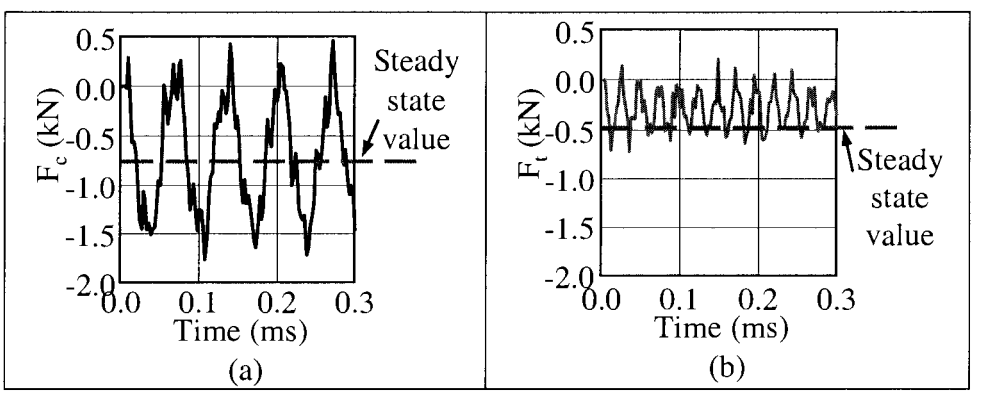

Figure 6.8: Assumed steady state value for (a) Cutting force F_c (b) Feed force F_t in FE (Tool + Holder).

The long transition region faced by FE (Tool + Holder) could be explained by looking into the material properties and geometry of the tool holder. As mentioned earlier, the FE cutting models built were dynamic systems that had stiffness and damping properties. By looking at Figure 6.6 and Figure 6.7, the oscillation gradually decayed,

thus FE cutting models were underdamped systems. Figure 6.9 shows the sketch of a typical step response of an under-damped system. The under-damped oscillation has transition and steady state region. The setting time (t_s) shown in Figure 6.9 is the amount of time for the oscillation to die away and settle to the steady state value (X_S). The setting time could be calculated using equation 6.1 (a).

$$t_{s(2\%)} = -\frac{\ln 0.02}{\xi\omega_n} = -\frac{\ln 0.02}{\xi\left(\sqrt{k/m}\right)} \qquad \text{6.1 (a)}$$

Where, ξ is the damping ratio, ω_n is the natural frequency, k is the overall stiffness, and m is the overall mass.

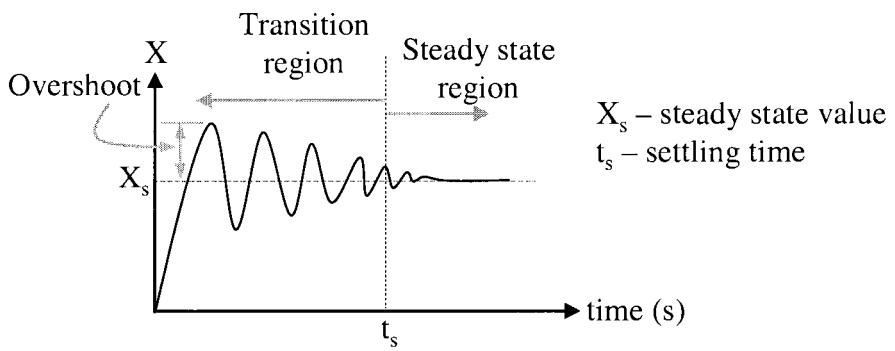

Figure 6.9: Sketch of graph that has under damped system.

In a stable under-damped system, the values of overshoot, X_s and t_s were affected by the overall structure material properties and geometry; the structure material properties and geometry affect the stiffness, damping ratio and mass value, thus affecting the settling time value. Table 6.2 shows the damping ratio, stiffness, mass and finally the settling time when only tool was being used and when both tool + holder were being used. Take note that the values of damping ratio, ξ was assumed to be 0.5. The value of stiffness k and mass m were calculated using FE implicit model (see Appendix B for details). When tool holder was included into the model, the under-damped dynamic

system took ten times longer than the model which only includes the tool. Thus, in order to have FE (Tool + Holder) to reach steady state values, the simulation would have to go as long as at least 50 ms. Building a model that simulates up to 50 ms will suffer from severe mesh distortion with ALE formulation and long computational time. Therefore in this research, it was assumed that F_c settled at average value, and F_t settled at the maximum peak value.

	Tool only	Tool + Holder
ξ (damping ratio)	0.05	0.05
k (stiffness, N/mm)	7.59×10^{5}	3.19×10^{5}
m (kg)	6.36×10^{-3}	124.81×10^{-3}
$t_{s(2\%)}$ (ms)	7.2	48.9

Table 6.2: Comparison of settling time for dynamic under-damped system.

6.1.2.3 Obtaining Predicted F_c and F_t from forces signature on FE (Tool + Holder + WP)

With reference to Figure 6.6 (b) and (c), the force and deflection signatures obtained by FE (Tool + Holder + WP) were similar to those obtained by FE (Tool + Holder). Except, the oscillation magnitude obtained by FE (Tool + Holder + WP) was a higher. Since the oscillation patterns were similar, the same method of acquiring predicted F_c and F_t from force signature on FE (Tool + Holder) will be used on FE (Tool + Holder + WP).

Due to inclusion of large workpiece geometry, FE (Tool + Holder + WP) was computationally more expensive than FE (Tool + Holder). Since the results obtained by both models produced results that were similar in pattern and magnitude, FE (Tool + Holder) was chosen to carry out Phase 2 and Phase 3.

6.2 PHASE 2: CALIBRATION OF COF IN FE CUTTING MODEL

Phase 2 work presented a new and simple method to calibrate the value of COF (μ) to be used in FE cutting models for one combination of tool (coated carbide) and workpiece material (AISI 1045). Figure 6.10 shows the steps of methodology for Phase 2. In this phase, all FE cutting models were built based on one cutting condition: cutting speed of 250 m/min, feed rate of 0.1 mm/rev. An initial guessed COF value (μ_i) was employed by the FE cutting model. The predicted FE output (F_c, F_t and t_c) compared with experimental data. The magnitude of COF to be used depended on how well the FE output agreed with experimental data. This was the criteria used to determine the COF.

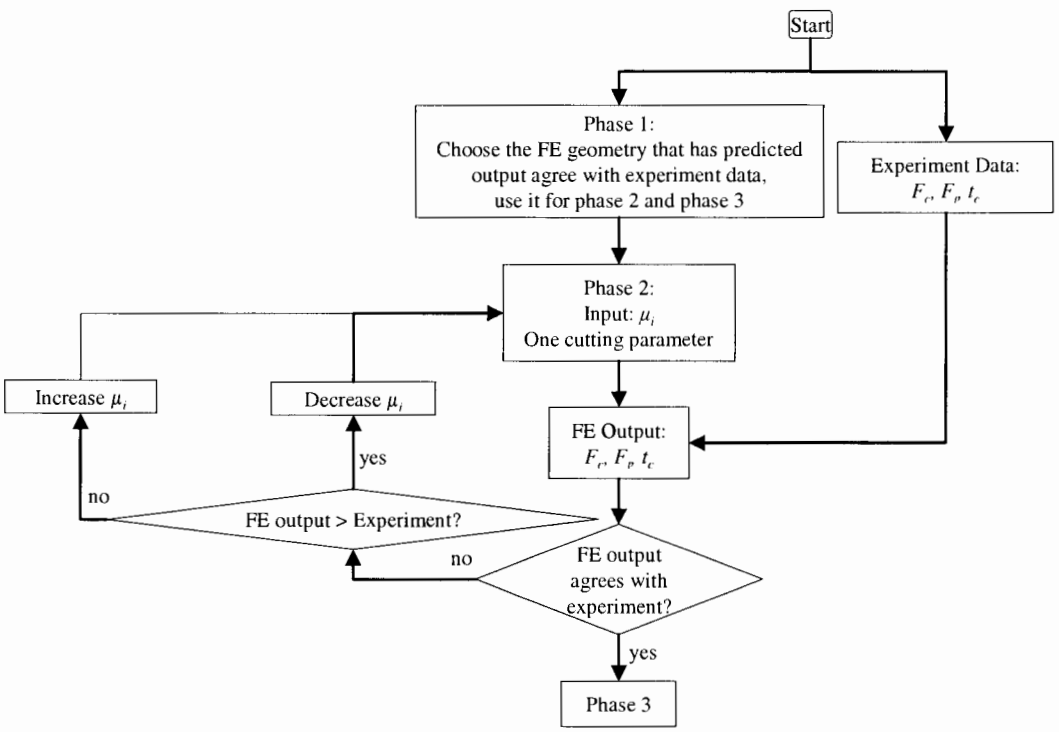

Figure 6.10: Flow chart for Phase 2 methodology.

The test matrix for Phase 2 is shown in Table 6.3. One cutting condition (f = 0.1 mm/rev, v = 250 m/min) was used to investigate the effect of different COF magnitude. Predicted

results obtained by each models was compared with experimental data. COF magnitude obtained from orthogonal cutting tests and substituting into equation 6.2 was also evaluated. Experimental work were carried out using one cutting speed (250 m/min) and varied three different feed rates (f = 0.05 mm/rev, 0.1 mm/rev and 0.2 mm/rev). The reason for carrying out three different feed rates experimentally was to find out the effect of feed rate on the average COF acquired from Merchant's circle.

$$\mu = \frac{F_c \sin\alpha + F_t \cos\alpha}{F_c \cos\alpha - F_t \sin a} \qquad (6.2)$$

	Finite Element Models				Experiment		
Speed (m/min)	250						
Feed (mm/rev)	0.1				0.05	0.10	0.20
COF, μ	0.10	0.15	0.20	0.50			
FE (Tool)	√	√	√	√			
FE (Tool + Holder)	√	√	√	√			
Experiment					√	√	√

Table 6.3: Phase 2 test matrix. All FE cutting models used α=-6°.

6.2.1 Experimental Work Analysis

Part of Phase 2 work was to investigate the effect of using Merchant's circle equation 6.2 to calculate COF. The F_c and F_t used in equation 6.2 were obtained experimentally. Figure 6.11 (a) shows the forces obtained experimentally with varying feed rate, and Figure 6.11 (b) shows the corresponding cutting force ratio (F_c/F_t). Both F_c and F_t increased with increasing feed rate. However, F_c increased more significantly than F_t with higher feed rate, thus causing the cutting force ratio (F_c/F_t) to increase with higher feed rate. The cutting force ratio at f = 0.05 mm/rev is less that one; F_t higher than F_c. The reason for lower cutting force ratio at low feed rate has been known to be due to the finite

tool cutting edge radius which generates ploughing component on F_t. The ploughing component was described as the size effect by Boothroyd [1989]. The term size effect refers to the increase in the amount of energy required to remove a unit volume of metal as feed rate decreases. At high feed rate, the portion of ploughing component was small compared to the cutting force. However, at small feed rate, the portion of ploughing component became significant and thus could not be neglected. The trends of experimental results obtained were in agreement with the early investigation made by Albercht [1960]. Albercht [1960] did a detailed investigation on the significance of ploughing in the metal cutting process. Experimental results showed that F_c increased with feed rate; whereas the thrust force F_t increased with increasing feed rate up to a certain maximum and become nearly a constant value. Albrecht suggested that the low cutting force ratio behavior at low feed rate was due to the ploughing component on the tool cutting edge. Furthermore, Albrecht [1960] concluded that by eliminating the ploughing effect on the cutting edge radius, the COF on the tool rake face did not change with cutting conditions. However when using Merchant's circle to calculate COF, increasing feed rate decreased COF, as shown in Figure 6.11 (c), which was not in agreement with Albrecht [1960] conclusion. Using merchant's circle to calculate COF for FE cutting models was still being used, for example Xie et. al. [2005] and Ozel et. al. [2000], leading to misconceptions that COF varied with cutting conditions.

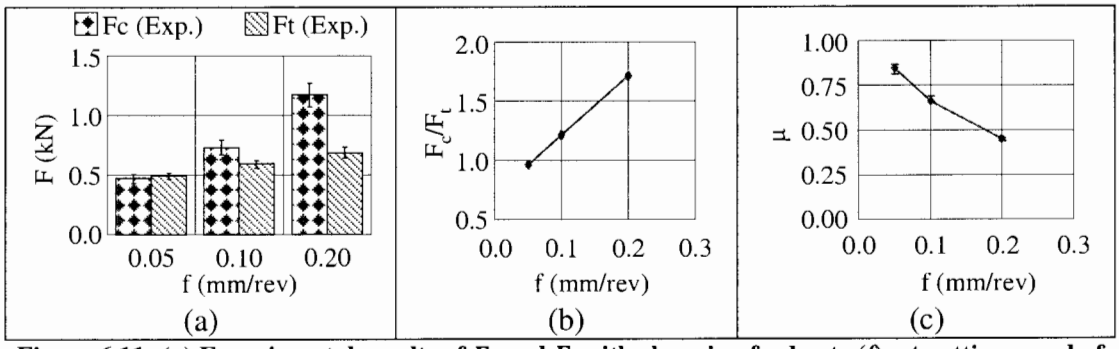

Figure 6.11: (a) Experimental results of F_c and F_t with changing feed rate (f), at cutting speed of v=250 m/min. (b) Experimental Cutting force ratio (F_c/F_t) with changing feed rate (f), at cutting speed of v=250 m/min. (c) Calculated μ with changing feed using Merchant's circle based on experimental data from (a).

6.2.2 Effect of Varying COF on Predicted Results

Figure 6.12 (a), (b) and (c) shows the effect of COF on predicted F_c, F_t and t_c respectively. Results from both conventional FE (Tool) and newly designed FE (Tool + Holder) geometries were presented for comparison purposes. In general, increasing COF caused F_c, F_t and t_c to increase. Shi et. al. [2002] also studied on the effect of varying COF on predicted results made by conventional FE cutting models and obtained the same trend; predicted F_c, t_c increased with larger values of COF. He suggested that COF could be calibrated by comparing experimentally measured results with numerically predicted results. However, no experimental validations were carried out. Figure 6.12 (a) shows that both conventional and newly designed FE geometries produced similar predicted F_c; values of COF ranging from 0.1 to 0.2 seemed to produce predicted F_c that agreed well with experimental F_c. Figure 6.12 (b) shows that even though the predicted F_t made by both conventional FE (Tool) and new FE (Tool + Holder) cutting models had the same trend when varying COF, only FE (Tool + Holder) cutting models could obtain predicted F_t similar to experimental result. When COF was at 0.5, the FE (Tool) could produce

predicted F_t that was close to experimental; however, F_c and t_c were over predicted. Figure 6.12 (c) shows that both FE (Tool) and FE (Tool + Holder) produced similar predicted t_c. For this tool and workpiece material combination, value of COF at 0.1 was able to produce good combinations of predicted F_c, F_t and t_c that agreed with experimental results; therefore this magnitude was used for the parametric study on Phase 3.

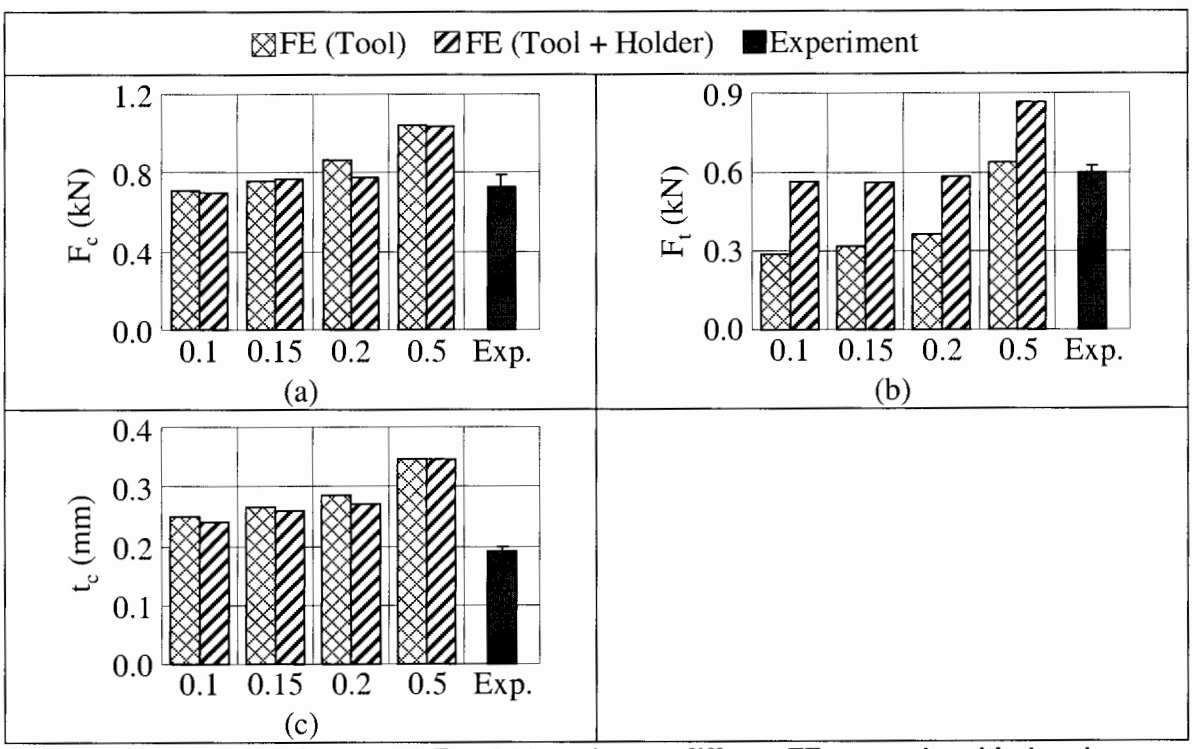

Figure 6.12: Predicted (a) F_c, (b) F_t and (c) t_c using two different FE geometries with changing μ compared with experimental data. Both FE cutting models and experimental works were carried out at f=0.1 mm/rev and v=250 m/min.

Figure 6.11 (c) showed that when $f = 0.1$ mm/rev, the magnitude of calculated COF was $\mu = 0.66$. From the results shown in Figure 6.12 (a), when $\mu = 0.5$, the predicted results obtained from FE (Tool + Holder) were already over predicted when compared to experimental results. Further increasing the COF magnitude would increase the difference between predicted and experimental data. In Phase 3 work, this point was further

emphasized with parametric study, and that the calculated COF with varying feed rate (shown on Figure 6.11 (c)) could not be applied on FE cutting models.

Looking at the microstructure of the chip formed also gave constructive information on the contact behavior along the tool-chip interface. Figure 6.13 (a) shows the microstructure of inhomogeneous continuous chip. The formation of inhomogeneous chip was due to the effect of dual phase structure of ferrite and pearlite. The softer ferrite grains (white areas) deformed more readily than the hard pearlite grains (darker areas), thus softer ferrite grain went through larger plastic strain than the pearlite grains. The strain mismatch between ferrite and pearlite grains lead to the formation of the irregularities on the chip free surface [Simoneau, 2007]. Another distinct feature that should be observed of the microstructure of the chip is that there is a continuous and uniform zone of built up layer (BUL) on the underside of the chip. The BUL on the underside of the chip was due to the deformation along the tool chip interface also known as the secondary deformation zone. The formation of BUL was also observed in the FE cutting model built which is shown on Figure 6.13 (b). The cutting condition used for both Figure 6.13 (a) and (b) was the same. The result contour plot of equivalent plastic strain showed that there is a thin continuous and uniform layer which plastic strain was much severe than any other region on the chip. The extreme plastic deformation on the chip underside showed that the contact condition along the tool-chip interface. This thin layer of material underwent high strain, large stress and elevated temperatures. Under these extreme conditions, the thin layer of workpiece material behaved like a viscous fluid. Trent [2000] defined the zone along the tool-chip interface where intense shear

strain occurred as the *flow-zone*. The thickness of the flow zone observed by Trent [2000] was often on the order of 25-50 μm. He mentioned that the shear strain within the *flow-zone* region was much more severe than the shear plane. Under this intense shear strain, the work material, in many ways, behaved more like an extremely viscous fluid than a normal solid. Jasper and Dautzenberg [2002 b] also noticed the BUL on the microstructure of the chip, and commented that BUL resemblance with boundary layer formed as a fluid forced to flow over a flat plate.

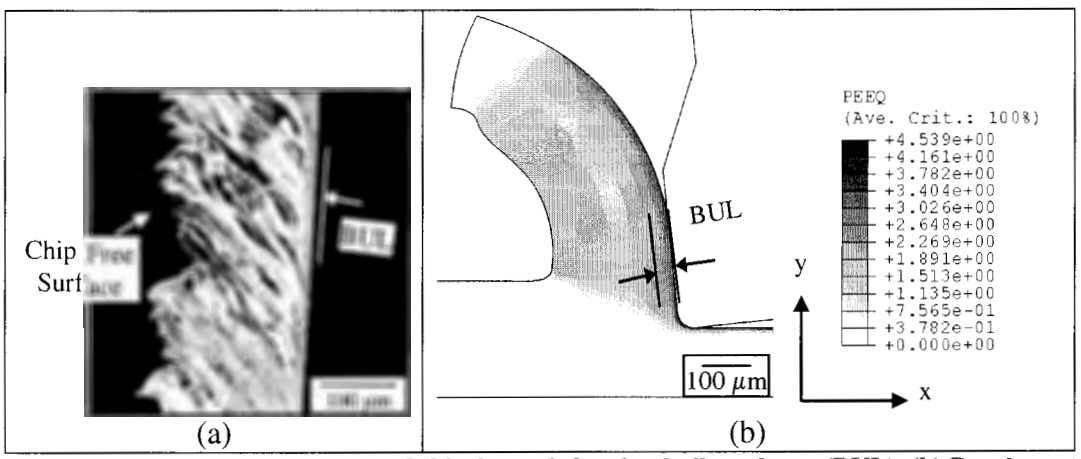

Figure 6.13: (a) Microstructure of chip formed showing built up layer (BUL). (b) Result contour plot of equivalent plastic strain when μ=0.1. Both figures were carried out at f=0.1 mm/rev, v=250 m/min.

6.2.3 Effect of Varying COF on General Steady-State Results

The use of Coulomb friction model with constant COF with cutting conditions was critiqued to have many limitations. The limitations were specifically directed at not being able to attain the extreme shear deformation on the tool cutting edge, and thus unable to capture the ploughing and the size effect on the cutting edge radius. Attempts on including tool cutting edge effect were done by increasing COF, or by applying different COF on the tool cutting edge and tool rake face [Haglund, 2008]. Authors who specifically investigated on the effect of tool cutting edge with FE cutting models agreed

on the research done by Albrecht [1960], and thus made attempts to continue and further improve the investigation [Arrazola, 2008]. In desperation to capture the ploughing effect in FE cutting models and solve the predicted F_t problem, friction models and COF values were being altered. Moreover, the values of COF on each different cutting condition are different. This contradicts with the early findings made by Albrecht [1960], who concluded that the same combination of tool and workpiece material, COF is constant with cutting conditions and COF is constant on the tool rake face. Due to the misconceptions regarding the limitations of employing Coulomb friction law in FE cutting models, it is thus critical to show the observations of some general steady state results when Coulomb friction law was being employed in FE cutting models. The effect of varying COF will also be discussed. Before further analyzing any results, the meaning of capturing tool cutting edge radius has to be clarified. The significant characteristics caused by tool cutting edge that researchers tried to capture in FE cutting models are:

1. Extreme plastic deformation and high temperature around the tool cutting edge radius that shows 'rubbing' of workpiece material,
2. Workpiece stagnant region on the tool cutting edge,
3. Size effect that influences the cutting force ratio,
4. Effect of tool cutting edge on chip formation,
5. Effect of tool cutting edge on chip formation through extrusion (micro-machining),
6. Size effect that influences temperature generation (micro-machining),
7. Effect of tool cutting edge on residual stresses,

Work done on Phase 2 explained point 1 and 2 of the tool cutting edge effect. Work done on Phase 3 illustrated point 3 and 4 of the tool cutting edge effect. Point 5, 6 and 7 of the tool cutting edge effect are beyond the scope of this thesis.

Figure 6.14 (a-f) compares the result contour plots of von mises stress, effective plastic strain and temperature on the tool-chip interface when two different values of COF (μ=0.1 and μ=0.5) were employed on FE cutting models. Several significant and obvious points could be made by observing these contour plots:

1. The extreme plastic deformation and temperature on the tool cutting edge was captured in FE cutting models when simple Coulomb friction model was employed.
2. Von mises stress on the tool chip interface was higher when μ=0.1 than when μ=0.5.
3. Equivalent plastic strain and temperature on the tool-chip interface were higher when μ=0.5 than when μ=0.1.
4. Chip thickness and contact length were higher when μ=0.5.

Shi et. al. [2002] used Lagrangian formulation to do research on the effect of COF on metal cutting in FEM. Shi et. al. [2002] comprehended that increase in COF caused increase in magnitude of stress on the tool-chip interface However, by looking at the contour plots shown on Figure 6.14 (a-f), it showed that increasing COF caused the region on tool-chip interface to increase equivalent plastic strain, temperature, contact length and decreased von mises stress. The increase in stress on the tool rake face as COF

value increased was also observed by Shet and Deng [2000], however, no explanation was offered with regards to that behavior.

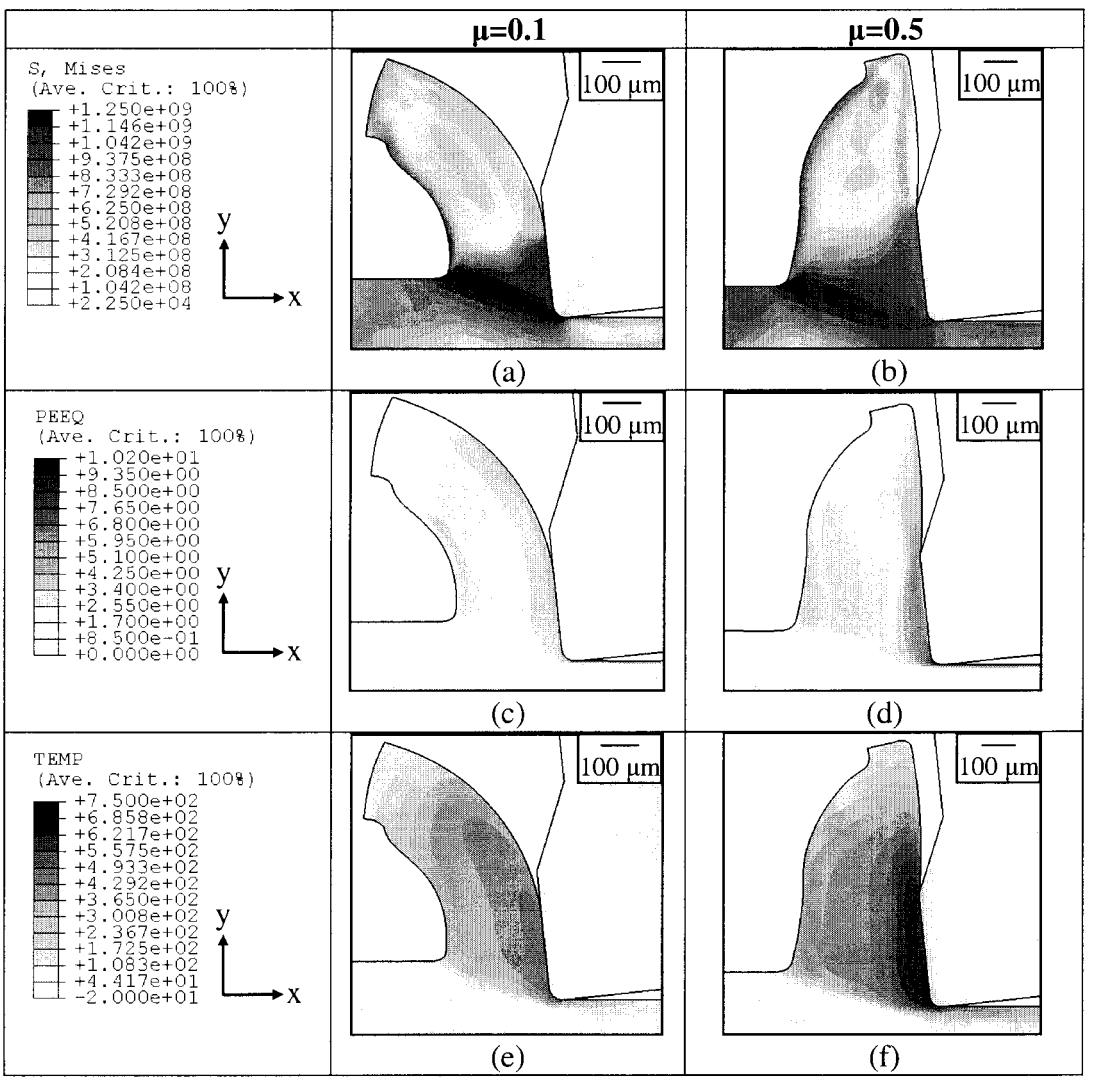

Figure 6.14: Result contour plots of tool-chip interface. Cutting condition is f=0.1 mm/rev and v=250 m/min. (a) and (b) von mises stress when μ=0.1 and μ=0.5 respectively. (c) and (d) Equivalent plastic strain when μ=0.1 and μ=0.5 respectively. (e) and (f) change in temperature when μ=0.1 and μ=0.5 respectively. All models include tool holder geometry.

In order to comprehend the behavior observed in Figure 6.14, it is crucial to understand the fundamentals of contact algorithm in FE codes and workpiece flow stress equation. As elaborated in Section 3.3, increasing COF in FE model did not increase the contact stresses, but caused the sticking region on the tool-chip interface to increase. When

sticking region increased, the equivalent plastic strain on the tool-chip interface also increased, causing higher plastic deformation to occur. Higher plastic deformation caused higher heat generation, thus increasing the temperature on the tool-chip interface.

It was factual in metal plasticity that high strain creates high stress; however Figure 6.14 (b) did not show the higher stress behavior as expected, the stress on the tool-chip interface decreased instead. The decrease in stress value on the tool chip interface while strain increased could be explained by understanding the Johnson-Cook material flow stress equation used (shown in Figure 6.15). The stress on the tool-chip interface did not increase when strain increased because the workpiece material AISI 1045 is sensitive to temperature change. Increase in temperature caused the stress to decrease. Therefore, even though the equivalent plastic strain on the tool-chip interface increased, the heat generation due to increase in plastic deformation caused a temperature increase significant enough to decreases stresses.

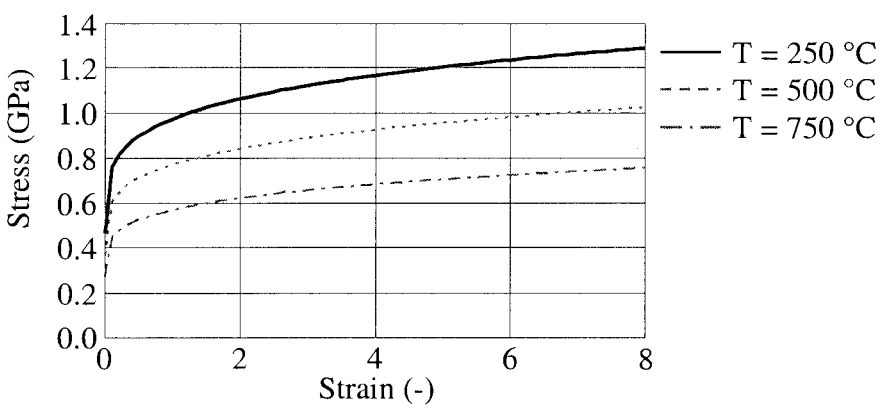

Figure 6.15: Stress-strain curve behavior of Johnson Cook equation for workpiece AISI 1045 with different temperature.

Another subject to be discussed is that employing simple Coulomb friction law on FE cutting models could also capture the stagnant region on the tool cutting edge. Figure

6.16 (a) and (b) shows the velocity profile when μ=0.1 and μ=0.5 respectively. On velocity profile, workpiece material stagnant region on the tool cutting edge occured when magnitude of velocity was close to zero. Stagnant region was formed due to the entrapment of workpiece material underneath the rounded tool cutting edge. The stagnant region formed acted as the first effective cutting edge [Nasr, 2007]. Beyond the stagnant region, the workpiece material flowed above the stagnated metal region to form chip, or flowed below the stagnated metal region and pressed into the newly machined surface. From the contour plots shown, it is visible that increase in COF caused the stagnant region formed to increase (indicating sticking region).

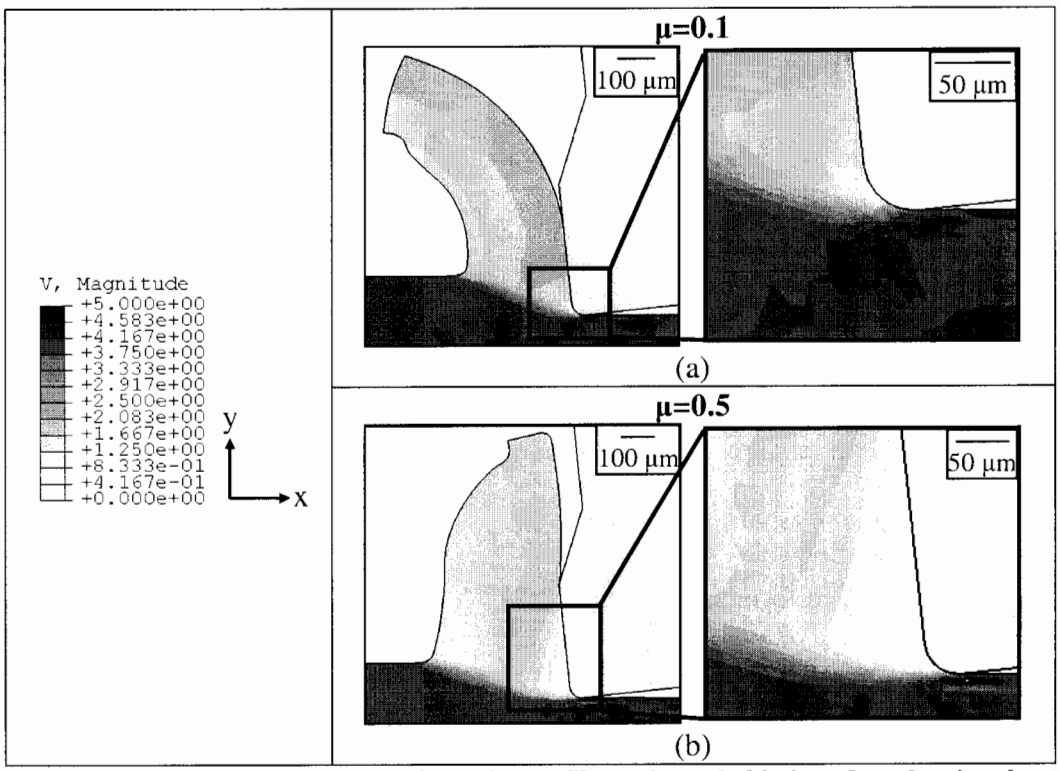

Figure 6.16: Result contour plots of velocity profile on the tool-chip interface showing the stagnant region when (a) μ=0.1 and when (b) μ=0.5. Cutting condition is f=0.1 mm/rev, v=250 m/min. Both models include tool holder geometry.

By examining Figure 6.16 (b) (When μ=0.5), the stagnant region occurred not only around the tool cutting edge, but extended all the way to the tool rake face. The shape of the large stagnant region formed was not rounded, but formed a right angled triangular shape positioned at an angle that created low shear angle on the primary shear zone. The low shear angle thus caused the large chip thickness to be formed. The large stagnant region ahead of the tool cutting edge also increased the 'rubbing' action against the machined surface. When μ=0.1, stagnant region also formed on the cutting edge region, however at a much smaller size. By observing Figure 6.16 (a), even though stagnant region formed was small when μ=0.1, the shape and position of the stagnant region still had a large influence on the shear angle formed. This further demonstrated the importance of effect of COF on the formation of stagnated metal zone.

Experimental validation to investigate the stagnated metal region formed was not carried out. The quick-stop experimental work found from the literature that had cutting parameter similar to the one being simulated in Figure 6.16 was done by Jasper and Dautzenberg [2002 b]. To comprehend how stagnated metal zone was formed, Jasper and Dautzenberg did a quick-stop experiment on AISI 1045 workpiece, collected the chip root. Figure 6.17 (b) shows the chip root picture taken from quick-stop experiment, and Figure 6.17 (a) shows the velocity contour plots obtained from FE cutting model when μ=0.1. Even though the cutting conditions used were not exactly the same, the picture obtained by Jasper and Dautzenberg [2002 b] still revealed information regarding the shape and size of the stagnated zone on the tool cutting edge region. The shape and size of the stagnated zone shown in Figure 6.17 (a) and (b) are similar. The area of stagnant

region obtained experimentally was much smaller than the one obtained from FE cutting model when μ=0.5. This further emphasized that COF calculated using merchant's circle could not be used in FE cutting models. It would be interesting to further investigate and study the formation and effect of the stagnated metal zone in metal cutting.

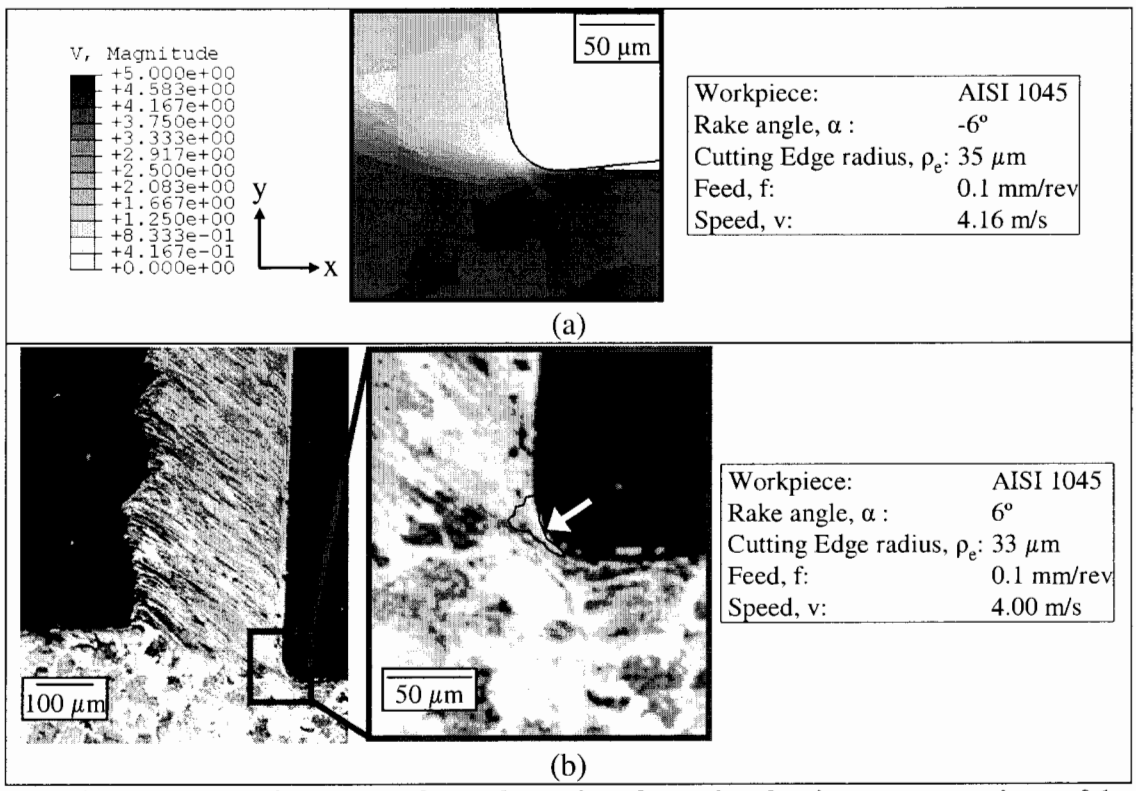

Figure 6.17: (a) the velocity contour plot on the cutting edge region showing stagnant region, μ=0.1. (b) chip root taken from quick-stop experiment, arrow indicating stagnant region [Jaspers, 2002 b].

6.3 PHASE 3: PARAMETRIC STUDY

The main objective of Phase 3 was to do a parametric study on the findings from Phase 1 and Phase 2. Results from Phase 1 shows that F_t could be predicted when the tool holder geometry was included into FE cutting models. Calibration of COF result from Phase 2 showed that μ=0.1 should be used for this particular combination of tool and workpiece material. However, the work done on Phase 1 and Phase 2 was only based on

one cutting condition. Therefore, Phase 3 of the work made use of the results obtained from Phase 1 and 2, and further tested the results with different cutting conditions. The flow chart for Phase 3 methodology is shown in Figure 6.18.

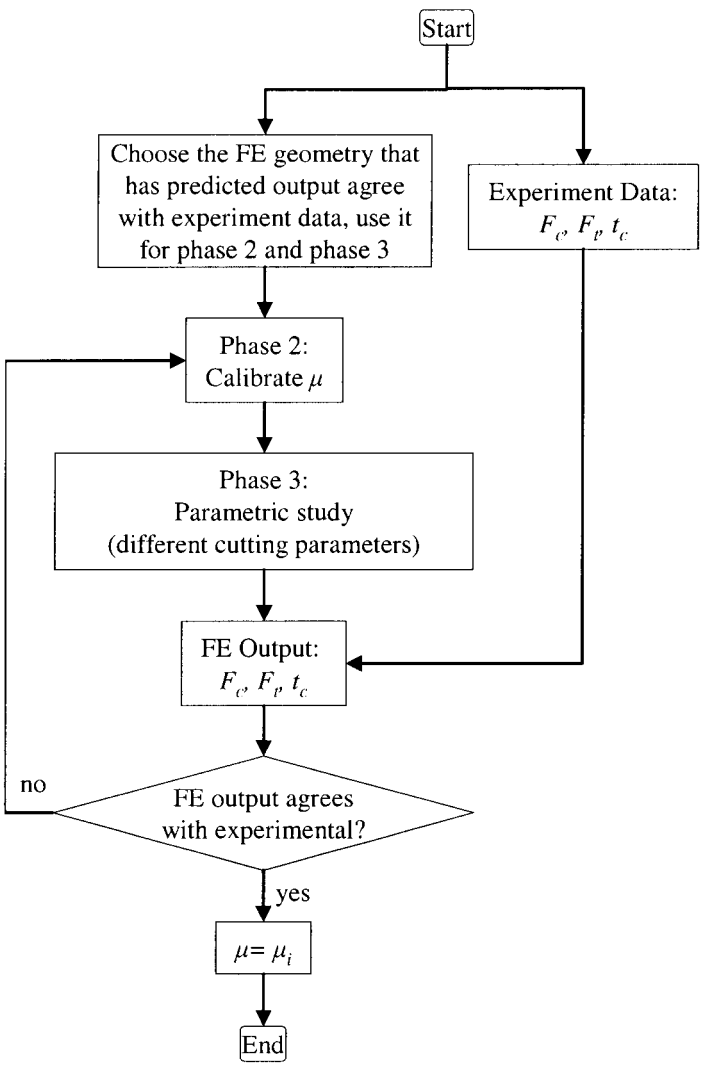

Figure 6.18: Flow chart for Phase 3 methodology.

Table 6.4 shows the test matrix for Phase 3 work. The effect of three different speeds and three different feeds were tested using COF of μ=0.1. Comparison of predicted forces and chip thickness with experimental data were made and discussed. Phase 3 work was

also to show that magnitude of COF to be used in FE models was not a function of process parameter, but a function of tool and workpiece material combination. The FE cutting models which did not include tool holder geometry were also included into Phase 3 test matrix. This was done for comparison purposes.

		FE (Tool)			FE (Tool + Holder)			Experiment		
Speed, v (m/min)		150	200	250	150	200	250	150	200	250
Feed, f (mm/rev)	0.05	√	√	√	√	√	√	√	√	√
	0.10	√	√	√	√	√	√	√	√	√
	0.20	√	√	√	√	√	√	√	√	√

Table 6.4: Phase 3 test matrix. All FE cutting models used μ=0.1.

6.3.1 Predicted Forces Analysis

Before analyzing the predicted forces obtained from FE cutting models, forces obtained experimentally were analyzed. Figure 6.19 (a) shows the effect of feed rate f and cutting speed v on the forces obtained experimentally. Both F_c and F_t increased with increasing feed rate. However, F_c increased more significantly than F_t with feed rate. As explained earlier in Section 6.2.1, this was due to the size effect. The size effect of varying feed rate on forces obtained could be illustrated clearly with the cutting force ratio obtained, see Figure 6.19 (b). With the speed range being tested, cutting speed had little effect on both F_c and F_t. This showed that the workpiece material was strain rate insensitive. The strain rate insensitive behavior of AISI 1045 was also being illustrated by the constant on Johnson-Cook material flow tress equation. AISI 1045 had a strain rate index C of 0.0132. The low value of strain rate index in J-C equation indicated that strain rate (cutting speed) had little effect on the stress strain behavior of the workpiece material.

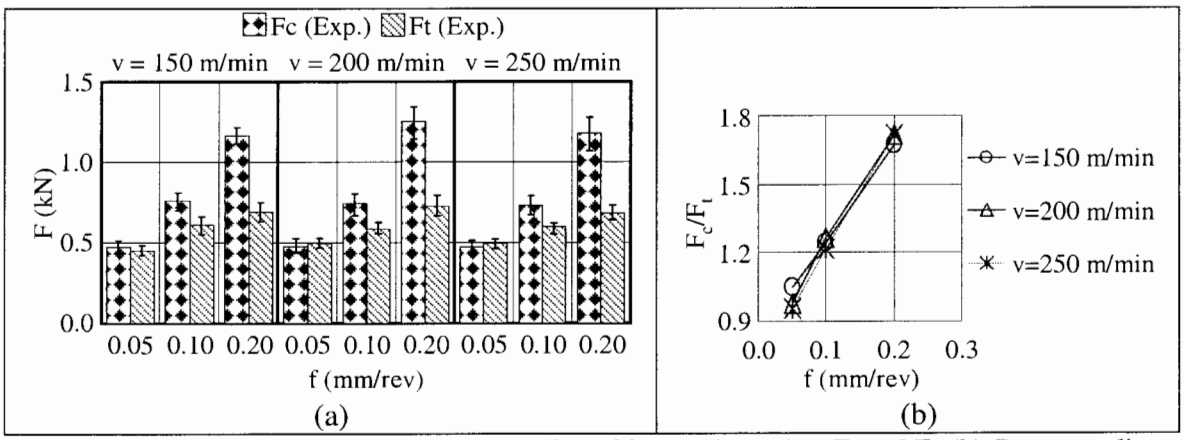

Figure 6.19: (a) Experimental results on the effect of feed and speed on F_c and F_t. (b) Corresponding cutting force ratio (F_c/F_t) obtained experimentally.

Parametric study of comparison of predicted F_c with experimental results is shown in Figure 6.20. Bear in mind that the results obtained from all FE cutting models used COF μ=0.1. Both FE (Tool) and FE (Tool + Holder) produced similar predicted F_c values. This showed that, even with varying cutting conditions, the tool holder geometry had little effect on the predicted F_c. Predicted F_c obtained increased with increasing feed rate, and similar with the trend obtained from experimental results, cutting speed v had little effect on F_c. Another interesting observation was that, F_c was under predicted at a low feed rate of 0.05 mm/rev, and F_c became over predicted as feed rate increased to 0.2 mm/rev. This different trend made at different feed rates was most probably due to the fact that the microstructure effect of workpiece material was not taken into consideration in the FE models. Without including the microstructure of workpiece material, the ploughing effect at low feed rate could not be fully captured, causing the predicted F_c to be lower than experimental results.

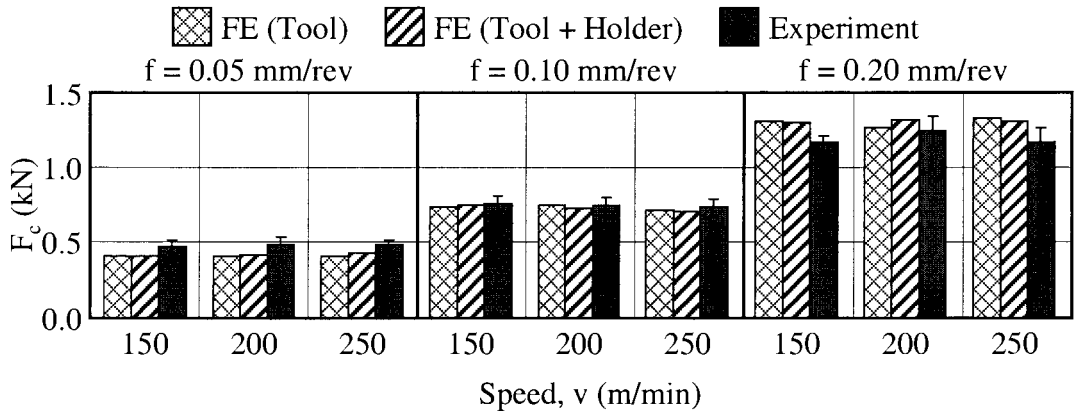

Figure 6.20: Comparison of predicted and experimental F_c with the effect of feed rate f and cutting speed v. All FE cutting models used μ=0.1.

The parametric study of comparison of predicted F_t with experimental results is shown in Figure 6.21. Predicted F_t obtained from both FE (Tool) and FE (Tool + Holder) increased with increasing feed rate, and like the trend obtained from experimental results, cutting speed has little effect on F_t. An important observation from the result shown was that at all cutting conditions, the FE cutting models which excluded tool holder geometry FE (Tool) could not predict F_t close to experimental results (maximum difference of 53%); while the FE models which included tool holder , FE (Tool + Holder) was able to predict Ft close to experimental results (maximum difference of 16%). With the parametric study made, it is evident that the under predicted thrust force F_t problem could be fixed by including the tool holder geometry into FE cutting models. Also, this showed that increasing COF is no a viable solution to fixing the under predicted *Ft*; with the same tool and workpiece material combination, COF used in FE cutting model should not be a function of cutting conditions.

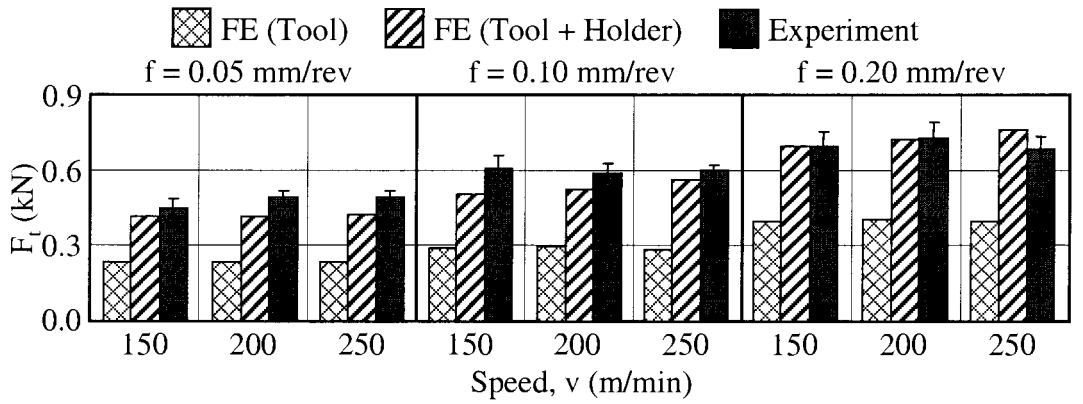

Figure 6.21: Comparison of predicted and experimental F_t with the effect of feed rate f and cutting speed v. All FE cutting models used μ=0.1.

Overall, predicted F_c and F_t made by FE (Tool + Holder) could capture the same trends of varying feed rate and varying cutting speed that was obtained experimentally. Most importantly, FE (Tool + Holder) could capture trend of cutting force ratio shown on Figure 6.22. Bear in mind that the predicted results in Phase 3 work were all obtained by using a constant COF of μ=0.1.

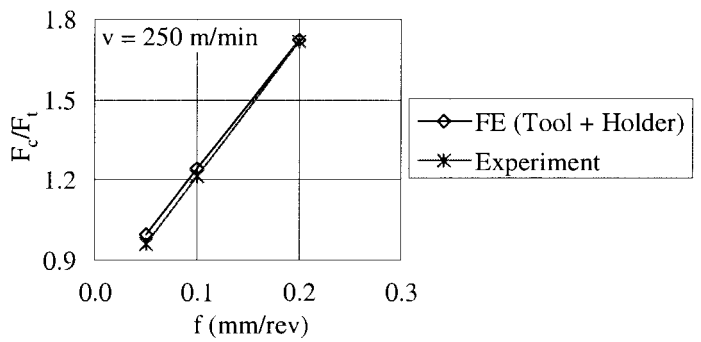

Figure 6.22: Comparison of predicted cutting force ratio (F_c/F_t) with experimental results.

6.3.2 Chip Formation Analysis

The pictures of microstructure of the chips obtained experimentally are shown on Figure 6.23. The chips obtained were all inhomogeneous continuous chips. The inhomogeneous deformation of the chip was due to the non-uniformly distributed

microstructure of the workpiece material. This inhomogeneous continuous chip could not be obtained by the FE cutting models built in this work; this was because of the assumption of homogenous workpiece material. By looking at the free surface of the chip, the inhomogeneous deformation on the chip was most severe at low feed rate of 0.05 mm/rev. This was because the average pearlite grain size of the workpiece microstructure was 103 μm, which was larger than the feed rate. Take note that on all the chips, there was always BUL on the chip underside.

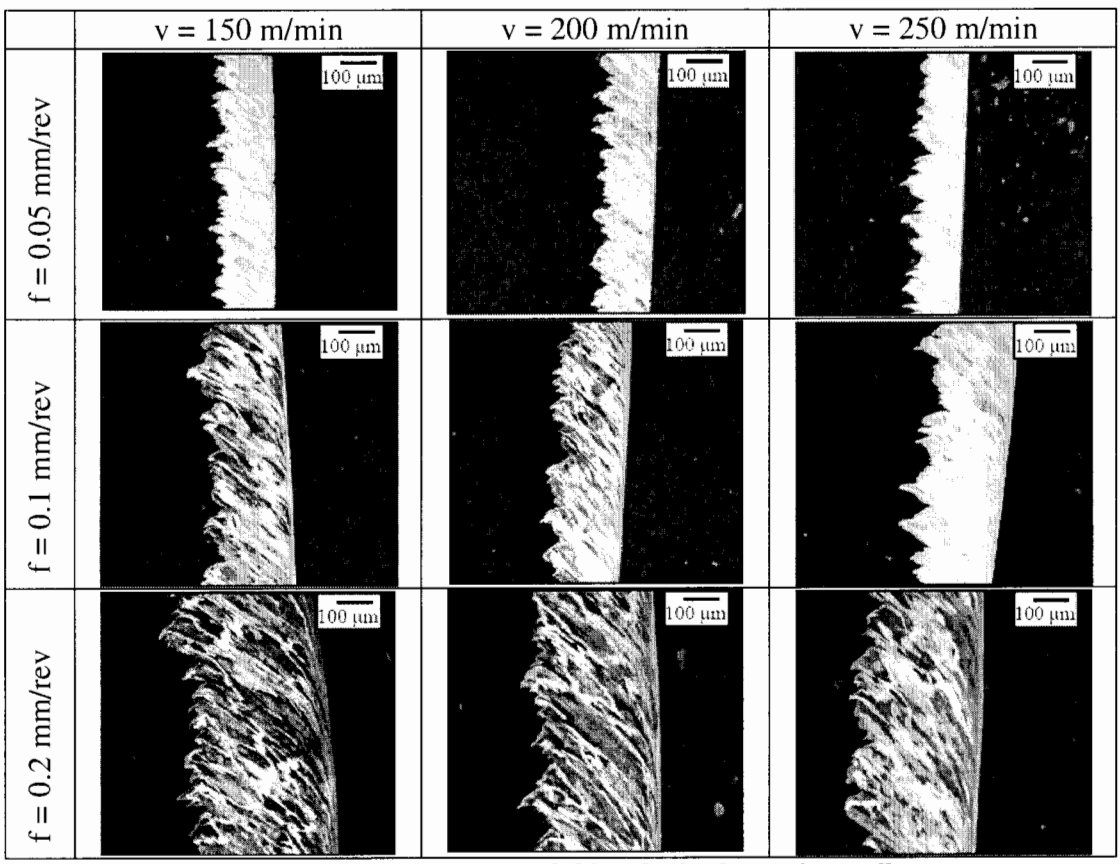

Figure 6.23: Microstructure of chips obtained experimentally.

Figure 6.24 (a) shows the experimental results on the effect of feed and speed on the chip thickness t_c. Chip thickness t_c increased with increasing feed rate f. A more effective way to analyze the effect of feed and speed on chip thickness was to look at the

cutting ratio (f/t_c) obtained, shown in Figure 6.24 (b). The cutting ratio obtained was always less than one, because t_c formed were always thicker than feed rate. Cutting ratio increased with increasing feed rate, and the trend was non-linear. At a low feed rate of 0.05 mm/rev, t_c formed was much larger than the feed rate (t_c ~2.5 times thicker than f); at high feed rate of 0.2 mm/rev, the t_c formed was closer to the value of feed rate (t_c ~1.5 times thicker than f). This was due to the combination of size effect caused by cutting edge radius and also due to the effect of workpiece microstructure. Within the range of speed tested, the cutting ratio obtained showed that increasing cutting speed caused t_c to decrease, however, the effect of cutting speed on t_c obtained was small.

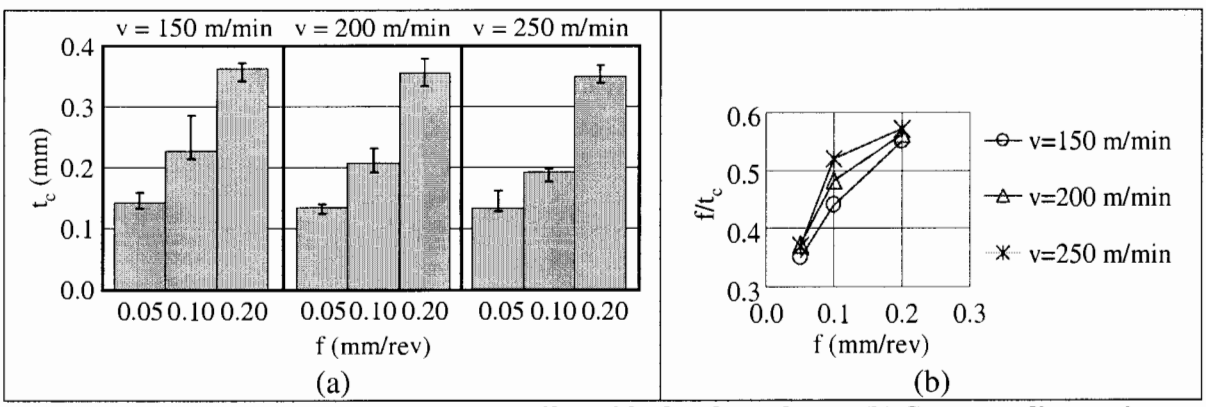

Figure 6.24 (a) Experimental results on the effect of feed and speed on t_c. (b) Corresponding cutting ratio (f/t_c) obtained experimentally.

Figure 6.25 explained the size effect caused by cutting edge radius on t_c formed. Figure 6.25 (a) and (b) illustrate the different effective rake angle (α) due to the effect cutting edge radius (ρ_e) at different feed rate. At a high feed rate (Figure 6.25 a), the tool rake angle was the effective rake angle acting on the workpiece material. As the feed rate decreased and approached cutting edge radius (Figure 6.25 b), the effective rake angle was no longer the tool rake angle and became more negative. When the effective rake

angle became more negative, the shear angle formed decreased and caused the chip formed to be thicker.

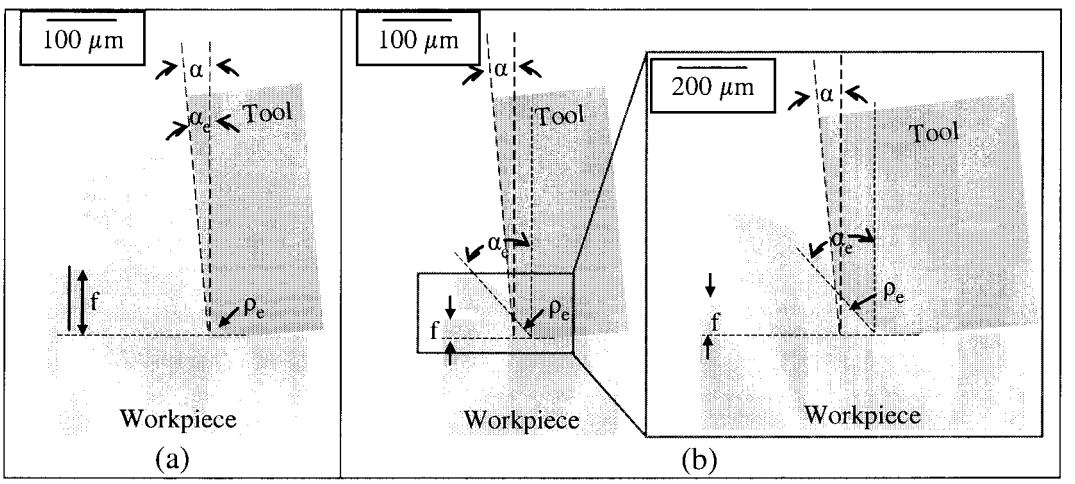

Figure 6.25: Effective rake angle α at (a) feed rate f higher than cutting edge radius ρ_e, and at (b) feed rate f near the cutting edge radius ρ_e.

The parametric study of comparison of predicted t_c with experimental results is illustrated in Figure 6.26 . Both FE (Tool) and FE (Tool + Holder) produced similar predicted t_c values. Similar with the trend obtained experimentally, increasing cutting speed caused the predicted t_c to decrease, however the effect was little. Bear in mind that the observations made were based on a limited range of cutting speed. The difference between predicted t_c with experimental data increased as feed rate increased (maximum of 25% from experimental results).

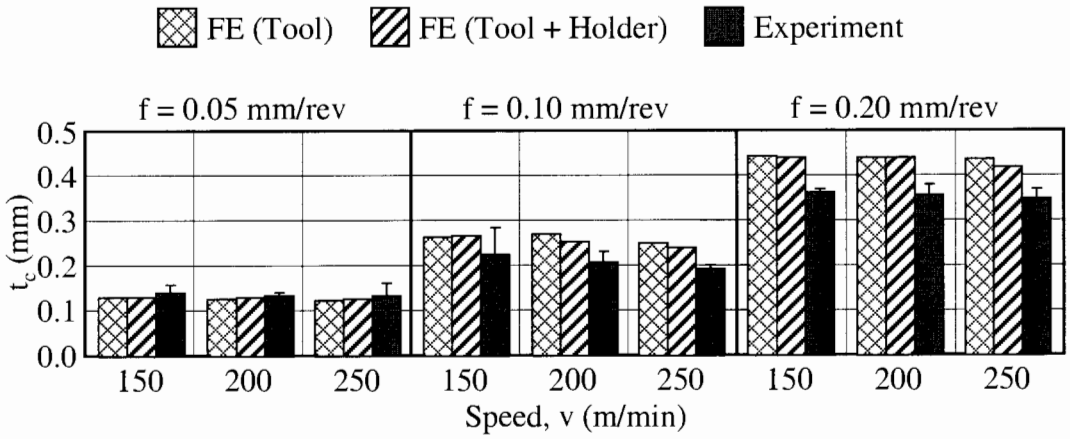

Figure 6.26: Comparison of predicted and experimental t_c with the effect of feed rate f and cutting speed v. All FE cutting models used μ=0.1.

Figure 6.27 shows predicted cutting ratio compared with experimental results. The predicted cutting ratio did not capture the significant drop in cutting ratio when feed rate was at 0.05 mm/rev. This effect was expected as it was mentioned that including workpiece microstructure became increasingly important as feed rate decreased. Thus by eliminating microstructure effect, some trends made by experimental results could not be captured by FE cutting models. The over predicted t_c (over predict by maximum of 25%) made by FE cutting models might be due to the constant value of the strain hardening index n in J-C flow stress equation. The constants value n of J-C equation available from literature might be higher than the actual value due to variation of workpiece material.

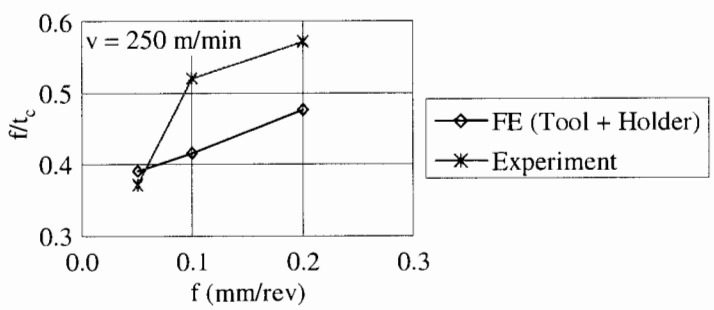

Figure 6.27: Comparison of predicted cutting ratio with experimental results at v=250 m/min, μ=0.1.

7 CONCLUSION

7.1 LITERATURE REVIEW

- ALE formulation in FE cutting models cannot be used effectively by only including adaptive mesh option. This is because severe mesh distortion around the tool cutting edge still persisted. Besides including adaptive mesh option, ALE formulation in FE cutting models should include pure Eulerian region around the tool cutting edge radius, then severe mesh distortion and chip separation criterion could be prevented. Refer to Figure 3.9 for partitioning scheme on the workpiece geometry when employing ALE formulation in FE cutting models.
- Detailed literature search on employing different friction models, different friction constants, different commercial FE codes and different process parameters showed that FE cutting models could not successfully predict both F_c and F_t that agree with experimental work. Past researched on force prediction were all carried out without including tool holder geometry.

7.2 RESULT AND DISCUSSION

- FE (Tool), FE (Tool + Holder) and FE (Tool + Holder + WP) produced similar predicted F_c and t_c. The predicted F_c and t_c obtained by the three FE cutting models agreed well within 4% and 13% difference with experimental data respectively.
- FE (Tool) predicted F_t that has 52% difference with experimental results. FE (Tool + Holder) and FE (Tool + Holder + WP) predicted feed force F_t that has 6% and 13%

difference with experimental data respectively. This shows that the missing tool holder geometry is the factor that caused under predicted F_t.

- In FE (Tool), the oscillation of force signatures obtained gradually decayed from a maximum value to a steady state value. Thus showing FE cutting models built are stable underdamped system.
- Oscillation of F_c signature obtained from FE (Tool) settled between its maximum and minimum value, therefore value of predicted F_c will be obtained by taking the average value form the F_c signature.
- Oscillation of F_t signature obtained from FE (Tool) settled at it maximum value, therefore value of predicted F_t will be obtained by taking the average of the peak values from the F_t signature.
- Including the tool holder and workpiece geometry into FE cutting model had influenced its dynamic system due to the change in overall structured stiffness and damping properties.
- In FE (Tool + Holder) and FE (Tool + Holder + WP): F_c and F_t signatures obtained were still within the transition region of an underdamped system. The model FE (Tool + Holder) and FE (Tool + Holder + WP) were not built long enough to reach steady state. Therefore, it was hypothesized that F_c and F_t signal will reach steady state at its average value and maximum value respectively.
- FE (Tool + Holder + WP) is computationally more expensive than FE (Tool + Holder). Since force and deflection oscillation signatures obtained by both FE (Tool + Holder)

and FE (Tool + Holder + WP) were similar in terms of pattern and magnitude, therefore FE (Tool + Holder) was chosen to carry out phase 2 and phase 3.

- COF calculated using Merchant's circle kept changing with process parameter, which is not in agreement with Albrecht [1960] conclusion.
- A new method of acquiring COF to be used in FE cutting model was presented. The magnitude of COF to be used in FE cutting models depended on how well the FE output (F_c, F_t and t_c) agree with experimental data. COF calibrated could only be used for the same pair of tool and workpiece material, however, COF should remain constant with varying process parameter.
- Increasing value of COF caused predicted F_c, F_t and t_c to increase. COF at 0.1 was able to produce good combinations of predicted F_c, F_t and t_c that agreed well with experimental results.
- Stagnated region formation on the tool cutting edge was captured by the FE cutting models built. The size of the stagnated region increases with COF.
- COF of 0.1 produced stagnated region that had similar shape and size to the chip root pictures taken by Jasper [2002 b]. COF of 0.5 produced stagnated region that was at least 5 times bigger than the one obtained by Jasper [2002 b] experimentally. This shows that increasing COF is not the right solution to capture ploughing.
- During parametric study, FE (Tool + Holder) using constant COF of 0.1 could produce both predicted F_c, F_t and t_c that have maximum difference of 14%, 16% and 25% when compared to experimental results respectively.

- Experimental results showed that cutting force ratio (F_c/F_t) increases with higher feed rate. This was due to the size effect. The trend and magnitude of increasing cutting force ratio (F_c/F_t) with feed rate could also be captured by FE (Tool + Holder).
- With the cutting speeds and feed rates tested experimentally, the chip form obtained was all inhomogeneous continuous chips. The cutting ratio (f/t_c) obtained experimentally increased with higher feed. This was due to the size effect. FE (Tool + Holder) could capture the trend of increasing cutting ratio (f/t_c) with feed rate. However, the drastic increase in cutting ratio (f/t_c) when feed rate change from 0.05 mm/rev to 0.1 mm/rev was not capture. This effect was due to the assumption of homogeneous workpiece material made by FE (Tool + Holder). Including workpiece microstructure effect becomes increasingly important as feed rate decreases.
- Parametric study showed that, with the same combination of tool and workpiece material, constant calibrated COF should be used in FE cutting models.

8. FUTURE WORKS

- Carry out experimental work and simulate FE (Tool + Holder) using different tool cutting edge radii. This work is to emphasize that it is unnecessary to increase COF in FE models to capture ploughing action around the tool cutting edge radius.
- Use a different combination of tool and workpiece material to calibrate COF and carry out parametric study. The results obtain here would confirm that:
    (a) COF changes with different combination of tool and workpiece material,
    (b) Value of COF will remain the same with changing process parameter.
- Carry out calibration of friction constants using other friction models (Model II to model VI) with FE (Tool + Holder). Do parametric study on each different friction models using the calibrated friction constants. Compare the predicted results and conclude on the ability of each different friction models.
- Investigate the ability of different friction models on predicting tool-chip contact length.
- Investigate on acquiring damping ratio of the tool holder structure, and applying it into FE cutting models that include tool holder geometry. This work could significantly decrease simulation time and allow shorter settling time, thus steady state predicted forces could be obtained.
- Re-design meshing scheme in order for FE (Tool + Holder) to be able to have a longer cut. The purpose of a longer cut is to obtain steady state forces signatures.

- Investigate the effect of including the workpiece microstructure properties into FE cutting models with ALE formulation.

9. REFERENCE

[ABAQUS, 2003] Hibbit H. D., Karlsson B.I. and Sorrensen, 2003, ABAQUS Online Documentation: Version 6.4-1, ABAQUS Inc.

[Albrecht, 1960] Albrecht P., 1960, 'New Developments in the Theory of the Metal Cutting Process Part I.', Journal of Engineering for Industry, Vol. 83, p. 348 – 358

[Arrazola, 2008] Arrazola P.J., Ugarte D., Dominguez X., 2008, 'A New Approach for the Friction Identification during Machining Through the use of Finite Element Modeling', International Journal of Machine Tools & Manufacture, Vol. 48, p. 173-183

[Arsecularatne, 1998] Arsecularatne J. A., Fowle R.F., Mathew P., 1998, 'Prediction of Chip Flow Direction, Cutting Forces and Surface Roughness in Finish Turning', Journal of Manufacturing Science and Engineering, Vol. 120 (1), p. 1-12

[Baker, 2003] Baker M., 2003, 'The Influence of Plastic Properties on Chip Formation', Computational Materials Science, Vol. 28, p.556-562

[Balaji, 1999] Balaji A. K., Sreeram G., Jawahir I. S., Lenz E., 1999, 'The Effects of Tool Thermal Conductivity on Tool-Chip Contact Length and cyclic Chip Formation in Machining with Grooved Tools', Annals of the CIRP, Vol. 48 (1), p. 33-38

[Balaji, 2002] Balaji A. K., Mohan V. S., 2006, 'An 'Effective Cutting Tool Thermal Conductivity' Based Model for Tool-Chip Contact in Machining with Multi-Layer Coated Cutting Tools', Machining Science and Technology, Vol. 6(3), p. 415-436

[Berhrens, 1999] Berhrens A., Westhoff B., 1995, 'Finite Element Modeling of High Speed Machining Process', 2nd International Conference on High Speed Machining, p. 185-190

[Bil, 2004] Bil H., Kilic S.E., Tekkaya E., 2004, 'A Comparison of Orthogonal Cutting Data from Experiments with Three Different Finite Element Models', International Journal of Machine Tool & Manufacture, Vol. 44, p. 933-944

[Boothroyd, 89] Boothroyd G. and Knight W.A., 1989, Fundamentals Of Machining And Machine Tools, Marcel Dekker, ISBN 0-8247-7852-9

[Buryta, 1994] Buryta D., Sowerby R., Yellowley I., 1994, 'Stress Distributions on the Rake Face During Orthogonal Machining', International Journal of Machine Tools and Manufacture, Vol. 34, p. 721-739

[Ceretti, 1996] Ceretti E., Fallbohmer P., Wu W. T., Altan T., 1996, 'Application of 2D FEM to Chip Formation in Orthogonal Cutting', Journal of Materials Processing Technology, Vol. 59, p. 169-180

[Childs, 1990], Childs T. H. C., Maekawa K., 1990, 'Computer Aided Simulation and Experimental Studies of Chip Flow and Tool Wear in the Turning of Low Alloy Steels by Cemented Carbide Tools', Wear, Vol. 139, p. 235-250

[Childs, 2006] Childs T. H. C., 2006, 'Friction Modelling in Metal Cutting', Wear, Vol. 260, p. 310-318

[Coelho, 2007] Coelho R. T., Ng E-G, Elbestawi M. A., 2007, 'Tool Wear When Turning Hardened AISI 4340 with Coated PCBN tools using Finishing Cutting Conditions', International Journal of Machine Tools & Manufacture, Vol. 47, p. 263-272

[D'Errico, 1999] D'Errico G. E., Bugliosi S., Calzavarini R., Cuppini D., 1999, 'Wear of Advanced Ceramics for Tool Materials', Wear, Vol. 225-229, p. 267-272

[Dirikolu, 2001] Dirikolu M. H., Childs T. H. C., Maekawa K., 2002, 'Finite Element Simulation of Chip Flow in Metal Machining', International Journal of Mechanical Sciences, Vol. 43, p. 2699-2713

[Fang, 2003] Fang F. z., Zhang G. X., 2003, 'An Experimental Study of Edge Radius Effect on Cutting Single Crystal Silicon', International Journal of Advance Manufacturing Technology, Vol. 22, p. 703-707

[Fang, 2004] Fang G., Zeng P., 2004, 'Effects of Tool Geometrical Parameters on the Chip Formation and Cutting Force in Orthogonal Cutting', Material Science Forum, Vol. 471-472, p. 16-20

[Fang, 2007] Fang N., Fang G., 2007, 'Theoretical and Experimental Investigation of Finish machining with a rounded edge tool', Journal of Materials Processing Technology, Vol. 191 (1-3), p. 331-334

[Filice, 2007] Filice, L., Micari, F., Ruzzuti, S., Umbrello, D., 2007, 'A Critical Analysis on the Friction Modelling in Orthogonal Machining', International Journal of Machine Tools & Manufacture, vol. 47, p. 709-714

[Grezsik, 2005] Grzesik W., Bartoszuk M., 2002, 'Finite Element Modelling of Temperature Distribution in the Cutting Zone in Turnining Processes with Differently Coated Tools', Journal of Materials Processing Technology, Vol. 164-165, p. 1204-1211

[Grezsik, 2002] Grzesik W., Zalisz Z., Nieslony P., 2002, 'Friction and Wear Testing of Multilayer Coatings on Carbide Substrates for Dry Machining Applications', Surface and Coatings Technology, Vol. 155, p. 37-45

[Grezsik, 1999] Grzesik W., 1999, 'The Role of Coatings in Controlling the Cutting Process when Turning with Coated Indexable Inserts', Journal of Material Processing Technology, Vol. 79, p. 133-143

[Guo, 2002 a] Guo Y. B., Liu C. R., 2002, '3D FEA Modeling of Hard Turning', Journal of Manufacturing Science and Engineering, Vol. 124, p. 189-199

[Guo, 2002 b] Guo Y. B., Liu C. R., 2002, 'FEM Analysis of Mechanical State on Sequentially Machined Surfaces', Machining Science and Technology, Vol. 6(1), p. 21-41

[Haglund, 2008] Haglund A.J., Kishawy H.A., Rogers R.J., 2008, 'An Exploration of Friction Models for the Chip-tool Interface using an Arbitrary Lagrangian-Eulerian Finite Element Model', Wear, Vol. 265, 452 – 460

[Huang, 1996] Huang J. M., Black J. T., 1996, 'An Evaluation of Chip Separation Criteria for the FEM Simulation of Machining', Journal of Manufacturing Science Engineering, Vol. 118, p.545-554

[Iqbal, 2007 a] Iqbal S. A., Mativenga P. T., Sheikh M. A., 2007, 'Characterization of Machining of AISI 1045 Steel over a Wide Range of Cutting Speeds, Part I', Journal of Engineering Manufacture, Vol. 221, p. 909-916

[Iqbal, 2007 b] Iqbal S.A., Mativenga P.T., Sheikh M.A., 2007, 'Characterization of Machining of AISI 1045 Steel over a Wide Range of Cutting Speeds. Part 2', Journal of Engineering Manufacture, Vol. 221, p. 917 – 926

[Jasper, 2002 a] Jaspers S. P. F. C., Dautzenberg J. H., 2002, 'Material Behavior in Conditions Similar to Metal Cutting: Flow Stress in the Primary Shear Zone', Journal of Materials Processing Technology, Vol. 122, p. 322-330

[Jasper, 2002 b] Jasper S. P. F. C., Dautzenberg J. H., 2002, 'Material Behavior in Metal Cutting: Strains, Strain Rates and Temperature in Chip Formation', Journal of Materials Processing Technology, Vol. 121, p. 123-135

[Jawahir, 1993] Jawahir I. S., Luttervelt V., 1993, 'Recent Developments in Chip Control: Research and Applications, CIRP Annals, Vol. 45 (1), p. 659-693

[Joyot, 1998] Joyot P., Rakotomalala R., Pantelo O., Touratier M. and Hakem N., 1998, 'A Numerical Simulation Of Steady State Metal Cutting', Proceedings Of The Institution of Mechanical Engineers, Vol. 212, p. 331-341

[Kalhori, 2001] Kalhori V., Modelling and Simulation of Mechanical Cutting, Ph. D. Thesis, Lulea University of Technology, Lulea

[Karpat, 2008] Karpat Y., Ozel T., 2008, 'Mechanics of High Speed Cutting with Curvilinear Edge Tools', International Journal of Machine Tools & Manufacture, Vol. 48, p. 195-208

[Kato, 1972] Kato S., Yamaguchi K., Yamada M., 1972, 'Stress Distribution at the Interface between Tool and Chip in Machining', Journal of Engineering and Industry, Vol. 94 B, p. 683-689

[Kishawi, 2006] Kishawy H. A., Haglund A., Balazinski M., 2006, 'Modelling of Material Side Flow in Hard Turning', Annals of the CIRP, Vol. 55(1), p. 855-858

[Klocke, 2001] Klocke F., Raedt H. W., Hoppe S., 2001, '2D-FEM Simulation of the Orthogonal High Speed Cutting Process', Machining Science and Technology, Vol. 5(3), p. 323-340

[Komanduri, 1981] Komanduri R. and Brown R. H., 1981, 'On the Mechanics of Chip Segmentation in Machining', Journal of Engineering for Industry, Vol. 103, p. 33-51

[Komanduri, 1986] Komanduri R. and Schroeder T.A., 1986, 'On Shear Instability On Machining A Nickel-Iron Based Superalloy', Journal of Engineering For Industry, Vol. 108, p. 93-100

[Komvopoulos, 1991] Konvopoulos K. and Erpenbeck S.A., 1991, 'Finite Element Modelling Of Orthogonal Metal Cutting', Journal Of Engineering For Industry, Vol. 113, p. 253-267

[Lee, 1995] Lee L. C., Liu X. D., Lam, K. Y., 1995, 'Determination of Stress Distribution on the Tool Rake Face using a Composite Tool', International Journal of Machine Tools & Manufacture, Vol. 35 (3), P. 373-382

[Li, 2002] Li K., Gao X. L., Sutherland J. W., 2002, 'Finite Element Simulation of the Orthogonal Metal Cutting Process for Qualitative Understanding of the Effects of Crater Wear on the Chip Formation Process', Journal of Materials Processing Technology, Vol. 127, p. 309-324

[Lin, 2001] Lin Z. C., Lo S. P., 2001, '2-D Discontinuous Chip Cutting Model by Using Strain Energy Density Theory and Elastic Plastic Finite Element Method', International Journal of Mechanical Sciences, Vol. 43, p. 381-398

[Ling, 1966] Ling F. F., Whitely R. L., Ku P. M., Peterson M. B., 1966, Friction and Lubrication in Metal Processing, The American Society of Mechanical Engineers

[Liu, 2000] Liu C. R., Guo Y. B., 2000, 'Finite Element Analysis of the Effect of Sequential Cuts and Tool-Chip Friction on Residual Stresses in a Machined Layer', International Journal of Mechanical Sciences, Vol. 42, p. 1069-1086

[Liu, 2007] Liu K., Melkote S. N., 2007, 'Finite Element Analysis of the Influence of Tool Edge Radius on Size Effect in Orthogonal Micro-Cutting Process', International Journal of Mechanical Sciences, Vol. 49, p. 650-660

[Mamalis, 2001] Mamalis A. G., Horvath M., Branis A. S., Manolakos D. E., 2001, 'Finite Element Simulation of Chip Formation in Orthogonal Metal Cutting', Journal of Materials Processing Technology, Vol. 110, p. 19-27

[Marusich, 2001] Marusich T. D., Thiele J. D., Brand C. J., 2001, 'Simulation and Analysis of Chip Breakage in Turning Processes', www.thirdwavesys.com

[McClain, 2000] McClain B., Thean W., Maldonado G. I., Fang X. D., 2000, 'Finite Element Analysis of Chip Formation in Grooved Tool Metal Cutting', Machining Science and Technology, Vol. 4(2), p. 305-316

[McClain, 2002] McClain B., Batzer S. A., Maldonado G. I., 2002, 'A Numeric Investigation of the Rake Face Stress Distribution in Orthogonal Machining', Journal Materials Processing Technology, Vol. 123, p. 114-119

[Miguelez, 2006] Miguelez H., Zaera R., Rusinek A., Moufki A., Molinari A., 2006, 'Numerical Modelling of Orthogonal Cutting: Influence of Cutting Conditions and Separation criterion', Journal of Physics IV France, Vol. 134, p. 417-422

[Monaghan, 1999] Monaghan J., MacGinley T., 1999, 'Modelling the Orthogonal Machining Process using Coated Carbide Cutting Tools', Computational Materials Science, Vol. 16, p. 275-284

[Movahhedy, 2000 a] Movahhedy M. R., Gadala M. S., Altintas Y., 2000, 'Simulation of Orthogonal Metal Cutting Process using an Arbitrary Lagrangian-Eulerian Finite Element Method', Journal of Materials Processing Technology, Vol. 103, p. 267-275

[Movahhedy, 2000 b] Movahhedy M. R., Gadala M. S., Altintas Y., 2000, 'Simulation of Chip Formation in Orthogonal Metal Cutting Process: an ALE Finite Element Approach', Machining Science and Technology, Vol. 4 (1), p. 15-42

[Nasr, 2007] Nasr M. N. A., Ng E-G, Elbestawi M. A., 2007, 'Modelling the Effects of Tool-Edge Radius on Residual Stresses when Orthogonal Cutting AISI 316L', International Journal of Machine Tools & Manufacture, Vol. 47, p. 401-411

[Ng, 2002 a] Ng E-G, Aspinwall D. K., 2002, 'Modelling of Hard Part Machining', Journal of Materials Processing Technology, Vol. 127, p. 222-229

[Ng, 2002 b] Ng E-G, El-Wardany T. L., Dumitrscu M., Elbestawi M. A., 2002, 'Physics-Based Simulation of High Speed Machining', Machining Science and Technology, Vol. 6 (3), p. 301-329

[Obikawa, 1996] Obikawa T., Usui E., 1996, 'Computational Machining of Titanium Alloy - Finite Element Modeling and a Few Results', Journal of Manufacturing Science and Engineering, Vol. 118 (2), p. 208-215

[Ohbuchi, 2003] Ohbuchi Y., Obikawa T., 2003, 'Finite Element Modeling of Chip Formation in the Domain of Negative Rake Angle Cutting', Journal of Engineering Materials and Technology, Vol. 125, p. 324-332

[Oxley, 89] Oxley P.L.B., 1989, Mechanics Of Machining: An Analytical Approach To Assessing Machinability, Ellis Horwood Limited, ISBN-0-7458-0007-6

[Ozel, 2000] Ozel T., Altan T., 2000, 'Determination of Workpiece Flow Stress and Friction at the Chip-Tool Contact for High-Speed Cutting', International Journal of Machine Tools & Manufacture, Vol. 40, p. 133-152

[Ozel, 2006] Ozel T., 2006, 'The Influence of Friction Models on Finite Element Simulations of Machining', International Journal of Machine Tools & Manufacture, Vol. 46, p. 518-530

[Ozel, 2007] Ozel T., Erol Z., 2007, 'Finite Element Modeling the Influence of Edge Roundness on the Stress and Temperature Fields Induced by High-Speed Machining', International Journal of Advance Manufacturing Technology, Vol. 35, p. 255-267

[Raczy, 2004] Raczy A., Elmadagli M., Altenhof W. J., Alpas A. T., 2004, 'An Eulerian Finite-Element Model for Determination of Deformation State of a Copper Subjected to Orthogonal Cutting', Metallurgical and Materials Transactions A, Vol. 35A, p.2393-2400

[Rech, 2006] Rech J., 2006, 'Influence of Cutting Tool Coatings on the Tribological Phenomena at the Tool-Chip interface in Orthogonal Dry Turning', Surface & Coatings Technology, Vol. 200, p. 5132-5139

[Sartkulvanich, 2005] Sartkulvanich P., Altan T., Gocmen A., 2005, 'Effects of Flow Stress and Friction Models in Finite Element Simulation of Orthogonal Cutting - A Sensitivity Analysis', Machining Science Technology, Vol. 9(1), p. 1-26

[Shaw, 2005] Shaw M. C., 2005, Metal Cutting Principles, Oxford Series on Advanced Manufacturing, ISBN-019514263

[Shet, 2000] Shet C., Deng X., 2000, 'Finite Element Analysis of the Orthogonal Metal Cutting Process', Journal of Materials Processing Technology, Vol. 105, p. 95-109

[Shi, 2002] Shi G., Deng X., Shet C., 2002, A Finite Element Study of the Effect of Friction in Orthogonal Metal Cutting, Finite Elements in Analysis and Design, Vol. 38, p.863-883

[Shi, 2004] Shi J., Liu C. R., 2004, 'The Influence of Material Models on Finite Element Simulations of Machining', Journal of Manufacturing Science and Engineering, Vol. 126, p. 849-857

[Shih, 1996] Shih A. J., 1996, 'Finite Element Analysis of the Rake Angle Effects in Orthogonal Metal Cutting', International Journal of Mechanical Science, Vol. 38(1), p. 1-17

[Simoneau, 2006] Simoneau A., Ng E., Elbestawi M. A., 2006, 'Chip Formation During Microscale Cutting of a Medium Carbon Steel', International Journal of Machine Tools and Manufacture, Vol. 46, p. 467-481

[Simoneau, 2007] Simoneau A., Ng E., Elbestawi M. A., 2006, 'Modeling the Effects of Microstructure in Metal Cutting', International Journal of Machine Tools and Manufacture, Vol. 47, p. 368-375

[Statia, 2006] Statia M. H., D'Alessandria M., Quinto D. T., Roundet F., Astort M. M, 2006, 'High-Temperature Tribological characterization of Commercial TiAlN Coatings', Journal of Physics: Condensed Matter, Vol. 18, p. 1727-1736

[Trent, 2000] TRENT E.M., 2000, Metal Cutting, Forth Edition, Butterworth-Heinemann Ltd, ISBN 0-7506-7069-X

[Umbrello, 2007] Umbrello D., Filice L., Rizzuti S., Micari F., Settineri L., 2007, 'On the Effectiveness of Finite Element Simulation of Orthogonal Cutting with Particular Reference to Temperature Prediction', Journal of Materials Processing Technology, Vol. 189, p. 284-291

[Usui, 1982] Usui E., Shirakashi T., 1982, 'Mechanics of Machining - from Descriptive to Predictive Theory. In on the Art of Cutting Metals-75 years later', ASME Publication PED, Vol. 7, p. 13-35

[Woon, 2008] Woon K. S., Rahman M., Fang F. Z., Neo K. S., Liu K., 2008, 'Investigation of Tool Edge Radius Effect in Micromachining: A FEM Simulation Approach', Journal of Materials Processing Technology, Vol. 195, p. 204-211

[Xie, 1998] Xie J. Q., Bayoumi A. E., Zbib H. M., 1998, 'FEA Modeling and Simulation of Shear Localized Chip Formation in Metal Cutting', International Journal of Machine Tools and Manufacture, Vol. 39, p. 1067-1087

[Xie, 2005] Xie L. J, Schmidt K., Schmidt C., Biesinger F., 2005, '2D FEM Estimate of Tool Wear in Turning Operation', Wear, Vol. 258, p. 147-1490

[Yang, 2002] Yang X., Liu C. R., 2002, 'A new Stress-Based Model of Friction Behavior in Machining and Its Significant Impact on Residual Stresses Computed by Finite Element Method', International Journal of Mechanical Sciences, Vol. 44, p.703-723

[Yen, 2004 b] Yen Y. C., Jain A., Chigurupati P., Wu W. T., Altan T., 2004, 'Computer Simulation of Orthogonal Cutting using a Tool with Multiple Coatings', Machining Science and Technology, Vol. 8 (2), p. 305-326

[Yen, 2004] Yen Y.C., Jain A., Altan T., 2004, ' A Finite Element Analysis of Orthogonal Machining using Different Tool Edge Geometries', Journal of Materials Processing Technology, Vol. 146, p. 72-8

[Zheng, 1997] Zheng B. H., Komanduri R., 1997, 'Modeling of Thermomehcanical Shear Instability in Machining', International Journal of Mechanical Science, Vol. 39 (11), p. 1273-1314

[Zorev, 1963] Zorev N. N., 1963, 'Interrelation Between Shear Processes Occuring Along Tool Face and on Shear Plane in Metal Cutting', ASME, New York, p. 42-49

APPENDIX A

For all FE cutting models which include tool holder geometry FE (Tool + Holder), method of obtaining predicted F_t from the force signature was fixed. F_t force signature from FE (Tool + Holder) was filtered as shown on Figure A1. The range of filtered signal data between the two dashed lines was within ~0.1 kN, this value was fixed for consistency purposes.

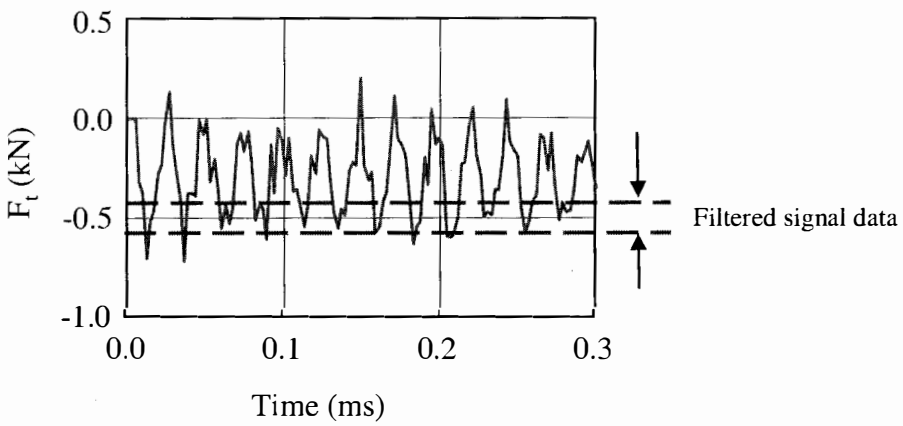

Figure A1: Filtered F_t signal data from FE (Tool + Holder)

APPENDIX B

It is assumed that the tool holder did not go through plastic deformation. Hooke's law of elasticity shown on equation B.1 was used to calculate the overall structure stiffness k of the tool holder, where F is the reactive force, and δ is the deflection.

$$F = -k\delta \quad \text{B.1}$$

Figure B1 (a) and (b) show the boundary condition of the FE models built to simulate the elastic deflection of the structure of the tool and the structure of the tool with the holder were built respectively. The reactive force F and structure deflection δ were obtained from the simulated models. Calculated overall structure stiffness is shown in Table B1. The results shows that the average structure stiffness for tool is 7.59×10^5 N/mm, and average overall structure stiffness for tool with holder is 3.19×10^5 N/mm.

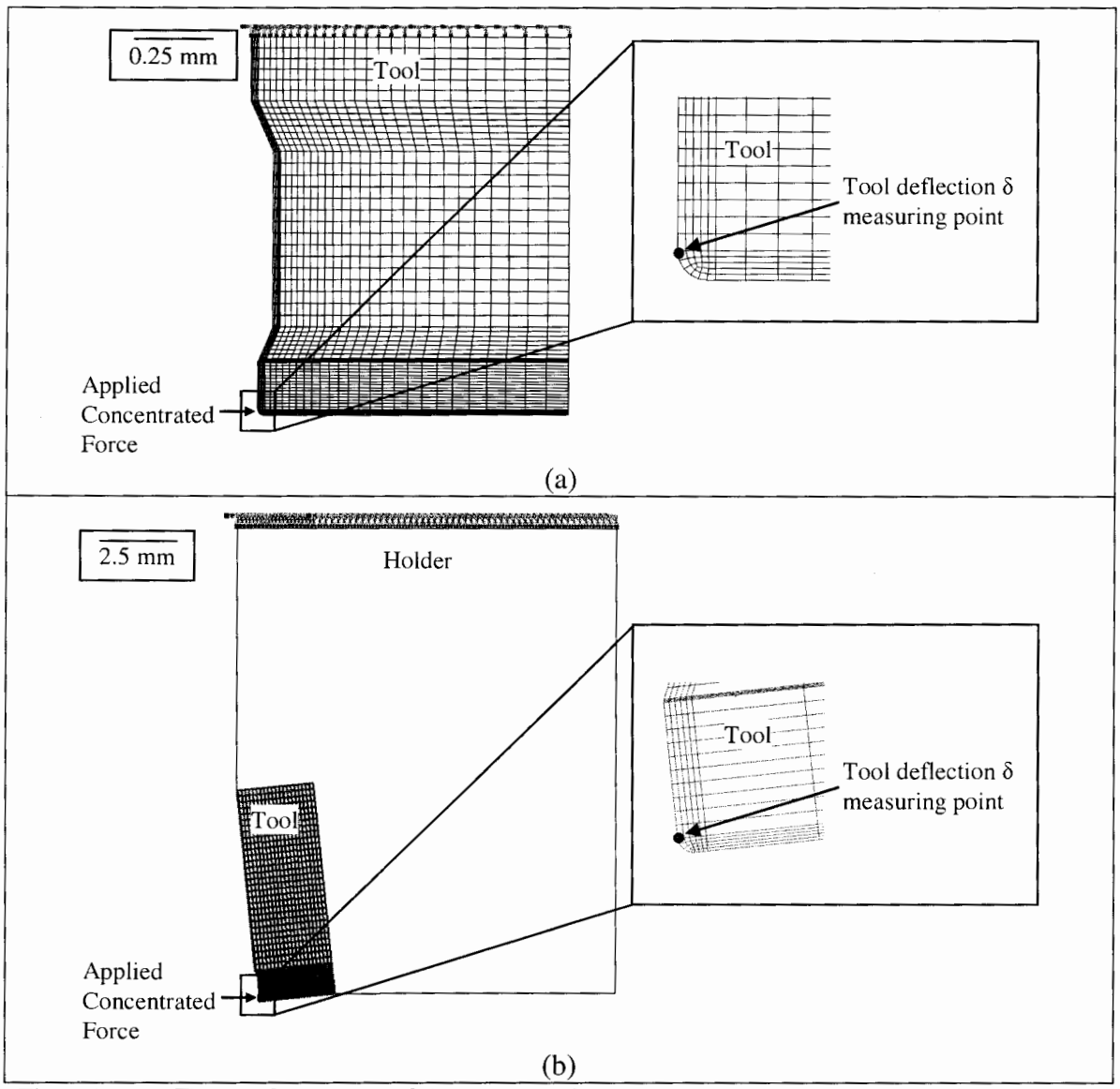

Figure B1: (a) FE model to measure *k* for the part of cutting tool structure. (b) FE model to measure *k* for the overall too and holder structure.

Tool				Tool + Holder		
δ (mm)	F (N)	$k = -F/\delta$ (N/mm)		δ (mm)	F (N)	$k = -F/\delta$ (N/mm)
1.32E-06	-1	7.59E+05		3.13E-06	-1	3.19E+05
2.63E-06	-2	7.59E+05		6.27E-06	-2	3.19E+05
4.61E-06	-3.5	7.59E+05		1.10E-05	-3.5	3.19E+05
7.57E-06	-5.75	7.59E+05		1.80E-05	-5.75	3.19E+05
1.20E-05	-9.125	7.59E+05		2.86E-05	-9.125	3.19E+05
1.87E-05	-14.1875	7.59E+05		4.45E-05	-14.1875	3.19E+05
2.87E-05	-21.7813	7.59E+05		6.82E-05	-21.7813	3.19E+05
4.37E-05	-33.1719	7.59E+05		1.04E-04	-33.1719	3.19E+05
6.62E-05	-50.2578	7.59E+05		1.57E-04	-50.2578	3.19E+05
9.99E-05	-75.8867	7.59E+05		2.38E-04	-75.8867	3.19E+05
1.51E-04	-114.33	7.59E+05		3.58E-04	-114.33	3.19E+05
2.27E-04	-171.995	7.59E+05		5.39E-04	-171.995	3.19E+05
3.40E-04	-258.493	7.59E+05		8.10E-04	-258.493	3.19E+05
4.72E-04	-358.493	7.59E+05		1.12E-03	-358.493	3.19E+05
6.04E-04	-458.493	7.59E+05		1.44E-03	-458.493	3.19E+05
7.36E-04	-558.493	7.59E+05		1.75E-03	-558.493	3.19E+05
8.68E-04	-658.493	7.59E+05		2.06E-03	-658.493	3.19E+05
9.99E-04	-758.493	7.59E+05		2.38E-03	-758.493	3.19E+05
1.13E-03	-858.493	7.59E+05		2.69E-03	-858.493	3.19E+05
1.26E-03	-958.493	7.59E+05		3.00E-03	-958.493	3.19E+05
1.32E-03	-1000	7.59E+05		3.13E-03	-1000	3.19E+05

Table B1: Calculated structure stiffness k for structure tool and for structure tool + holder.